Exploiting Structure and Input-Output Properties in Networked Dynamical Systems

Ana Sofia Rufino Ferreira

Electrical Engineering and Computer Sciences
University of California at Berkeley

Technical Report No. UCB/EECS-2015-245
http://www.eecs.berkeley.edu/Pubs/TechRpts/2015/EECS-2015-245.html

December 17, 2015

Exploiting Structure and Input-Output Properties in Networked Dynamical Systems

by

Ana Sofia Rufino Ferreira

A dissertation submitted in partial satisfaction of the

requirements for the degree of

Doctor of Philosophy in Engineering

in

Electrical Engineering and Computer Sciences

in the

Graduate Division

of the

University of California, Berkeley

Committee in charge:

Professor Murat Arcak, Chair
Professor Claire Tomlin
Professor Andrew Packard

Fall 2015

Exploiting Structure and Input-Output Properties in Networked Dynamical Systems

Abstract

Exploiting Structure and Input-Output Properties in Networked Dynamical Systems

by

Ana Sofia Rufino Ferreira

Doctor of Philosophy in Engineering in Electrical Engineering and Computer Sciences

University of California, Berkeley

Professor Murat Arcak, Chair

Large coupled networks of individual entities arise in multiple contexts in nature and engineered systems to produce rich dynamics and achieve complex behaviors. As the state-space dimension increases, the certification of stability and performance properties of these nonlinear dynamical systems becomes an intractable problem. In this thesis we develop decomposition methods that break up such convoluted systems into components of smaller dynamics whose behavior is dependent on the state of the neighboring components. These methods explore useful input-output properties of the subsystems in conjunction with the topology of their interconnections, providing results that scale well to large-scale networks.

We begin by developing a mathematical approach to analyze spatial pattern formation in developmental biology that combines graph-theoretical and dynamical systems methods to systematically predict the emergence of patterns. This approach models the contact between cells by a graph and exploits its symmetries to create partitions of cells into classes of equal fate. Using monotone systems theory, we derive verifiable conditions that determine whether patterns consistent with such partitions exist and are stable. Then, we propose an engineered synthetic circuit that mimics contact inhibition by using diffusible molecules to spontaneously generate sharply contrasting patterns. Using a compartmental model, we determine a condition that serves as a parameter tuning guide for patterning.

We next focus on exploring the symmetric topology of the interconnection to provide efficient certification of performance properties of large networks. Performance certification can be cast as a distributed optimization problem for which the existence of a solution is equivalent to the existence of a solution with repeated variables. We demonstrate that fast certification of stability and performance is possible by searching over solutions in a reduced order domain.

Finally, motivated by the stochastic behavior of biological networks, we provide stochastic stability results for systems modeled by stochastic differential equations. We use stochastic passivity properties of the subsystems and a diagonal stability condition of the interconnection matrix together with the passivity gains to guarantee stochastic stability and noise-to-state stability.

To my godmother Ascenção,
so I never forget my roots.

To my friend Floraine,
so I never forget to travel.

Contents

List of Figures

List of Tables

Acknowledgments

Aside from the PhD itself, my journey at Berkeley has been quite a personal transformation. The richness, quirkiness, diversity and intelligence of the people I had the pleasure to interact with makes me feel like playdough being shaped in all sorts of ways. I have had the most fun here. I have also developed a healthy sense self-criticism and understand that I have neither the skill nor wit to write an acknowledgment page that shows my full appreciation for everyone involved in this journey, both inside and outside of academia.

First and foremost, I would like to thank my advisor Murat Arcak. Some of my self-criticism developed from my interactions with him and his attention to detail in all things. He has taught me about preparedness, clarity and correctness. Murat is incredible at making time for me and everyone in the group, and for always providing an insightful suggestion when I struggled.

My undergraduate advisor, João Sousa, is the person responsible for my admission to Berkeley. He helped me immensely in the preparation of my graduate school applications, and has always been genuinely interested in my personal and professional progress. I still remember how he once told me that Berkeley, the school and the city, would be the best place for me. No doubt about that.

The support from the Pinto-Fialon Scholarship, Prof. Deolinda Adão in the Portuguese Studies Department, and the Portuguese Foundation for Science and Technology, has been essential for my success. Having participated in the admissions committee has made me understand the advantage of guaranteed funding for the first years of graduate school.

Academically, I have appreciated the interactions, discussions and research directions suggested by my qualifying committee members Andy Packard, Claire Tomlin, and Venkat Anantharam. I also had the privilege to collaborate in multiple publications with Eduardo Sontag, Michel Maharbiz, Adam Arkin, Justin Hsia and Chris Meissen. One of the things I will miss the most are the research meetings with multiple faculty: the brainstorm of ideas, the crazy hypotheses, and the stories were inspirational to me. I feel fortunate to have participated in many meetings, reading groups, lunches and coffee breaks with my research group: Yusef Shafi, Sam Coogan, John Maidens, Eric Kim, Jonathan Tu, Erin Summers, Justin Hsia and Chris Meissen; some barely related with work.

I am forever grateful to my friend Richard for taking me to Yosemite for the first time and sparking my admiration for nature. Finally, I end with an incomplete list of my Berkeley friends with whom I have enjoyed cooking, eating, drinking, picnicking, concertgoing, traveling, hiking and backpacking: Aude, Ryan, Maria, Emily, Richard, Sylvia, Floraine, Max, Mike, Jackie, Johnny, Edna, Georgia, Katerina, Sergey, Shang, Matt, Kay, Alan; my sailing community of friends: Moni, Bob, Lori, Sallie, Jan, Don, Rajat; and the Portuguese com-

munity in Berkeley: Luís, Elói, Maria, Diogo, Catarina, Gonçalo. Proper acknowledgements would include a short sentence about each one of you and why you are all special to me in your own way. At the intersection of all these, the best and most unexpected adventures have been with Cory, my partner in crime.

While Berkeley has become my home, I never forget my roots, and how hard it is for my parents and siblings to see me so rarely.

Chapter 1

Introduction

Networked systems are formed by components that behave in accordance to the output of their corresponding neighboring or communicating components. These ubiquitous systems occur in nature and in engineered systems. However, most existing analytical methods do not scale to large networks. Efficient and scalable certification techniques for such large-scale systems are imperative. In this thesis, we develop new approaches for the analysis of networked dynamical systems that exploit the interconnection structure of their components together with relevant input-output properties, such as passivity and monotonicity. This approach decouples the certification problem into two. First, we examine analytical conditions for the individual subsystems that guarantee the relevant input-output properties without knowledge about the interconnection. Then, we derive conditions for the interconnection by representing each subsystem as an appropriate abstraction of its input-output behavior.

The thesis addresses three main topics. In Chapters 2 and 3 we address pattern formation in developmental biology and inspect the existence and stability of spatial patterns in networks of biological cells. We employ tools from graph theory to identify symmetries and equitable partitions in the network, and show that such partitions are templates of repeated dynamics that allow for the dimensionality reduction of the analysis. In Chapter 3 we address a cellular biological mechanism by which cells compete with its neighbors through contact, while Chapter 4 focuses on the design and analysis of an engineered synthetic circuit with similar lateral inhibition properties but in which communication is achieved with the use of diffusible molecules. In the second part, Chapter 4, we extend the use of symmetries to the certification of performance properties. In several optimization problems with linear constraints, symmetries imply that the existence of a solution is equivalent to the existence of a solution with repeated elements, and thus one needs to search over a reduced number of variables. We show how to achieve efficient performance certification by exploring this reduction in semidefinite programming problems. Finally, Chapter 5 addresses nonlinear systems driven by noise, that are modeled by stochastic differential equations. Sufficient conditions are provided to guarantee stochastic stability in probability and noise-to-state stability by exploiting stochastic passivity properties and diagonal stability of the passivity

matrix together with the interconnection matrix.

1.1 Preliminaries

We consider a networked system to be a large dynamical system that can be decomposed into several decoupled subsystems $H_i : u_i \to y_i$, $i = 1, ..., N$, with exogenous disturbances d and performance output e, and a communication topology defined by an interconnect matrix $M \in \mathbb{R}^{N\times N}$, see Figure 1.1. The input/output relation is determined by $\left[\begin{smallmatrix} u \\ e \end{smallmatrix}\right] = M \left[\begin{smallmatrix} y \\ d \end{smallmatrix}\right]$ and the subsystems H_i are described by the nonlinear dynamics $\dot{x} = f(x, u)$, $y = h(x, u)$.

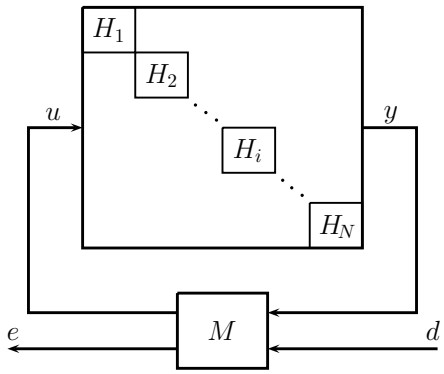

Figure 1.1: Networked System.

In Chapters 2-4, we interpret the interconnection matrix M as the adjacency matrix of a graph $\mathcal{M}$ and explore its symmetric properties. For each subsystem H_i we use monotonicity properties to show stability and emergence of spatial patterns in biological cell networks, Chapters 2 and 3; and we use dissipativity properties in Chapter 4. We study stochastic systems in Chapter 5 and explore properties of stochastic passivity and noise-to-state stability. We consider closed systems in Chapters 2 and 3, *i.e.*, without d and e; Chapter 4 addresses systems with exogenous d and e; and Chapter 5 considers systems driven by noise.

Algebraic Graph Theory and Symmetries

A *graph* $\mathcal{G}$ consists of a set of vertices, $V = \{1, ..., N\}$, and edges E, where every edge connects two vertices. In this thesis, we consider both directed and undirected graphs. In the former, each edge has a tail vertex and a head vertex, and there is a notion of orientation. The latter can be seen as an undirected graph where each edge shows up in pairs of opposite directions. Each edge might include a binary value (1 or 0, if nodes are connected or not), or include a weight between nodes, $w_{i,j}$. We will use the notion of connectedness in undirected graphs, which dictates that every pair of vertices is connected through a path of one or several edges. Next, we define symmetry properties in graphs, [55].

Automorphisms

A symmetry in a graph is normally understood as a transformation, *e.g.*, rotation, reflection, that preserves the topology of the graph edges. Formally, in a weighted graph $\mathcal{G}(V, E)$, an *automorphism* is a permutation of the vertices $g : V \to V$ such that if $(i, j) \in E$ then also $(gi, gj) \in E$ and $w_{i,j} = w_{gi,gj}$, where gi denotes the image of vertex i under permutation g. The set of all automorphisms of $\mathcal{G}$ forms a group designated by *automorphism group*,

$$Aut(\mathcal{G}) = \Big\{ g : V \to V \;\Big|\; (gi, gj) \in E \text{ and } w_{i,j} = w_{gi,gj} \;\text{ for all } (i, j) \in E \Big\}.$$

A subset H of the automorphism group $Aut(\mathcal{G})$ that is closed under composition and inverse is called a *subgroup*. Given a subgroup of the automorphism group, $H \subseteq Aut(\mathcal{G})$, the vertices of $\mathcal{G}$ can be partitioned into sets of vertices that permute with each other, which we call *orbits*. The orbit of index $i \in V = \{1, ..., N\}$ under the action of H is defined as:

$$O_i = \Big\{ j \in V \;\Big|\; gi = j \;\text{ for some } g \in H \subseteq Aut(\mathcal{G}) \}.$$

The orbits form an *equivalence class* given by the *equivalence relation* $\sim$, where

$$i \sim j \;\text{ if }\; j \in O_i.$$

Due to symmetry, at each vertex u in an orbit O_i, the sum of edge weights coming from all elements in another orbit O_j, must be constant regardless of the choice of u in O_i. Therefore, the action of a subgroup $H \subseteq Aut(\mathcal{G})$ defines a *quotient graph* $\mathcal{G}/H$ whose vertices are the orbits of V, and the edges represent the sum of the edge weights between a vertex $u \in O_i$ and all vertices in O_j, [55].

Example: Consider the undirected cyclic graph with five vertices, represented in Figure 1.2a. This graph is rich in symmetries. In fact, this is a *vertex-transitive* graph, since for any two vertices $i, j \in V$ there exists an automorphism $g \in Aut(\mathcal{G})$ that permutes i into j. Consider the subgroup $H \subset Aut(\mathcal{G})$ formed by the identity permutation together with the permutation along the vertical axis represented in Figure 1.2b, $H = \{(1, 2, 3, 4, 5) \to (1, 2, 3, 4, 5), (1, 2, 3, 4, 5) \to (1, 5, 4, 3, 2)\}$. The action of H permutes vertices 2 with 5, and 3 with 4, and the orbits of graph $\mathcal{G}$ become $O_1 = \{1\}$, $O_2 = \{2, 5\}$, and $O_3 = \{3, 4\}$, see 1.2c. For this orbit partition, the corresponding quotient graph is represented in Figure 1.2d, which in this example is a directed graph.

Adjacency Matrix

The *adjacency matrix* of graph $\mathcal{G}$ is the matrix $M \in \mathbb{R}^{N \times N}$ where entry m_{ij} is equal to 0 if there is no edge between vertices i and j, otherwise m_{ij} equals the edge weight $w_{i,j}$. Let R be the permutation matrix that represents a permutation $g \in Aut(\mathcal{G})$. Then, due to symmetry,

$$RM = MR.$$

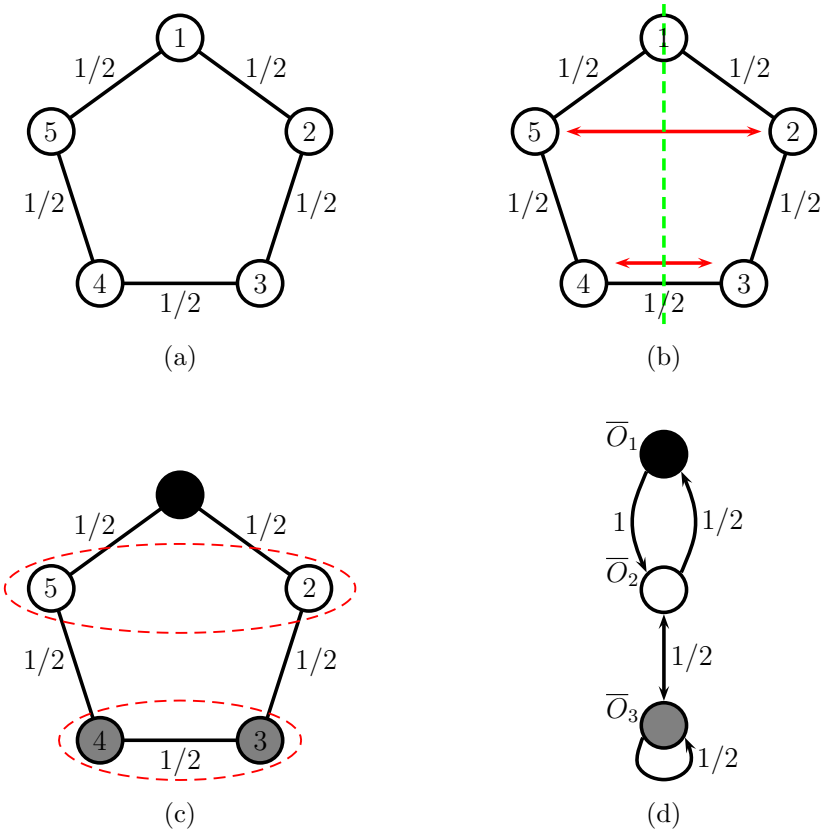

Figure 1.2: Example of a cyclic graph with five vertices: original graph in (a); symmetry along vertical axis in (b); orbit partition due to the action of subgroup H, composed by the vertical symmetry and the identity, in (c), and corresponding quotient graph, in (d).

Consider a subgroup $H \subseteq Aut(\mathcal{G})$ and let r be the corresponding number of distinct orbits. Define the matrix $Q \in \mathbb{R}^{N \times r}$ such that $q_{ij} = 1$ when vertex i is in orbit j, and $q_{ij} = 0$ otherwise. The following holds,

$$MQ = Q\overline{M},$$

where $\overline{M} \in \mathbb{R}^{r \times r}$ is the quotient matrix, which corresponds to the adjacency matrix of the quotient graph $\mathcal{G}/H$. The following are the adjacency matrices of the graph $\mathcal{G}$ and the

quotient graph $\mathcal{G}/H$ in Figure 1.2:[1]

$$M = \begin{bmatrix} 0 & 1/2 & 0 & 0 & 1/2 \\ 1/2 & 0 & 1/2 & 0 & 0 \\ 0 & 1/2 & 0 & 1/2 & 0 \\ 0 & 0 & 1/2 & 0 & 1/2 \\ 1/2 & 0 & 0 & 1/2 & 0 \end{bmatrix} \qquad \overline{M} = \begin{bmatrix} 0 & 1 & 0 \\ 1/2 & 0 & 1/2 \\ 0 & 1/2 & 1/2 \end{bmatrix}.$$

Remark: Note that the eigenvalues of $\overline{M}$ are also eigenvalues of M. Moreover, since each vertex of the quotient graph represents an orbit, we can find a correspondence between the eigenvectors of M and $\overline{M}$. Consider an eigenvector $v \in \mathbb{R}^N$ of M with corresponding eigenvalue λ, and let $\overline{v} \in \mathbb{R}^r$ be the vector with entries $\{\overline{v}\}_k = \frac{1}{|O_k|} \sum_{u \in O_k} v_u$. If $\overline{v}$ is not a zero vector, then it is an eigenvector of $\overline{M}$ with corresponding eigenvalue λ. On the other hand, an eigenvector v corresponding to λ of M can also be chosen from the eigenvector $\overline{v}$ for λ of $\overline{M}$, by repeating the elements of $\overline{v}$ over the indices in the same orbit, [17].

In Chapters 2 and 3 we use the more general notion of equitability, which is based on vertex partitions and their edge weights. For the graph $\mathcal{G}(V, E)$ with adjacency matrix M, a partition of the vertex set V into classes $O_1, ..., O_r$ is *equitable* if there exist $\overline{m}_{ij}$, $i, j = 1, ..., r$ such that

$$\sum_{v \in O_j} m_{uv} = \overline{m}_{ij} \quad \forall u \in O_i.$$

This means that the sum of the normalized edge weights from some vertex in a class O_i into all the vertices in a class O_j is invariant of the choice of the vertex in class O_i. The notions of quotient graph and quotient matrix also apply for equitable partitions. The quotient matrix $\overline{M}$ is formed by the entries $\overline{m}_{ij}$.

Indeed, the action of each subgroup H of the full automorphism group $Aut(\mathcal{G})$ defines an equitable partition. Note that, the action of H on V partitions the vertex set into *orbits*, $O_i = \{hi \,|\, h \in H\}$, such that $O_j = O_i$ for all $j \in O_i$. Let r be the number of distinct orbits under the subgroup H, and relabel them as $\{\overline{O}_1, \ldots, \overline{O}_r\}$. This orbit partition is indeed equitable, because the sum $\sum_{k \in \overline{O}_j} m_{i^* k} = \overline{m}_{ij}$ is constant independently of the choice of $i^* \in \overline{O}_i$.

Monotone Systems

A *monotone* system is one that preserves a partial ordering of the initial conditions as its trajectories evolve. The partial ordering is defined with respect to a *positivity cone* K in the Euclidean space that is closed, convex, pointed ($K \cap (-K) = \{0\}$), and has nonempty

[1] where $Q = \begin{bmatrix} 1 & 0 & 0 \\ 0 & 1 & 0 \\ 0 & 0 & 1 \\ 0 & 0 & 1 \\ 0 & 1 & 0 \end{bmatrix}$

interior. For such cone, $x \preceq \hat{x}$ means that $\hat{x} - x \in K$; $x \prec \hat{x}$ means that $x \preceq \hat{x}$ and $x \neq \hat{x}$; and $x \ll \hat{x}$ means that $\hat{x} - x$ is in the interior of K.

Given the positivity cones K^U, K^Y, K^X, for the input, output, and state spaces, the dynamical system $\dot{x} = f(x,u)$, $y = h(x)$ is said to be *monotone* if $x(0) \preceq \hat{x}(0)$ and $u(t) \preceq \hat{u}(t)$ for all $t \geq 0$ imply that the resulting solutions satisfy $x(t) \preceq \hat{x}(t)$ for all $t \geq 0$, and that the output map is such that $x \preceq \hat{x}$ implies $h(x) \preceq h(\hat{x})$, [4].

Useful properties include the fact that the linearization of a monotone system around a steady-state (x^*, u^*) is also a monotone system with respect to the same positivity cone [3]. Moreover, it has been shown that the stability of a linear monotone system with positive feedback can be determined by the steady-state gain of the open-loop system, [39].

Stochastic Differential Equations

We consider continuous-time nonlinear stochastic systems driven by noise:

$$dx = f(x)dt + l(x)\Sigma dw.$$

The noise, $w(t)$, is an independent standard Wiener process, and $\Sigma = \{\sigma_{ij}\}$ is a nonnegative-definite matrix, where σ_{ij} represents the intensity with which the j^{th} source of uncertainty influences the i^{th} state.

The stochastic system above, with $f(0) = 0$ and $l(0) = 0$, has an equilibrium at the origin that is said to be *globally stable in probability* if the sample paths of the process starting at point x_0 at time $t = 0$ remain within a prescribed neighborhood of the origin with probability tending to one as x_0 tends to zero, [31], *i.e.*, if $\forall \epsilon > 0$, $\exists \gamma \in \mathcal{K}$ such that

$$P\{|x(t)| \leq \gamma(|x_0|)\} \geq 1 - \epsilon, \quad \forall t \geq 0, \forall x_0 \in \mathbb{R}^n.$$

It is *globally asymptotically stable in probability* if it is globally stable in probability and the trajectories eventually converge to the equilibrium.

A stochastic counterpart of the Lyapunov theory will be used to show stochastic stability. For the system above, assume that there exists a storage function $V(x)$ that is nonnegative and radially unbounded, and such that

$$\mathcal{L}V(x) \triangleq \frac{\partial V}{\partial x} f(x) + \frac{1}{2}\mathrm{Tr}\left\{\Sigma^\top l(x)^\top \frac{\partial^2 V}{\partial x^2} l(x)\Sigma\right\} \leq -S(x), \quad \forall x,$$

for some function $S(x)$. When $S(x)$ is a nonnegative (positive) function, the origin is globally (asymptotically) stable in probability, [66]. The infinitesimal generator $\mathcal{L}V(x)$ is a partial differential operator and defines a notion of expected derivative, since $\mathcal{L}V(x) =$

$\lim_{t\to 0} \frac{E[V(x(t)]-V(x_0)}{t}$. Note that the first term corresponds to the deterministic part of the system, while the second term is always positive when $V(x)$ is a convex storage function, which makes stochastic stability harder to achieve. However, in some cases, it might be possible to construct storage functions with negative concavity in some intervals, that show global stability in probability of the origin even if the deterministic part is not globally attractive at the origin.

We use the notion of *noise-to-state stability* (NSS) in cases of unknown noise intensity Σ and nonvanishing noise at the origin, $l(0) \neq 0$, [31]. A system is NSS when its state is bounded in probability, *i.e.*, for any $\epsilon > 0$, there exists a $\mathcal{KL}$ function β, and a $\mathcal{K}_\infty$ function δ, such that

$$P\left\{|x| < \beta(|x_0|, t) + \delta\left(|\Sigma\Sigma^\top|_F\right)\right\} \geq 1 - \epsilon \quad \forall t \geq 0.$$

Consider now the controlled stochastic nonlinear system

$$\begin{cases} dx = f(x,u)dt + l(x,u)\Sigma dw \\ y = h(x,u) \end{cases}$$

The system is *stochastic dissipative* if the storage function is such that

$$EV(x(t)) - V(x(s)) \leq E\int_s^t W\big(x(\tau), u(\tau)\big)d\tau,$$

where W is the supply rate. Equivalently, $\mathcal{L}V(x) \leq W(x,u)$. In Chapter 5, we choose $W(x,u) = h(x,u)^\top u - S(x)$. When there exists a positive semidefinite (definite) function $S(x)$, the system is called *stochastic (strictly) passive*, [45]. It is *stochastic output strictly passive* (sOSP) if $S(x) = \frac{1}{\gamma}h(x)^\top h(x)$, and γ is said to be a gain.

Note that, we recover the deterministic notion of dissipativity when $l(x) \equiv 0$, [110]. In Chapter 4, we consider problems that address quadratic supply rates,

$$W(x,u) = \begin{bmatrix} u \\ h(x,u) \end{bmatrix}^\top X \begin{bmatrix} u \\ h(x,u) \end{bmatrix}.$$

For example, to certify an L_2-gain from scalar $u(t)$ to $y(t)$ choose $X = \left[\begin{smallmatrix} \gamma^2 & 0 \\ 0 & -1 \end{smallmatrix}\right]$, which implies that $\|y\|_2^2 \leq \gamma^2\|u\|_2^2 + V(x(0))$.

1.2 Summary of the Thesis

In biology, multicellular developmental processes rely on spatial patterning to initiate differentiation. Even though the majority of results on patterning investigate diffusion-driven mechanisms, lateral inhibition is a common pattern formation mechanism where cell-to-cell

contact signaling induces neighboring cells to compete and diverge into sharply contrasting fates that can initiate developmental processes such as segmentation or boundary formation. Known examples of lateral inhibition are the Notch pathway in Metazoans and contact-dependent inhibition (CDI) in *E. coli*.

In Chapter 2, we analyze spatial patterns on networks of cells where adjacent cells inhibit each other through contact signaling. We represent the network as a graph where each vertex represents the dynamics of identical individual cells and where graph edges represent cell-to-cell signaling. To predict steady-state patterns we find equitable partitions of the graph vertices and assign them into disjoint classes. Equitable partitions of the contact graph allow for a systematic identification of patterns. We use results from monotone systems theory to prove the existence of patterns that are structured in such a way that all the cells in the same class have the same final fate. To study the stability properties of these patterns, we rely on the graph partition to perform a block decomposition of the system and reduce its dimension. Then, to guarantee stability, we provide a small-gain type criterion that depends on the input-output properties of each cell in the reduced system. Finally, we discuss pattern formation in stochastic models. With the help of a modal decomposition we show that noise can enhance the parameter region where patterning occurs. The results in this chapter appear in [40].

Despite the vigorous research on elucidating natural pathways such as Notch-Delta and CDI, a synthetic lateral inhibition system for pattern formation has not been successfully engineered. In order to achieve patterning with synthetic circuits, we propose a compartmental lateral inhibition system, in Chapter 3, where contrasting patterns between neighboring compartments emerge due to communication via diffusible molecules. Our proposed construct consists of a set of compartments interconnected by channels, where in each compartment we place a colony of cells that can produce diffusible molecules to be detected by the neighboring colony. We equip each cell with an inhibitory circuit that reacts to the detected signal, so that the more diffusible molecules detected in one compartment, the less production in that colony. To prevent auto-inhibition, we utilize two orthogonal diffusible quorum sensing molecules and design two inhibitory circuits each of which detects only one type of molecule and produces the other type.

We derive analytical conditions that guarantee contrasting patterning in this spatially-distributed construction by defining the cell network as a graph, where each compartment corresponds to a vertex, and each graph edge corresponds to a diffusion channel between two compartments. We model the diffusion with the Laplacian matrix of the weighted graph and use a notion of equitable partition to provide existence and stability conditions of contrasting patterns. Finally, we propose and analyze a synthetic circuit which is currently under implementation. The results in this chapter appear in [42, 43].

We also exploit symmetries in the interconnection topology of a networked system, in Chapter 4, to provide a dimensionality reduction in the certification of stability and performance. The certification method provides a guarantee with respect to exogenous distur-

bances and output performance, and exploits the dissipativity properties of the subsystems, thus the conservatism introduced by the reduction is minimal when the subsystems possess similar dissipativity characteristics. We combine this reduction with distributed optimization techniques and robust dissipativity analysis, and show that the number of decision variables in the global optimization constraint can be reduced, as well as its size in several cases. This leads to the efficient analysis of large networks. To certify frequency dependent properties, we also extend the results to a state-space variant of integral quadratic constraints (IQCs). The results in this chapter have been submitted to IEEE Transactions on Control of Network Systems, [44].

Finally, in Chapter 5, we analyze the stability of large-scale nonlinear stochastic systems, represented as an interconnection of lower-order stochastic subsystems. Stochastic stability in probability and noise-to-state stability are addressed using Lyapunov theory. The method proposed proves network stability by using appropriate stochastic passivity properties for its subsystems, and a linear matrix inequality for the structure of their interactions. In particular, stability is established by the diagonal stability of a dissipativity matrix, which incorporates information about the passivity properties of the systems, together with the interconnection matrix. Due to the difficulty of determining the equilibrium of such large-scale systems, we derive equilibrium-independent conditions for the verification of the relevant stochastic passivity properties of the subsystems. To certify noise-to-state stability, we provide sufficient conditions that rely only on the system state and, thus, are independent of the noise intensity. We illustrate the proposed approach on a class of biological reaction networks. The results in this chapter appear in [41].

Chapter 2

Pattern Formation in Lateral Inhibition Systems using Graph Partitions

Spatial patterning is crucial for multicellular developmental processes [51, 111]. The majority of theoretical results on pattern formation rely on diffusion-driven instabilities, proposed by Turing [101] and further studied by other authors [50, 33, 84]. Although some early events in developmental biology employ diffusible signals, most of the patterning that leads to segmentation and fate-specification relies on contact-mediated signals. In particular, lateral inhibition [96] is a cell-to-cell contact signalling mechanism that leads neighboring cells to compete and diverge to contrasting states of differentiation. An example of lateral inhibition is the Notch pathway, where neighboring cells compete through the binding of Notch receptors and Delta ligands [26].

Analytical results that pursue explicit conditions for patterning by lateral inhibition, such as [26, 107, 87, 49], study simple networks with only a few cells, and do not reveal the variety of patterns that may arise in large networks. A broader dynamical model for lateral inhibition is proposed in [8], and results that are independent of the size of the network are presented. In this reference, the large-scale network is viewed as an interconnection of individual cells, each defined by an input-output model. The contact signaling is represented by an undirected graph, where each vertex is a cell, and a link between two vertices represents the contact between two cells. Results for the instability of the homogeneous steady-state and the existence of two-level patterns for bipartite contact graphs are presented in [8].

In this chapter, we use the model introduced in [8] and derive results for pattern formation on a general contact graph, recovering the results of [8] for bipartite graphs as a special case. Our main idea is to partition the graph vertices into disjoint classes, where the cells in the same class have the same final fate. We use algebraic properties of the graph and tools from monotone systems theory [92] to prove the existence of steady-states that

are patterned according to these partitions. We then address the stability of these patterns by decomposing the system into two subsystems. The first describes the dynamics on an invariant subspace defined according to the partition; and the second describes the dynamics transversal to this subspace. We provide a small-gain type criterion [105, 32], that relies only on the dynamics of the first invariant subspace.

A key property that the graph partition must satisfy is that the sum of the normalized edge weights from one vertex in another class into all those vertices in some class is independent of the choice of vertex. Partitions with this property are called *equitable* and allow us to study a reduced model where all vertices in the same class have the same state. As examples of equitable partitions, we study bipartite graphs and graphs with symmetries. Permutations of the graph nodes that leave the edge set invariant are called automorphisms [55], and the set of all automorphisms of the graph has a group structure. We show that subgroups of the full automorphism group, which can be found with numerical tools such as [46], can be used to identify equitable partitions.

Symmetry reduction has been explored in dynamical systems and bifurcation theory [77, 98, 56]. In particular, the idea of clustering the graph vertices into classes of synchronized states has been studied [98, 56, 106]. The notion of equitable partitions in this chapter is related to the definition of balanced relations and synchrony subspaces introduced in [98, 56], and similarly the reduced models defined by the equitable partitions correspond to the notion of quotient networks in these references. However, our results are the first to combine symmetry with monotone systems properties to characterize the emergence of steady-state patterns in lateral inhibition systems. These results are readily applicable to various lateral inhibition models [26, 96] and specify the ranges of meaningful biological parameters that yield patterning.

Other uses of symmetry properties in control theory include dimension reduction and block decomposition of semidefinite programming problems, such as fastest mixing Markov chains on the graph [17, 19], and sum-of-squares [48]. Symmetry has also been explored to investigate controllability in agreement problems [88].

Finally, we discuss the formation of patterns in stochastic models and show that noise can enhance the parameter region where patterning occurs. Such enlargement of the parameter region by stochasticity has been observed for Turing patterns in [15, 22, 60]. Although lateral inhibition is a fundamentally different mechanism than Turing's diffusion-driven patterning, we follow an approach similar to [60], and show that high-frequency spatial modes can be excited by noise, even when the homogeneous steady-state is stable.

In Section 2.1, we define the model and introduce necessary graph theoretical concepts. In Section 2.2, we present the main result of the chapter, which provides conditions for the existence of steady-state patterns. In Section 2.3, we apply the main results to graphs

with symmetries, and present examples. In Section 2.4, we present a decomposition that is helpful for the stability analysis of steady-state patterns, and derive a small-gain stability type criterion. Finally, in Section 2.5, we discuss stochastic models and pattern formation driven by noise.

2.1 Lateral Inhibition Model

We represent the cell network by an undirected and connected graph $\mathcal{G} = \mathcal{G}(V, E)$, where the set of vertices V represents a group of cells, and each edge $e \in E$ represents a contact between two cells. The connectivity between cells i and j is represented by the nonnegative constant $w_{i,j} \in \mathbb{R}_{\geq 0}$. We let $w_{i,j} = 0$ when i and j are not in contact, and $w_{i,j} > 0$ when they are in contact. A common choice is to select $w_{i,j} = 1$; however, to be more general and to allow distinct contact signal strengths, we allow weights other than 0 and 1. Since this *contact graph* is undirected, the weights must satisfy $w_{i,j} = w_{j,i}$.

Let N be the number of cells and define the *scaled adjacency matrix* $M \in \mathbb{R}^{N\times N}$ of $\mathcal{G}$ as:

$$m_{ij} = d_i^{-1} w_{i,j}, \tag{2.1}$$

where the scaling factor is the node degree $d_i = \sum_j w_{i,j}$. The structure of M is identical to the transposed probability transition matrix of a reversible Markov Chain (*i.e.*, let π be a stationary distribution such that $\pi_i = d_i / \sum_k d_k$, for $i = 1, ..., N$, then $\pi_i m_{ij} = \pi_j m_{ji}$). Therefore, M is nonnegative and row-stochastic, *i.e.*, $M\mathbf{1}_N = \mathbf{1}_N$, where $\mathbf{1}_N \in \mathbb{R}^N$ denotes the vector of ones, and it has real valued eigenvalues and eigenvectors.

Consider a network of identical cells $i = 1, \ldots, N$ each described by the dynamical model:

$$\begin{cases} \dot{x_i} &= f(x_i, u_i) \\ y_i &= h(x_i) \end{cases} \tag{2.2}$$

where $x_i \in \mathcal{X} \subset \mathbb{R}^n$ describes the state in cell i (typically, a vector of reactant concentrations), $u_i \in \mathcal{U} \subset \mathbb{R}$ is an aggregate input from neighboring cells, and $y_i \in \mathcal{Y} \subset \mathbb{R}$ represents the output of each cell that contributes to the input to its neighbors. We represent the cell-to-cell interaction by

$$u = My \tag{2.3}$$

where M is the scaled adjacency matrix of the contact graph as in (2.1), $u \triangleq [u_1 \ldots u_N]^\top$, and $y \triangleq [y_1 \ldots y_N]^\top$. This means that the input to each cell is a weighted average of the outputs of adjacent cells.

Standing Assumptions. We assume that $f(\cdot, \cdot)$ and $h(\cdot)$ are continuously differentiable, and that for each constant input $u^* \in \mathcal{U}$, system (2.2) has a globally asymptotically stable steady-state

$$x^* \triangleq S(u^*), \tag{2.4}$$

that is also a hyperbolic equilibrium (*i.e.*, $\frac{\partial f}{\partial x}|_{(x^*,u^*)}$ has no eigenvalues on the imaginary axis). Furthermore, we assume that the map $S : \mathcal{U} \to \mathcal{X}$ and the map $T : \mathcal{U} \to \mathcal{Y}$, defined as:

$$T(\cdot) \triangleq h(S(\cdot)), \tag{2.5}$$

are continuously differentiable, and that $T(\cdot)$ is a positive, bounded, and decreasing function. The decreasing property of $T(\cdot)$ is consistent with the lateral inhibition feature, since higher outputs in one cell lead to lower values in adjacent cells. An example of such a map is the transfer function of a biochemical inverter, see [113, 109].

Note that the steady-states of the system (2.2)-(2.3) are given by $x_i = S(u_i)$ in which $u_1, \ldots, u_N$ are solutions of the equation:

$$u = M\mathbf{T}_N(u), \tag{2.6}$$

where

$$\mathbf{T}_N(u) = [T(u_1), \ldots, T(u_N)]^\top. \tag{2.7}$$

In particular, since M is row-stochastic, (2.6) admits a solution that is homogeneous across all cells, *i.e.*, $u_i = u^*$ for all $i = 1, \ldots, N$, where u^* is the unique fixed point of $T(\cdot)$, *i.e*,

$$T(u^*) = u^*. \tag{2.8}$$

We refer to the corresponding steady-state $x_i^* = S(u^*)\ \forall i$ as the homogeneous steady-state (HSS) of the interconnection. We now give a sufficient condition for the instability of the HSS. This condition is similar to [8, Theorem 1] but our proof does not rely on the monotonicity assumption ([4]) made in [8].

Lemma 1. *Consider the system* (2.2)-(2.3). *Let* λ_N *be the smallest eigenvalue of* M, *and let* u^* *be as in* (2.8). *Then, if*

$$|T'(u^*)|\lambda_N < -1, \tag{2.9}$$

the homogeneous steady-state $x_i = x^* \triangleq S(u^*)$, $i = 1, \ldots, N$, *is unstable.*

Proof. The linearization of (2.2)-(2.3) about the HSS can be brought to a block-diagonal form consisting of the matrices $A + \lambda_k BC$, where λ_k denote the eigenvalues of M, $A \triangleq \frac{\partial f(x,u)}{\partial x}|_{(x,u)=(x^*,u^*)}$, $B \triangleq \frac{\partial f(x,u)}{\partial u}|_{(x,u)=(x^*,u^*)}$, and $C \triangleq \frac{\partial h(x)}{\partial x}|_{x=x^*}$, as in [8, Proof of Theorem 1]. We thus guarantee instability of the HSS if one of the matrices $A+\lambda_k BC$, for $k = 1, \ldots, N$ has a positive eigenvalue. Furthermore, we note from (2.11) that $T'(u^*) = -CA^{-1}B$. This means that, given the assumption (2.9), we just need to prove that the condition $1 + \lambda_k CA^{-1}B < 0$ implies that $A + \lambda_k BC$ has a positive eigenvalue. To show this, we will make use of the multiplication property of determinants and Claim 2 below. Given the second statement in Claim 2, if we prove that $1 + \lambda_k CA^{-1}B < 0$ implies $(-1)^n det(A + \lambda_k BC) < 0$, then we can conclude that $A + \lambda_k BC$ has a positive eigenvalue and, therefore, the HSS is unstable.

Note that by assumption, any constant input has an hyperbolic globally asymptotically stable steady-state, which implies that A is Hurwitz, and therefore that, from the first part of Claim 2, $(-1)^n det(A) > 0$. The next inequality then follows from the condition that $det(1 + \lambda_k CA^{-1}B) < 0$:

$$\begin{aligned}(-1)^n det(A + \lambda_k BC) &= (-1)^n det(A) det(I_n + \lambda_k BCA^{-1}) \\ &= (-1)^n det(A) det(1 + \lambda_k CA^{-1}B) < 0, \end{aligned} \tag{2.10}$$

where the second equality holds from Sylvester's Determinant Theorem [2]. We then conclude that $A + \lambda_k BC$ has a positive and real eigenvalue. □

Claim 2. *If $A \in \mathbb{R}^{n\times n}$ is Hurwitz then $(-1)^n det(A) > 0$. If $(-1)^n det(A) < 0$ then A has a positive and real eigenvalue.*

Proof. To prove the claim, note that the characteristic polynomial of A can be written as $det(\lambda I_n - A) = (\lambda - \lambda_1)\dots(\lambda - \lambda_n)$, where $\lambda_1, \dots, \lambda_n$ are the eigenvalues of A. Then, the following holds: $det(-A) = det(-I_n A) = (-\lambda_1)\dots(-\lambda_n)$, and also $(-1)^n det(A) = (-1)^n \lambda_1 \dots \lambda_n$. □

Lemma 3 (In [8], Proof of Theorem 1)**.** *Consider the system* (2.2) *with static input-output map $T(\cdot)$ as in* (2.5)*. The following equality holds*

$$T'(u) = -C_w A_w^{-1} B_w \tag{2.11}$$

where $C_w \triangleq \left.\frac{\partial h(x)}{\partial x}\right|_{x=S(w)}$, $A_w \triangleq \left.\frac{\partial f(x,u)}{\partial x}\right|_{(x,u)=(S(w),w)}$, and $B_w \triangleq \left.\frac{\partial f(x,u)}{\partial u}\right|_{(x,u)=(S(w),w)}$.

2.2 Identifying Steady-State Patterns

To identify nonhomogeneous steady-states, we use equitable graph partitions. For a weighted and undirected graph $\mathcal{G}(V, E)$ with scaled adjacency matrix M, a partition π of the vertex set V into classes $O_1, \dots, O_r$ is said to be *equitable* if there exist $\overline{m}_{ij}$, $i, j = 1, \dots, r$, such that

$$\sum_{v\in O_j} m_{uv} = \overline{m}_{ij} \quad \forall u \in O_i. \tag{2.12}$$

This definition is a modification of [55, Section 9.3] which considers a partition based on the weights of the graph $w_{i,j}$ instead of the scaled weights m_{ij} in (2.1). We let the *quotient matrix* $\overline{M} \in \mathbb{R}^{r\times r}$ be formed by the entries $\overline{m}_{ij}$, which is also a row-stochastic matrix and its eigenvalues are a subset of the eigenvalues of M, as can be shown with a slight modification of [55, Theorem 9.3.3]. As we will further discuss, equitable partitions are easy to identify in bipartite graphs and in graphs with symmetries.

We now search for nonhomogeneous solutions to (2.6) in which the entries corresponding to cells in the same class have the same value. This means that we examine the reduced set of equations

$$z = \overline{M}\mathbf{T}_r(z), \tag{2.13}$$

where $\overline{M}$ is the quotient matrix of the contact graph $\mathcal{G}$, and $z \in \mathbb{R}^r$. The patterns determined from the solutions of (2.13) are structured in such a way that all cells in the same class have the same fate, *i.e*,

$$u_i = z_j \text{ for all } i \in O_j. \tag{2.14}$$

Thus, an equitable partition defines a "template" for a pattern, and a steady-state consistent with this template exists if (2.13) has a nonhomogeneous solution. To determine if (2.13) has a nonhomogeneous solution, we define the *reduced graph* $\mathcal{G}_\pi$ to be a simple graph in which the vertex set is $\tilde{V} = \{O_1, \ldots, O_r\}$ and the edge set is

$$\tilde{E} = \{(O_i, O_j) : i \neq j,\ \overline{m}_{ij} \neq 0 \text{ or } \overline{m}_{ji} \neq 0\}. \tag{2.15}$$

Assumption 4. *The reduced graph $\mathcal{G}_\pi$ is bipartite.*

Note that, although $\overline{m}_{ii}$ may take nonzero values, we omit self-loops in the definition of $\mathcal{G}_\pi$; therefore, this assumption does not rule out self-loops in the quotient matrix. In the following theorem, we determine whether there exists a solution to the reduced set of equations (2.13) other than the homogeneous solution $z^* = u^*\mathbf{1}_r$.

Theorem 5. *Let π be an equitable partition of the vertices of $\mathcal{G}$ such that Assumption 4 holds. Let v_r be the eigenvector of $\overline{M}$ associated with the smallest eigenvalue $\overline{\lambda}_r$. If $T(\cdot)$ is positive, bounded, and decreasing, and if $T'(u^*)$ is such that*

$$|T'(u^*)|\overline{\lambda}_r < -1, \tag{2.16}$$

then there exists a solution of (2.13) *other than*

$$z^* = u^*\mathbf{1}_r. \tag{2.17}$$

Proof. Consider the auxiliary dynamical system:

$$\begin{bmatrix} \dot{z}_1 \\ \vdots \\ \dot{z}_r \end{bmatrix} = -\begin{bmatrix} z_1 \\ \vdots \\ z_r \end{bmatrix} + \overline{M}\begin{bmatrix} T(z_1) \\ \vdots \\ T(_{z_r}) \end{bmatrix} \triangleq F(z), \tag{2.18}$$

where $z \in \mathbb{R}^r_{\geq 0}$ lies in the positive orthant, since $\overline{M}$ is nonnegative and $T(\cdot)$ is a positive function. Note that around the homogeneous steady-state $z^* = \mathbf{T}_r(z^*)$, the Jacobian matrix

$$DF(z^*) = -I_r + T'(u^*)\overline{M} \tag{2.19}$$

is nonpositive (since $\overline{M}$ is nonnegative, and from (2.16), $T'(u^*) < 0$).

We show that under a coordinate transformation the auxiliary system in (2.18) is *cooperative*. The system is said to be cooperative if $\frac{\partial F_i(z)}{\partial z_j} \geq 0$ for $i \neq j$ and $z \in R^r$, see [92, Definition 3.1.3]. Cooperativity is a particular case of monotonicity with respect to the standard cone. Following the bipartite property of $\mathcal{G}_\pi$ in Assumption 4, we define a partition $J \subset \{1, \ldots, r\}$ and $J' = \{1, \ldots, r\} \backslash J$ such that no two vertices in the same set are adjacent. Let $\epsilon_j = 0$ if $j \in J$ and $\epsilon_j = 1$ if $j \in J'$, and choose the transformation Rz to be

$$R = \text{diag}((-1)^{\epsilon_1}, \ldots, (-1)^{\epsilon_j}, \ldots, (-1)^{\epsilon_r}). \tag{2.20}$$

Since the reduced graph is bipartite, $R^{-1}\overline{M}R = R\overline{M}R$ is a matrix similar to $\overline{M}$ and all of its off-diagonal elements are nonpositive. In the new coordinates Rz, the Jacobian matrix in (2.19) becomes $J \triangleq R(DF(z^*))R$ and has nonnegative off-diagonal elements. This means that the system is cooperative.

To prove the existence of a solution $\tilde{z} \neq z^*$ of (2.13), we will show: (i) that the largest real part of the eigenvalues of J (designated by $s(J)$) is positive with associated eigenvector $v \gg 0$ (*i.e.*, all elements are positive); and (ii) that the solutions of (2.18) are bounded. These two facts guarantee the existence of a steady-state $\tilde{z} \neq z^*$, because (i) implies that solutions that start at $z^* + \epsilon v$ for sufficiently small ϵ have a positive derivative and will be increasing with respect to the standard order [92, Theorem 4.3.3]. Combined with the boundedness property (ii), this implies that the solution converges to a steady-state $\tilde{z} \neq z^*$, *cf.* [92, Proposition 3.2.1]. We complete the proof by ascertaining (i) and (ii):

(i) Note that J is a quasi-positive and irreducible matrix (this is because the reduced graph is connected, and $T'(u^*) \neq 0$). Then, we conclude from a Corollary to the Perron-Frobenius Theorem for quasi-positive matrices [92, Corollary 4.3.2] that there exists an eigenvector $v \gg 0$ such that $Jv = s(J)v$. The eigenvalues of J are all real and given by

$$-1 + \overline{\lambda}_k T'(u^*), \ k = 1, \ldots, r, \tag{2.21}$$

where $\overline{\lambda}_k$ are the eigenvalues of $\overline{M}$. Therefore, $s(J) = -1 + T'(u^*)\overline{\lambda}_r$. From condition (2.16) we conclude that $s(J) > 0$ with positive eigenvector v, and that $v_r = Rv$ is an eigenvector of $\overline{M}$ associated with $\overline{\lambda}_r$ (*i.e.*, $\overline{M}Rv = \overline{\lambda}_r Rv$).

(ii) Since the transformed cooperative system is monotone with respect to the standard cone $R^r_{\geq 0}$, we conclude that $z^* + R^r_{\geq 0}$ and $z^* - R^r_{\geq 0}$ are forward invariant. Furthermore, since $T(\cdot)$ is bounded and decreasing (and $T(u^*) = u^*$), there exists an hypercube $[0, \overline{u}]^r$, with $0 < u^* < \overline{u}$ which is also forward invariant. This can be seen from the fact that at $z = 0$, $F(z) = \overline{M}T(0) \geq 0$, and at $z = \overline{u}$, $F(z) \leq 0$ (since $\overline{u} > T(\overline{u})$). The sets

$$S_1 = (z^* + R^r_{\geq 0}) \cap [0, \overline{u}]^r \text{ and } S_2 = (z^* - R^r_{\geq 0}) \cap [0, \overline{u}]^r, \tag{2.22}$$

are forward invariant. Therefore, we conclude from [92, Theorem 4.3.3], there exists an equilibrium point $\tilde{z} \neq z^*$, and it satisfies (2.13).

□

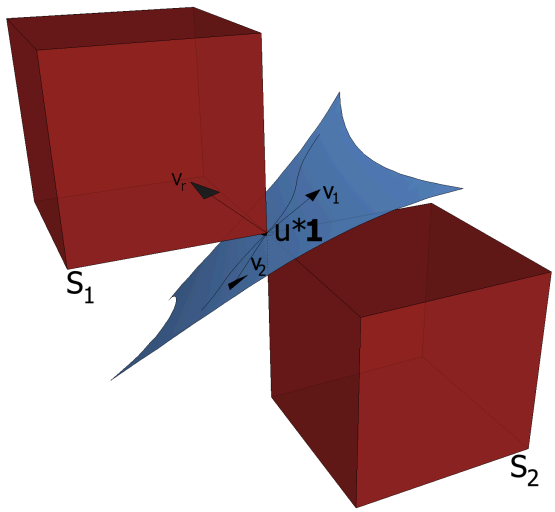

Figure 2.1: Graphical sketch of the proof. The red areas represent the forward invariant and bounded sets S_1 and S_2. Despite the fact that there might exist a stable manifold (blue) intersecting $u^*\mathbf{1}_r$, when condition (2.16) holds, the eigenvector v_r corresponding to the smallest eigenvalue of $\overline{M}$ (λ_r) lies inside S_1 and S_2. Since this also implies that the largest eigenvalue of J is positive, we conclude any trajectories starting at $u^*\mathbf{1}_r + \epsilon v_r$ for any $\epsilon > 0$, inside the cones, converge to $\tilde{z} \neq z^*$.

Remark 6. *Given the resemblance between the conditions* (2.9) *and* (2.16)*, one may ask when the two conditions coincide; that is, when the instability criterion for the HSS* (2.9) *also guarantees the existence of a nonhomogeneous steady-state pattern* (2.16)*. We see that* (2.9) *and* (2.16) *depend only on the smallest eigenvalue of* M *and* $\overline{M}$*, respectively. Furthermore, it is known that the eigenvalues of* $\overline{M}$ *are a subset of the eigenvalues of* M*, see [17]. Thus, the equivalence of conditions* (2.9) *and* (2.16) *depend on the eigenvalues that are preserved or lost in the reduction from* M *to* $\overline{M}$*. If the smallest eigenvalue of* M *is preserved, then* (2.9) *and* (2.16) *are identical. Otherwise, the range of* $T'(u^*)$ *in* (2.16) *is a strict subset of* (2.9)*.*

Example 1: Checkerboard Patterns in Bipartite Graphs

Suppose that the contact graph $\mathcal{G}$ is bipartite, and choose O_1 and O_2 to be the partition such that every edge can only connect a vertex in O_1 to a vertex in O_2. Then, up to vertex relabeling, the scaled adjacency matrix of $\mathcal{G}$ can be written as

$$M = \begin{bmatrix} 0 & M_{12} \\ M_{21} & 0 \end{bmatrix}. \tag{2.23}$$

Since the rows of M_{12} (and also rows of M_{21}) sum up to 1, we conclude that π, consisting of sets O_1 and O_2, is an equitable partition. Moreover, the reduced graph $\mathcal{G}_\pi$ is itself bipartite

(*i.e.*, Assumption 4 holds), and matrix $\overline{M}$ is given by

$$\overline{M} = \begin{bmatrix} 0 & 1 \\ 1 & 0 \end{bmatrix}. \tag{2.24}$$

Since the eigenvalues of $\overline{M}$ are $\overline{\lambda}_1 = 1$ and $\overline{\lambda}_2 = -1$, the next Corollary follows.

Corollary 7. *Let $\mathcal{G}$ be bipartite, and define a partition $O_1 \subset \{1, \ldots, N\}$ and $O_2 = \{1, \ldots, N\} \backslash O_1$ such that no two vertices in the same set are adjacent. Then, if*

$$|T'(u^*)| > 1, \tag{2.25}$$

there exists a steady-state $x = S(u)$ such that $u = [u_1 \ldots u_N]$ is a vector where $u_i = z_1$ if $i \in O_1$, $u_i = z_2$ if $i \in O_2$, and $z_1 \neq z_2 \neq u^*$.

The steady-state defined by Corollary 7 results in a "checkerboard" pattern as in Figure 2.3A, since it has distinct states for adjacent cells: $x_i = S(z_1) \quad if \quad i \in O_1$ and $x_i = S(z_2) \quad if \quad i \in O_2$. As discussed in Remark 6, since the smallest eigenvalue of M is preserved in $\overline{M}$, condition (2.25) coincides with (2.9). For bipartite graphs, the HSS loses stability where the checkerboard steady-state appears.

2.3 Graphs with Symmetries

An important class of equitable partitions results from graph symmetries, which are represented by graph automorphisms. For a weighted graph $\mathcal{G}(V, E)$, an *automorphism* is a permutation $g : V \to V$ such that if $(i, j) \in E$ then also $(gi, gj) \in E$ and $w_{i,j} = w_{gi,gj}$, where gi denotes the image of vertex i under permutation g. The set of all automorphisms of $\mathcal{G}$ forms a group designated by *automorphism group*, $Aut(\mathcal{G})$. A subset H of a full automorphism group $Aut(\mathcal{G})$ is called a *subgroup* if H is closed under composition and inverse.

Since any subgroup of the full automorphism group of a graph leads to an equitable partition, we conclude by Theorem 5 that any orbit partition generated by a subgroup of $Aut(\mathcal{G})$ is a candidate for a pattern structured according to this partition.

The computation of automorphism groups and the identification of the reduced order systems become cumbersome as the size and symmetries of the graphs increase. However, these can be obtained from computer algebra systems with emphasis on computational group theory, such as GAP [46].

Example 2: Two-Dimensional Mesh
Consider a two-dimensional mesh with wrap-arounds as in Figure 2.2. Since the graph is bipartite, an equitable partition is given by the two disjoint subsets of vertices $O_1 = \{1, 3, 6, 8, 9, 11, 14, 16\}$, and $O_2 = \{2, 4, 5, 7, 10, 12, 13, 15\}$. From Corollary 7, we conclude

that a pattern with final value u_1 for all cells in O_1, and u_2 for all cells in O_2, with $u_1 \neq u_2 \neq u^*$, is a steady-state of the network when $|T'(u^*)| > 1$; see Figure 2.3A.

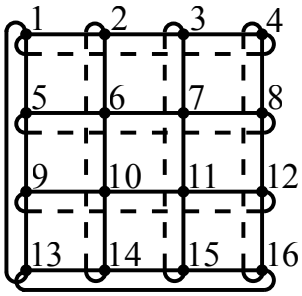

Figure 2.2: Graph representation for a two-dimensional mesh with wraparounds.

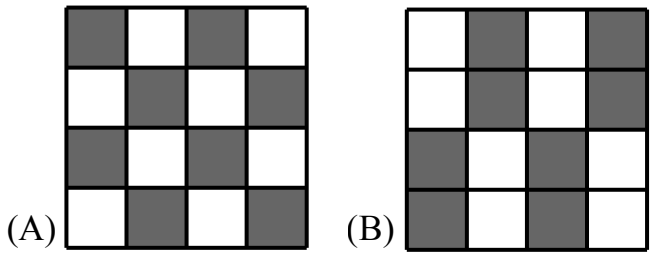

Figure 2.3: Steady-state patterns for the graph in Figure 2.2.

We next consider the automorphism subgroup that is generated by a combination of two cell rotations in the horizontal direction, one cell rotation in the vertical direction, and one cell rotation in both vertical and horizontal directions. This subgroup leads to the orbits $O_1 = \{1, 3, 5, 7, 10, 12, 14, 16\}$, $O_2 = \{2, 4, 6, 8, 9, 11, 13, 15\}$. The quotient matrix associated with this partition is given by

$$\overline{M}_B = \begin{bmatrix} \frac{1}{4} & \frac{3}{4} \\ \frac{3}{4} & \frac{1}{4} \end{bmatrix},$$

and has eigenvalues $-1/2$ and 1. Therefore, from Theorem 5, a nonhomogeneous steady-state given as in Figure 2.3B exists if $|T'(u^*)| > 2$.

In this example, we predict the existence of two steady-state patterns. We note that the HSS loses stability for the same parameter range (when $|T'(u^*)| > 1$) where the checkerboard steady-state in Figure 2.3A appears. As discussed in Remark 6, this is a result of the smallest eigenvalue of M being preserved in $\overline{M}$. However, the steady-state pattern in Figure 2.3B only appears for the parameter range $|T'(u^*)| > 2$, and this is due to the fact that $\lambda_N = -1$

is lost in $\overline{M}_B$ with this choice of equitable partition.

Since $|T'(u^*)|$ may be interpreted as the intensity of competition between neighboring cells, this example demonstrates that more intense competition can generate new steady-states with interesting patterns clustering among the cells. In fact, the dependence of condition (2.16) on $T'(u^*)$ provides a bifurcation parameter that guarantees the instability of the homogeneous steady-state and the existence of contrasting stead-state patterns.

Example 3: Two-dimensional Hexagonal Cyclic Lattice
The number of distinct equitable partitions in a hexagonal lattice of cells is considerably large [106]. We use the computational algebra algorithms in [46] to find all the possible two-level equitable partitions obtained by automorphism subgroups in a 6×6 cyclic lattice. Five distinct partitions, each with two classes, are plotted in Figure 2.4.

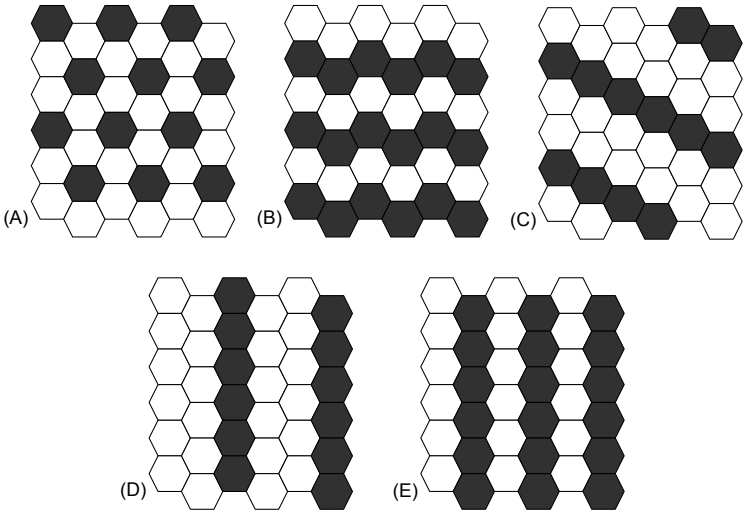

Figure 2.4: Five distinct partitions, each with two classes, in a 6×6 two-dimensional cyclic hexagonal lattice obtained by symmetries on the contact graph.

For these partitions, we have the following scaled adjacency matrices of the auxiliary systems:

$$\overline{M}_A = \begin{bmatrix} 0 & 1 \\ \frac{1}{2} & \frac{1}{2} \end{bmatrix}, \overline{M}_B = \begin{bmatrix} \frac{1}{3} & \frac{2}{3} \\ \frac{2}{3} & \frac{1}{3} \end{bmatrix}, \overline{M}_C = \begin{bmatrix} \frac{1}{3} & \frac{2}{3} \\ \frac{1}{3} & \frac{2}{3} \end{bmatrix},$$

and $\overline{M}_D = \overline{M}_C$, $\overline{M}_E = \overline{M}_B$. For each matrix we have the following smallest eigenvalue $\overline{\lambda}_A = -1/2$, $\overline{\lambda}_B = \overline{\lambda}_E = -1/3$, and $\overline{\lambda}_C = \overline{\lambda}_D = 0$. We thus conclude from Theorem 5 that the steady-state represented by pattern A in Figure 2.4 exists when $|T'(u^*)| > 2$, and patterns B, E are steady-states when $|T'(u^*)| > 3$. Theorem 5 is inconclusive for patterns C, D. The condition for instability of the HSS occurs as the condition for existence of pattern A is met ($|T'(u^*)| > 2$), while patterns B and E are only guaranteed to occur for a stricter parameter range, see Remark 6.

Example 4: Soccerball Pattern on a Buckminsterfullerene Graph
The next example addresses a larger graph, with 32 cells. It is motivated by the truncated icosahedron solid, also known as the *Buckminsterfullerene* [55], formed by 12 regular pentagonal faces, and 20 regular hexagonal faces, see Figure 2.5. In this case, we assume that each face is a vertex and that two vertices are connected if the corresponding faces have a common edge.

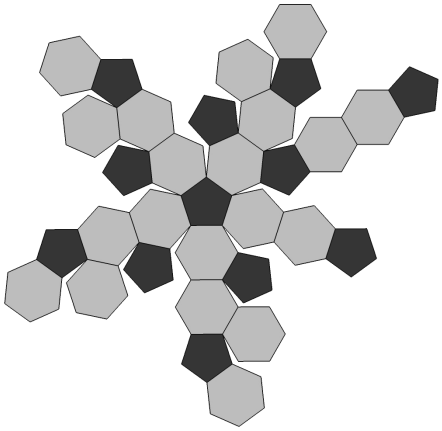

Figure 2.5: Cell network and soccerball pattern for the Buckminsterfullerene graph.

The full automorphism group leads to two orbits, one that consists of all the regular pentagon cells (O_P), and the second orbit encloses all the regular hexagon cells (O_H). The quotient matrix associated with the orbit partition is then

$$\overline{M} = \begin{bmatrix} 0 & 1 \\ 1/2 & 1/2 \end{bmatrix}. \tag{2.26}$$

This matrix has eigenvalues 1 and $-1/2$. Therefore, we conclude from Theorem 5, that a steady-state as in Figure 2.5 exists when $|T'(u^*)| > 2$. Note that this coincides with the instability condition for the HSS, see Remark 6.

Example 5: Nonbipartite and Nonsymmetric Equitable Partition
As discussed above, both bipartitions and automorphism subgroups (symmetries) lead to equitable partitions. However, these are not the only cases that lead to equitable partitions. Consider the graph in Figure 2.6 with partition $C_1 = \{3, 6\}$, and $C_2 = \{1, 2, 4, 5, 7, 8\}$. This partition is equitable, but it does not result from an automorphism subgroup (for instance, there is no automorphism exchanging vertices 1 and 4), and the graph is also not bipartite (due to the odd length cycles).
The quotient matrix is the same as in Example 4, we conclude that a two level steady-state pattern formed by cells C_1 and C_2 exists when $|T'(u^*)| > 2$.

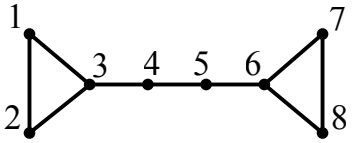

$$\overline{M} = \begin{bmatrix} 0 & 1 \\ 1/2 & 1/2 \end{bmatrix}$$

Figure 2.6: Example of an equitable partition that is neither bipartite nor a symmetry ($C_1 = \{3, 6\}$, $C_2 = \{1, 2, 4, 5, 7, 8\}$).

For a general network, it has been proven in [1] that the set of all equitable partitions, which is a lattice, can be determined from the network adjacency matrix.

2.4 Stability Analysis of Patterns

In the previous sections we discussed the existence of nonhomogeneous steady-states for the cell network (2.2)-(2.3). To qualify as viable patterns, these steady-states must be asymptotically stable. Determining stability for these steady-states may become a cumbersome task due to the nonlinearity and large order of the network of cells. To simplify this task, we decompose the system into an appropriate interconnection of lower order subsystems that arise from the structure of the equitable partition considered in the previous section.

Network Decomposition

Note that an equitable partition defines an invariant subspace for the full system (2.2)-(2.3) where $x_i = x_j$ for vertices i and j in the same class. Therefore, the steady-states identified using an equitable partition of the contact graph lie on the corresponding invariant subspace. For a partition of dimension r, $(O_1, \ldots, O_r)$, the reduced order dynamics on this subspace consists of r subsystems as defined in (2.2), coupled by $u = \overline{M}y$.
Let the steady-state be defined by

$$x_i = S(u_i),\ i = 1, \ldots, N \quad \text{with} \quad u_i = z_j \quad \text{if} \quad i \in O_j, \tag{2.27}$$

where $[z_1, \ldots, z_r]$ is a solution of (2.13). The linearization at this steady-state has the form

$$\dot{\tilde{x}} = (A + BMC)\tilde{x}, \tag{2.28}$$

where $A \in \mathbb{R}^{Nn \times Nn}$ is a block-diagonal matrix where the i-th block is equal to:

$$A_j \triangleq \frac{\partial f(x,u)}{\partial x}|_{(x_j,u_j)}, \quad \text{if} \quad i \in O_j. \tag{2.29}$$

In addition, $B \in \mathbb{R}^{Nn \times N}$ and $C \in \mathbb{R}^{N \times Nn}$ are block-diagonal matrices structured similarly to A, with $B_j = \frac{\partial f(x,u)}{\partial u}|_{(x_j,u_j)}$, and $C_j = \frac{\partial h(x)}{\partial x}|_{x_j}$.

To decompose (2.28) into two subsystems, we select a representative vertex V_i for each class O_i. The set of r representatives of each class defines the state of the subsystem on the invariant subspace. To see this, let Q be a matrix in $\mathbb{R}^{N\times r}$, where $q_{i,j} = 1$ if cell i is in class j, and $q_{i,j} = 0$ otherwise. Since the partition is equitable, we conclude that

$$MQ = Q\overline{M}. \tag{2.30}$$

Letting $T \triangleq [Q\ R]$ where R is a matrix in $\mathbb{R}^{N\times(N-r)}$ with columns that, together with those of Q, form a basis for $\mathbb{R}^N$, we conclude that there exist matrices U and P such that

$$M[\ Q\quad R\ ] = [\ Q\quad R\ ]\begin{bmatrix} \overline{M} & U \\ 0 & P \end{bmatrix} \triangleq T\tilde{M}. \tag{2.31}$$

The matrix T is invertible and, thus, defines a similarity transformation from M to $\tilde{M}$. Note that the upper left diagonal block of $\tilde{M}$ is the matrix $\overline{M}$, which describes the reduced order subsystem defined by the representative vertices.

Next, we study a particular choice of the matrix R that gives a meaningful variable representation to the transverse subspace dynamics. Let the columns of R be given by standard vectors e_i, defined as $e_{ij} = \delta_{ij}$, $j = 1,\ldots,N$; and further select the columns of R to be e_i, $i \in \{O_1\backslash V_1,\ldots,O_r\backslash V_r\}$, in such a way that if $i \in O_p\backslash V_p$, $j \in O_q\backslash V_q$, and $p < q$, then e_i is in a column before e_j, *i.e.*, the column with non-zero entry i is placed before the column with entry j if vertex i is in a class with smaller index than the class of vertex j.

For this choice of R, we conclude from [29, Section 5.3] that the change of variables

$$\hat{x} = (T^{-1}\otimes I_n)\tilde{x} \tag{2.32}$$

leads to the decomposition of the linearized dynamics into two subsystems: (i) an invariant subspace defined by the r representative cells of each class, *i.e*, V_i $i = 1,\ldots,r$; and (ii) a transverse subspace, that corresponds to the distance of each non-representative cell to its corresponding class representative. The new state variables are then,

$$\hat{x}_i = \begin{cases} \tilde{x}_{V_i}, & i = 1,\ldots,r \\ \tilde{x}_k - \tilde{x}_{V_j}, & i = r+1,\ldots,N \end{cases}, \text{ where } k \in O_j\backslash V_j. \tag{2.33}$$

Therefore, the linearized system is decomposed into the representative subsystem S_R and the transverse subsystem S_D,

$$S_R = \{A_R, B_R, C_R\} \text{ and } S_D = \{A_D, B_D, C_D\}, \tag{2.34}$$

where $A_R = \text{blkdiag}(A_1, A_2,\ldots,A_r)$, and A_D is also a block-diagonal matrix, with the remaining repeated entries of A being given by A_j in (2.29), and ordered by the index

$j = 1, \ldots, r$. A structure identical to A_R and A_D follows for B_R, B_D, and C_R, C_D. To see why the linearized system decomposes into S_R and S_D, note that

$$\dot{\tilde{x}} = (T^{-1} \otimes I_n)(A + BMC)(T \otimes I_n)\tilde{x} = (\tilde{A} + \tilde{B}\tilde{M}\tilde{C})\tilde{x}, \tag{2.35}$$

where

$$\begin{aligned} \tilde{A} &\triangleq T^{-1} \otimes I_n A T \otimes I_n \\ &\triangleq \mathrm{diag}(A_1, A_2, \ldots, A_r, A_1, \ldots \\ &\qquad \ldots, A_1, A_2, \ldots, A_2, \ldots, A_r, \ldots, A_r) \\ &\triangleq \mathrm{diag}(A_R, A_D), \end{aligned} \tag{2.36}$$

and $\tilde{B}$ and $\tilde{C}$ are defined analogously to $\tilde{A}$. This means that a necessary and sufficient condition for the asymptotic stability of (2.28) is the stability of the matrices

$$A_R + B_R\overline{M}C_R \quad \text{and} \quad A_D + B_D P C_D. \tag{2.37}$$

In a typical large-scale system, the matrix $A_R + B_R\overline{M}C_R$ is of low dimension but the size of $A_D + B_R P C_D$ may be prohibitively large.

A Small-Gain Criterion for Stability

In this section, we provide a small-gain type condition [105, 32] for stability. This condition is only sufficient, but it requires checking the spectral radius of a matrix whose dimension is the same as that of $\overline{M}$. Thus, it is easier to apply than checking stability of both matrices in (2.37).

Consider again the linearization introduced in (2.29). This describes a network with interconnection defined by $u = My$ and where each individual cell is given by the following linearized subsystem:

$$H_i : \left\{ \begin{array}{rcl} \dot{\tilde{x}}^i &=& A^i\tilde{x}^i + B^i\tilde{u}^i \\ \tilde{y}^i &=& C^i\tilde{x}^i \end{array} \right. , \tag{2.38}$$

where $A^i = A_j$, if $i \in O_j$ as in (2.29), and similarly for B^i and C^i, see Figure 2.7. Note that $H_i = H_j$ if $i, j \in O_k$. Recall that A^i is Hurwitz, and assume that each linearized subsystem H_i is observable [23].

Since subsystems in the same class have identical models, they have identical $\mathcal{L}_2$-gains. Let γ_i denote an $\mathcal{L}_2$-gain of each subsystem in class i, and let Γ be a diagonal matrix with entries

$$\{\Gamma\}_{jj} = \gamma_i \quad \text{for} \quad j \in O_i. \tag{2.39}$$

The following Lemma provides a small-gain criterion for the stability of the cell network around the steady-state pattern.

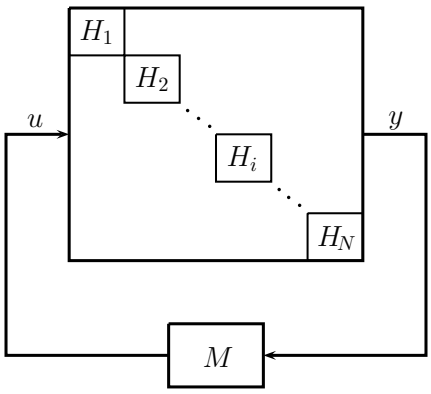

Figure 2.7: Linearized system interconnection with H_i, $i = 1, \ldots, N$ independent subsystem.

Lemma 8. *Consider the network* (2.2)-(2.3)*. The steady-state pattern defined by* (2.27) *is locally asymptotically stable if*

$$\rho(M\Gamma) < 1, \tag{2.40}$$

where Γ *is as in* (2.39)*, and* $\rho(\cdot)$ *represents the spectral radius.*

Proof. Since each linearized subsystem H_i, in (2.38), has bounded $\mathcal{L}_2$-gain, by the Bounded Real Lemma [34], we conclude that there exists a positive definite matrix Q_i such that, for $V_i(z) = z^\top Q_i z$, we have $\dot{V}_i(x^i, u^i) \leq \gamma_i^2 u^{iT} u^i - y^{iT} y^i$. Let $D = \text{diag}(d_1, \ldots, d_n)$, where d_i is some positive constant, and let $V(x) = \sum_i d_i V_i$. We then obtain,

$$\begin{aligned} \dot{V}(x) = \sum_i d_i \dot{V}_i(x^i, u^i) &\leq u^\top D\Gamma^2 u - y^\top D y \\ &= y^\top ((\Gamma M)^\top D(\Gamma M) - D) y, \end{aligned} \tag{2.41}$$

where $u = [(u^1)^\top \ldots (u^N)^\top]^\top$, $y = [(y^1)^\top \ldots (y^N)^\top]^\top$, and the second equality follows from the fact that $u = My$. From inequality (2.41), we conclude that the steady-state (2.27) is stable if there exists a positive diagonal matrix D such that $D - (\Gamma M)^\top D(\Gamma M)$ is positive definite. This is equivalent to the condition that $I - \Gamma M$ be a M-matrix, see [7, Theorem 2]. Therefore, since the spectra of $M\Gamma$ is the same as ΓM, and since assumption (2.40) implies that $I - \Gamma M$ is a nonsingular M-matrix, see [14, Definition 6.1.2], we conclude stability of the interconnection.

Finally, since $\dot{V}(x)$ is negative semidefinite, we conclude from LaSalle's Invariance Principle [64] and from properties of linear systems ([90]), that every trajectory converges to the unobservable subspace of the system. Furthermore, under the same assumption, and since each H_i is observable, we conclude that each trajectory must converge to the singleton $\{0\}$. Thus, the steady-state (2.27) is locally asymptotically stable. □

We now show that (2.40) is equivalent to $\rho(\overline{M}\,\overline{\Gamma}) < 1$, where

$$\overline{\Gamma} = \text{diag}(\gamma_1, \ldots, \gamma_r). \tag{2.42}$$

This result simplifies the verification of this small-gain stability condition to the reduced system S_R in (2.34) with interconnection matrix $\overline{M}$.

Lemma 9. *Consider an equitable partition π of $\mathcal{G}$. Then,*

$$\rho(\overline{M}\,\overline{\Gamma}) = \rho(M\Gamma), \tag{2.43}$$

where $\overline{M}$ is as in (2.12)*, and $\overline{\Gamma}$ is as in* (2.42)*.*

Proof. First, note that $\overline{M}\,\overline{\Gamma}$ is a nonnegative irreducible matrix. Thus, by the Perron-Frobenius Theorem [14], we conclude that $r = \rho(\overline{M}\,\overline{\Gamma}) > 0$ is an eigenvalue of $\overline{M}\,\overline{\Gamma}$ with corresponding eigenvector $\overline{v} \gg 0$.
Claim: $r > 0$ is also an eigenvalue of $M\Gamma$ with corresponding eigenvector v such that entries $v_i = \overline{v}_j$ if $i \in O_j$.
According to this claim, we conclude that v is a positive eigenvector. Therefore, by appealing again to the Perron-Frobenius Theorem, and since $M\Gamma$ is also a nonnegative irreducible matrix, we conclude that v has to be the eigenvector associated with eigenvalue $r = \rho(M\Gamma)$.

To prove the claim, note that matrix Γ is positive diagonal with repeated entries for vertices in the same class. Therefore, since the vertex partition is equitable for the scaled adjacency graph M, then it is also equitable when we consider a modified adjacency graph $M\Gamma$, *i.e.*,

$$\sum_{v \in O_j} p_{uv}\gamma_{jj} = \overline{p}_{ij}\gamma_{jj} \quad \forall u \in O_i, \tag{2.44}$$

where $\overline{p}_{ij}$ is as defined in (2.12). From this observation we see that this claim is a generalization of the Lifting Proposition in [17], which holds not only for partitions obtained through an automorphism subgroup but also for any equitable partition. The proof of the claim follows similarly to the proof of the Lifting Proposition, with matrices $M\Gamma$ and $\overline{M}\,\overline{\Gamma}$ as in (2.44). □

Combining Lemma 8 and Lemma 9 we obtain the following stability condition.

Theorem 10. *Consider the network* (2.2)-(2.3)*. The steady-state pattern defined by* (2.27) *is locally asymptotically stable if*

$$\rho(\overline{M}\,\overline{\Gamma}) < 1. \tag{2.45}$$

Special Case: Bipartite Graph

Consider the special case of a bipartite graph, with a partition π consisting of two classes, chosen so that no two vertices in the same set are adjacent. As discussed in Example 1, the quotient matrix $\overline{M}$ is given by

$$\overline{M} = \begin{bmatrix} 0 & 1 \\ 1 & 0 \end{bmatrix}. \tag{2.46}$$

Therefore, the eigenvalues of $\overline{M}\,\overline{\Gamma}$ are $\pm\sqrt{\gamma_1\gamma_2}$. The next result follows trivially from Theorem 10.

Corollary 11. *Assume that the contact graph $\mathcal{G}$ of the cell network (2.2)-(2.3) is bipartite, and that there exists a steady-state $u \in R^N$ such that $u_i = z_1$ if $i \in O_1$ and $u_i = z_2$ if $i \in O_2$, with $z_1 \neq z_2 \neq z^*$, as in Corollary 7. This steady-state solution is locally asymptotically stable if*

$$\gamma_1\gamma_2 < 1, \tag{2.47}$$

where γ_1 and γ_2 are $\mathcal{L}_2$-gains of the linearized subsystems around z_1 and z_2, respectively.

In the particular case where the $\mathcal{L}_2$-gain is identical to the dc-gain:

$$\gamma_i = -C^i(A^i)^{-1}B^i = -T'(z_i), \tag{2.48}$$

the local asymptotic stability condition in (2.47) reduces to

$$T'(z_1)T'(z_2) < 1. \tag{2.49}$$

The $\mathcal{L}_2$-gain is indeed equal to the dc-gain when each subsystem (2.2) is input-output monotone [3], as assumed in [8]. We have thus recovered Theorem 2 in [8] which used the condition (2.49) to prove the existence of stable checkerboard patterns. Unlike the proof in [8], which relies heavily on monotonicity properties, here we have made the less restrictive assumption that the $\mathcal{L}_2$-gain be equal to the dc-gain.

Remark 12. *Several results discussed in [26] for the Delta-Notch lateral inhibition model are recovered in this chapter. In particular, that the HSS is unstable when the inhibition mechanism is sufficiently strong (condition (2.9)), and that the instability of HSS for patterns with two distinct levels implies the existence of pairs of inhomogeneous steady-states, since condition (2.16) is identical for a pattern with opposite high/low cell output. Our results study pattern motifs that form equitable partitions, and therefore, are consistent with the patterning rule that low level cells cannot be completely surrounded by other low level cells. On the other hand, the pattern in Figure 2.3B conflicts with the patterning rule that no two high notch cells lie next to each other. We have found a set of parameters for the Delta-Notch model (Example 6 below), where such pattern is stable. However, only very few simulations can converge to such pattern, specially if starting close to the HSS. We believe its region of convergence to be fairly small compared to the "checkerboard" pattern, and thus the reason why such patterns had not been found through simulation.*

2.5 Noise Driven Patterning

In the previous sections, we provided sufficient conditions for the instability of the homogeneous steady-state and the emergence of patterned steady-states. We now focus on the case where the HSS is locally asymptotically stable, but where the persistence of noise can

generate spatial patterns. This means that noise can enhance the parameter regime where patterns emerge. A similar situation was observed for Turing patterns [15, 22, 60]. Following [60], we will use tools from robust control, namely, an $\mathcal{H}_2$-norm analysis (see [115]), to characterize the sensitivity of each spatial mode to noise. We show with an example that the highest frequency spatial mode (associated with the smallest eigenvalue of the interconnection M) is more sensitive to noise and, thus, predominant in stochastic simulations, when the HSS is on the verge of instability.

We now consider a stochastic differential equation (SDE) of the linearization of system (2.2)-(2.3) representing the state variations around the HSS, x^*:

$$\left\{ \begin{array}{rcl} d\tilde{x}_i &=& A^*\tilde{x}_i dt + B^*\tilde{u}_i dt + G^* dw_i \\ \tilde{y}_i &=& C^*\tilde{x}_i \end{array} \right. \tag{2.50}$$

where $G^* \in \mathbb{R}^{n\times r}$, $w^i(t)$ is an $r-$dimensional independent standard Wiener process; and where A^* is given by

$$A^* = \frac{\partial f(x,u)}{\partial x}|_{(x^*,u^*)}. \tag{2.51}$$

Similarly, $B^* = \frac{\partial f(x,u)}{\partial u}|_{(x^*,u^*)}$, and $C^* = \frac{\partial h(x)}{\partial x}|_{x^*}$.

When considering systems representing biochemical reactions, r will typically be the number of reactions in each cell, and the linearized system represents a linear approximation of the system's variation around the equilibrium point defined by HSS [63, 60]. The full interconnection of the linearization is the following,

$$d\tilde{x} = (I_N \otimes A^* + M \otimes B^*C^*)\,\tilde{x}dt + (I_N \otimes G^*)dw. \tag{2.52}$$

We apply a change of coordinates that decomposes the system into N independent problems, each of dimension n,

$$\hat{x} = (V^{-1} \otimes I_n)\tilde{x}, \tag{2.53}$$

where the columns of matrix V are the eigenvectors of the adjacency matrix M, i.e. vectors $\{v_1, \ldots, v_N\}$ associated with $\lambda_1, \ldots, \lambda_N$. The full system decomposes into N spatial modes governed by:

$$d\hat{x}_k = (A^* + \lambda_k B^*C^*)\hat{x}_k dt + G^* d\hat{w}, \quad k = 1, \ldots, N, \tag{2.54}$$

where $\hat{x}_k \in \mathbb{R}^n$. Unlike $\tilde{x}_i$, which represents a vector of concentrations in cell i, $\tilde{x}_k$ represents an aggregate concentration vector for spatial mode k. The $\mathcal{H}_2$-norm for each of these independent SDE modes is given by the covariance of the linearized state, *i.e.*, $Q_k \triangleq \mathbb{E}\left[\hat{x}_k\hat{x}_k^\top\right] \in \mathbb{R}^{n\times n}$, which is the positive semidefinite solution of the following Lyapunov equation [47],

$$(A^* + \lambda_k B^*C^*)Q_k + Q_k(A^* + \lambda_k B^*C^*)^\top + G^*(G^*)^\top = 0. \tag{2.55}$$

The $\mathcal{H}_2$-norm is then defined by

$$\mu_k \triangleq Tr\{\overline{C}Q_k\overline{C}^\top\} \tag{2.56}$$

where $\overline{C}$ is chosen such that $\overline{C}\tilde{x}_i$ is the concentration of interest to be designated as the output. Given this decomposition, the covariance of each mode Q_k provides the $\mathcal{H}_2$-norm of each spatial mode. This norm can be interpreted as the sensitivity of each spatial mode to noise.

Example 6: Delta-Notch Lateral Inhibition in a Ring of Cells
We consider the Notch pathway, where Delta and Notch are trans-membrane proteins that allow cell-to-cell signaling. In this mechanism, Delta ligands in one cell will bind to Notch receptors in a neighboring cell and trans-activate them. This leads to the release of the Notch intracellular domain, which in turn inhibits the production of Delta in the same cell [26]. The following dynamical system describes such behavior:

$$\left\{ \begin{array}{rcl} \dot{x}_1^i &=& -\gamma_1 x_1^i + g_1(x_2^i) \\ \dot{x}_2^i &=& -\gamma_2 x_2^i + g_2(\langle x_1^j \rangle_i) \end{array} \right. , \tag{2.57}$$

where $\langle \cdot \rangle_i$ denotes the average over all the output of all cells adjacent to i, and

$$g_1(s) = \frac{b}{1+s^r}, \quad g_2(s) = \frac{as^p}{1+s^p},$$

with $\gamma_1 > 0$, $\gamma_2 > 0$, $a > 0$, $b > 0$, $r > 0$, $p > 0$. The states x_1^i and x_2^i in each cell $i = 1, \ldots, N$ represent the concentrations of Delta, and the intracellular domain of Notch, respectively. Parameter γ_j represents the degradation rate of the corresponding species, the decreasing property of $g_1(\cdot)$ represents the inhibition of Delta production by the intracellular domain of Notch, and the increasing property of $g_2(\cdot)$ represents the trans-activation of intracellular Notch due to Delta. In this example, we consider an N-cell cycle. Thus, the neighboring cells of cell i, are the ones with index $mod(i-1, N)$ and $mod(i+1, N)$.

Note that this dynamical system can be written in same form as (2.2)-(2.3):

$$\left\{ \begin{array}{rcll} \dot{x}_1^i &=& -\gamma_1 x_1^i + \frac{b}{1+(x_2^i)^r} & \\ \dot{x}_2^i &=& -\gamma_2 x_2^i + \frac{a(u^i)^p}{1+(u^i)^p} & i = 1, \ldots, 16, \\ y^i &=& x_1^i & \end{array} \right. \tag{2.58}$$

where the interconnection is defined by (2.3), with M being the scaled adjacency matrix for the 16-node cyclic graph (and with $w_{i,j} = 1$ if cells i and j are adjacent in the cycle). The linearization of (2.58) at the HSS yields:

$$A^* = \begin{bmatrix} -\gamma_1 & -\frac{rb(x_2^*)^{r-1}}{(1+(x_2^*)^r)^2} \\ 0 & -\gamma_2 \end{bmatrix} \quad B^* = \begin{bmatrix} 0 \\ \frac{ap(x_1^*)^p}{(1+(x_1^*)^p)^2} \end{bmatrix}, \tag{2.59}$$

and $C^* = [1\ 0]$. Finally, we choose the noise term G^* to be:

$$G^* = \begin{bmatrix} -\gamma_1 x_1^* & \frac{b}{1+(x_2^*)^r} & 0 & 0 \\ 0 & 0 & -\gamma_2 x_2^* & \frac{ax_1^*}{1+(x_1^*)^p} \end{bmatrix}, \tag{2.60}$$

whose structure is motivated by the Chemical Langevin Equation approximation, [54, 65]. In this example, $G^*(G^*)^\top$, is a 2-by-2 diagonal matrix. Since we are considering the output of each cell to be x_1^i, consider $\overline{C} = [1\ 0]$. Therefore, to calculate the $\mathcal{H}_2$-norm of each spatial mode we need to solve (2.55) for $\{Q_k\}$, $k = 1, \ldots, N$. We choose the parameters to be $\gamma_1 = \gamma_2 = 1$, $a = 8$, $b = 2.1$, $p = 2$, and $r = 1$. By doing so, we have $T'(u^*) = -0.9931$. For such parameters, it can be calculated that the HSS is stable, and that the steady steady is very close to instability (*cf.* (2.9)).

Modes	1	2/3	4/5	6/7	8/9	10/11	12/13	14/15	16
λ_k	-1	-0.9239	-0.7071	-0.3827	0	0.3827	0.7071	0.9239	1
μ_k	53.9812	4.834	1.5697	0.9192	0.6907	0.5880	0.5369	0.5123	0.5049

Table 2.1: $\mathcal{H}_2$-Norm μ_k for each spatial mode $k = 1, \ldots, N$.

The results for $\mathcal{H}_2$ under such parameters are in Table (2.1). We note that the norm is much larger for Mode 1, for which the associated eigenvector is composed of alternating $\{+1, -1\}$ entries, related to a checkerboard (or on-off) pattern. Indeed, in Figure 2.8 (Left), we see that under noise, a nonstationary on-off wave is persistent along the horizontal axis (individual cells), as we progress in time (vertical axis). Figure 2.8 (Right) shows a stochastic simulation for a larger ring of cells, where it is easier to see a striped on-off pattern.

In this particular case, we see that the on-off patterns arising from the stochastic simulations are nonstationary, unlike what is expected in the deterministic case (with the instability of the HSS). The reason why these nonstationary patterns arise is due to the fact that both on-off or off-on pattern can occur in this interconnection, and the initial conditions determine to which one the system converges. The noise introduces a persistent change in the system's state, thus forcing the pattern to shift along the cell cycle.

2.6 Conclusions

In this chapter we presented analytical results to predict steady-state patterns for large-scale lateral inhibition systems, independent of network size. We have shown that equitable partitions provide templates for steady-state pattern candidates, as they identify invariant subspaces where the fate of cells in the same class is identical. We proved the existence of steady-state patterns by relying only on the static input-output model of each cell and the algebraic properties of the contact graph. One limitation in these results is the assumption that the reduced graph is bipartite. This assumption is not overly restrictive, since it holds, for instance, in the study of two-level steady-state patterns. Nevertheless, the generalization to a larger class of graph partitions that do not necessarily result in bipartite reduced graphs needs to be considered. Since this assumption was made to be able to identify an orthant as the positivity cone, a possible relaxation would be to investigate monotonicity with respect

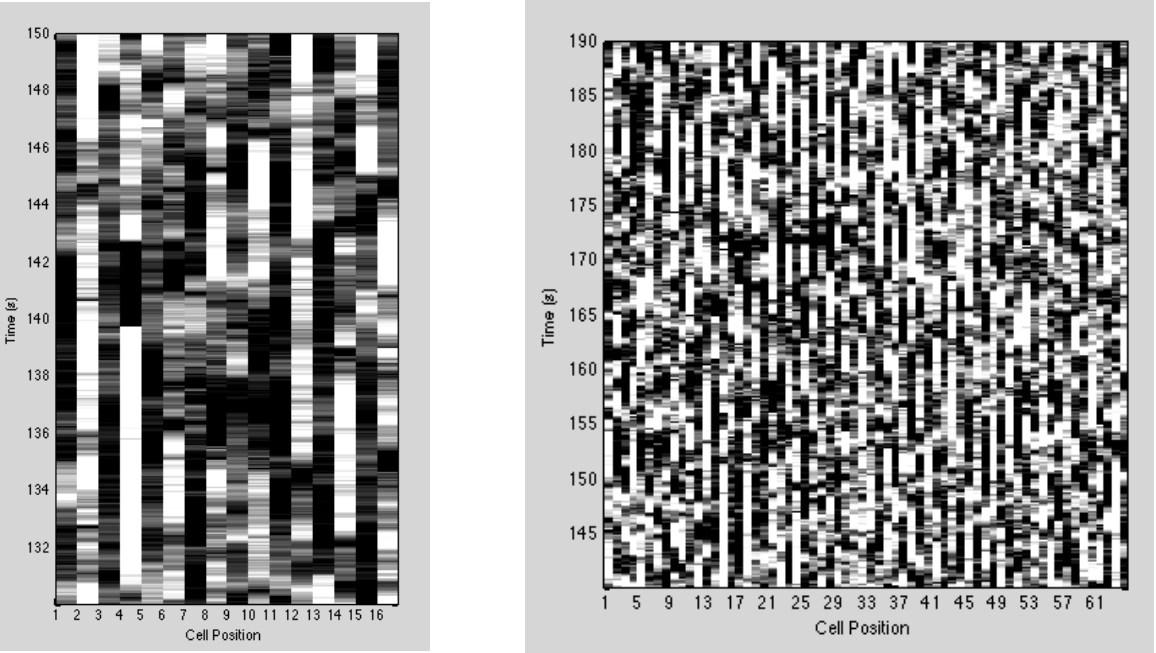

Figure 2.8: Stochastic simulation of Delta-Notch in a cyclic interconnection, where each cell behavior is governed by (2.50). Cell output results over time. (Left) 16-cell cycle; (Right) 64-cell cycle.

to other cones. The proposed procedure assumes a single-input single-output model for each cell. However, there exists evidence that cell-to-cell contact inhibition mechanisms may depend on more than a single species, [97]. Several results can be extended to multiple-input multiple-output cells by including further monotonicity assumptions in the dynamics of each cell.

We have analyzed the stability of steady-state patterns by providing a decomposition into a representative subsystem S_R and a transverse subsystem S_D. We provided a small-gain stability type criterion, which relies only on the reduced order subsystem S_R to guarantee stability of the steady-state patterns. A critical topic for further work in the stability analysis of these patterns is to provide a better characterization of their domains of attraction. As discussed in Section 2.4, we found analytical conditions that guarantee convergence of such steady-state patterns with neighboring high notch cells, contrary to the rule obtained from simulation in [26]. However, we suspect that their regions of attraction are fairly small and potentially not intersecting the neighborhood of the HSS.

Finally, we discussed how the parameter regime where patterns emerge can be enhanced by noise. We connected such results with the $\mathcal{H}_2$-norm of decomposed modes, which allowed the prediction of predominant spatial modes.

One practical limitation of the model introduced in this chapter is the assumption that the contact graph is constant, and thus it does not account for the mobility of cellular organisms, nor for the continuous growth and division of cells. There are, however, several applications where this assumption might still be acceptable: In developmental biology, there are certain developmental phases that involve long periods between cell divisions [51]; In synthetic biology, it is possible to inhibit cell growth without affecting transcription or translation [89], and there are also methods to guarantee the immobilization of cells [112]. Regardless of that, it is imperative to investigate the robustness of the patterning behavior with respect to changes in the contact graph.

Chapter 3

Compartmental Lateral Inhibition Systems

Multicellular developmental processes rely on spatial patterning to initiate differentiation [51, 111]. Commonly-studied methods of pattern formation include diffusion-driven instability [101, 78, 61], gradient or density detection [12, 72], locally-synchronized oscillators [30], and lateral inhibition [68, 26, 96]. Lateral inhibition is a mechanism where cell-to-cell signaling induces neighboring cells to compete and diverge into sharply contrasting fates, enabling developmental processes such as segmentation or boundary formation [79]. The best-known example of lateral inhibition is the Notch pathway in Metazoans where membrane bound Delta ligands bind to the Notch receptors on the neighboring cells. This binding releases the Notch intracellular domain in the neighbors, which then inhibits their Delta ligand production [85, 26, 97, 8]. Recent discoveries have shown that lateral inhibition is not limited to complex organisms: a contact-dependent inhibition (CDI) system has been identified in *E. coli* where delivery via membrane-bound proteins of the C-terminus of the gene *cdiA* causes down regulation of metabolism [6, 5, 108]. Despite the vigorous research on elucidating natural pathways such as Notch and CDI, a *synthetic* lateral inhibition system for pattern formation has not been developed.

In this chapter, we propose a *compartmental* lateral inhibition system that is able to spontaneously generate contrasting patterns between neighboring compartments. Our system consists of a set of compartments interconnected by channels as in Figure 3.1. In each compartment, we place a colony of cells that produce diffusible molecules to be detected by the neighboring colonies. We equip each cell with an inhibitory circuit that reacts to the detected signal, *i.e.*, the more diffusible molecules are detected in one compartment, the less production in that colony. To prevent auto-inhibition, we use two orthogonal diffusible quorum sensing pairs [27] and design two inhibitory circuits each of which detects only one type of molecule and produces the other type. In the examples of Figure 3.1, cells of type A produce a diffusible molecule X that is only detectable by cells of type B, and cells of type B produce a diffusible molecule Y which is only detectable by A.

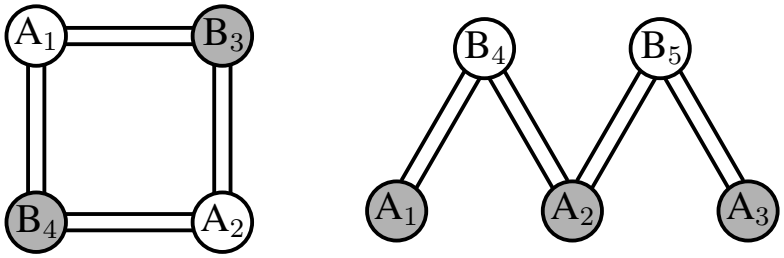

Figure 3.1: Compartmental lateral inhibition systems with cells of type A and B, where contrasting patterns between neighboring compartments emerge. In each compartment A_i (B_i) we place a colony with cells of type A (B) that communicate through channels. Each cell type can only detect signaling molecules produced by the other type, preventing auto-inhibition.

To derive conditions under which this system will exhibit contrasting patterns, we define the cell network as a graph where each compartment corresponds to a vertex. The diffusion of molecules between two compartments occurs through the channels and is represented by the graph edges. We model the diffusion with a compartmental model, and represent the compartment-to-compartment communication by the Laplacian matrix of the weighted graph. The edge weights depend on the distance between the compartments and the diffusivity of the quorum sensing molecules. We then use the graph-theoretic notion of *equitable partition* to ascertain the existence of contrasting steady-state patterns. Equitable partitions reduce the steady-state analysis to finding the fixed points of a scalar map, and each fixed point represents a steady-state where all the compartments of the same type have the same final value. We also show that the slope of the scalar map at each fixed point provides a stability condition for the respective steady-states. Finally, we propose and model a synthetic circuit with cells of type A and B, which is currently under implementation, and apply our analysis to show that it is capable of patterning.

In Chapter 2, we have used graph theoretical results to analytically determine patterning by lateral inhibition using a contact inhibition model for networks of identical cells. In this chapter, we analyze a diffusion model that allows two cell types which is critical for avoiding auto-inhibition. The notion of *equitable partition* is equivalent in both chapters. In the former it is defined in terms of the adjacency matrix of the contact graph, while in the latter, it is based on the Laplacian matrix defined by the channel topology.

Reaction-diffusion mechanisms have been widely used in the past to achieve spatial pattern generation with synthetic systems; mostly relying on one-way communication achieved through either the external spatiotemporal manipulation of the cell's chemical environment [25, 93, 74], the precise positioning of cells containing different gene networks which secrete

or respond to diffusible signals [12, 13], or the interplay between cell growth and gene expression [86]. A two-way communication mechanism using orthogonal quorum sensing systems has been employed to demonstrate a predator-prey system in [11]. Unlike these results, this chapter achieves spatial patterning by lateral inhibition by using orthogonal quorum sensing systems and by positioning colonies of cells inside compartments that are connected by channels.

In Section 3.1 we define the model for the proposed compartmental system and demonstrate how equitability allows to determine the existence of contrasting steady-state patterns. Under equitability and monotonicity assumptions, we derive a scalar condition for stability of such steady-state patterns, in Section 3.2. Finally, in Section 3.3, we propose a synthetic lateral inhibition circuit and analyze its patterning behavior.

3.1 An Analytical Test for Patterning

Composing a Compartmental Lateral Inhibition Model

We propose a network of N_A compartments of type A and N_B compartments of type B that communicate through diffusible molecules. Each cell of type A produces diffusible species X, and only cells of type B are equipped with a receiver species that binds to X and forms a receiver complex. Similarly, the diffusible species Y is produced by cells of type B and detected by cells of type A. We represent the dynamics in each cell type with three modules: the transmitter module where species X (or Y) is produced and released; the receiver module where Y (or X) is detected, and an inhibitory module which inhibits the transmitter activity in the presence of the receiver complex.

To facilitate the analysis, we separate the transmitter module of A and receiver module of B, and merge them into a "transceiver" block for the diffusible species X, which also includes the diffusion process. Similarly, the transceiver block of Y is composed by the transmitter module of B and the receiver module of A. The cell network is represented in Figure 3.2. Each compartment is represented with a block labeled H_A or H_B, corresponding to the inhibitory circuit of types A and B, respectively. The concentration of the autoinducer synthase for the production of X (respectively, Y) is denoted by y_A (y_B), and R_A (R_B) is the concentration of the receiver complex, the result of Y (X) binding to the receiver protein.

The transceiver blocks incorporate diffusion in an ordinary differential equation compartmental model that describes the concentrations of the diffusible species at each compartment. We define an undirected graph $\mathcal{G} = \mathcal{G}(V, E)$ where each element of the set of vertices V represents one compartment, and each edge $(i, j) \in E$ represents a channel between compartments i and j. For each edge $(i, j) \in E$ we define a weight $d_{ij} = d_{ji}$ (and $d_{ij} = 0$ if compartments i and j are not connected). The constant d_{ij} is proportional to the diffusivity of the species

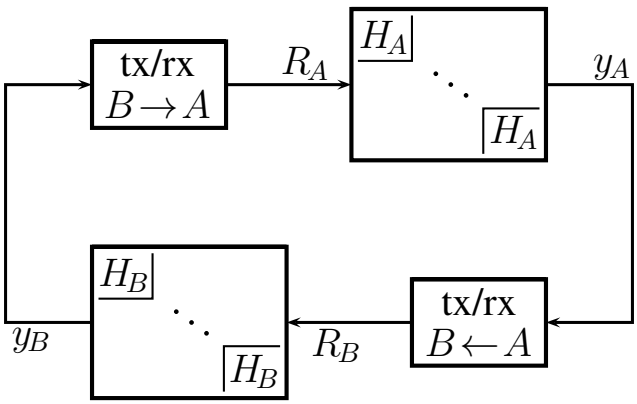

Figure 3.2: Cell network with two types of compartments A and B communicating through diffusion. For each type of diffusible species, the transceiver includes the dynamics of the senders' transmitter modules, the receivers' detection modules, and the diffusion process.

and inversely proportional to the square of the distance between compartments i and j. We define the weighted Laplacian of the graph to be:

$$\{L\}_{ij} = \begin{cases} -\sum_{j=1}^{N} d_{ij} & \text{if } i = j \\ d_{ij} & \text{if } i \neq j. \end{cases} \tag{3.1}$$

The dynamical model of the transceiver tx/rx for X is then represented by:

$$\text{tx/rx}_{A\to B} : \begin{cases} \begin{bmatrix} \dot{X}_A \\ \dot{X}_B \end{bmatrix} &= \begin{bmatrix} \Gamma_X(X_A, y_A) \\ \Phi_X(X_B, R_B) \end{bmatrix} + L \begin{bmatrix} X_A \\ X_B \end{bmatrix} \\ \dot{R}_B &= \Psi_X(X_B, R_B), \end{cases} \tag{3.2}$$

where $X_A \in \mathbb{R}^{N_A}_{\geq 0}$ represents the concentration of species X in compartments A due to production, $X_B \in \mathbb{R}^{N_B}_{\geq 0}$ the concentration of species X at compartment B due to diffusion, and $R_B \in \mathbb{R}^{N_B}_{\geq 0}$ the concentration of complexes at compartment B formed by the binding of species X with a receiver molecule. The functions $\Gamma_X(\cdot,\cdot) \in \mathbb{R}^{N_A}_{\geq 0}$, $\Phi_X(\cdot,\cdot) \in \mathbb{R}^{N_B}_{\geq 0}$, and $\Psi_X(\cdot,\cdot) \in \mathbb{R}^{N_B}_{\geq 0}$ are concatenations of the decoupled elements $\gamma^i_X(X^i_A, u^i) \in \mathbb{R}_{\geq 0}$, $i = 1, ..., N_A$, $\phi^j_X(X^j_B, R^j_B) \in \mathbb{R}_{\geq 0}$ and $\psi^j_X(X^j_B, R^j_B) \in \mathbb{R}_{\geq 0}$, $j = 1, ..., N_B$, and assumed to be continuously differentiable. The function $\gamma^i_X(\cdot,\cdot)$ models the production and the degradation of X in compartment i of type A, the function $\phi^j_X(\cdot,\cdot)$ models the degradation of X and the binding of X with the receiver protein in compartment j of type B, and $\psi^j_X(\cdot,\cdot)$ models the binding of the receiver complex in compartment j of type B. The transceiver $\text{tx/rx}_{B\to A}$ for Y is defined similarly, by changing X to Y and switching indices A with B in (3.2).

Assumption 13. *For each constant input $y^*_A \in \mathbb{R}^{N_A}_{\geq 0}$ (and $y^*_B \in \mathbb{R}^{N_B}_{\geq 0}$), the system* (3.2) *has a globally asymptotically stable steady-state (X^*_A, X^*_B, R^*_B), which is a hyperbolic equilibrium,*

i.e., the Jacobian has no eigenvalues on the imaginary axis. Furthermore, there exist positive and increasing functions $T_{AB}^{tx/rx}:\mathbb{R}_{\geq 0}^{N_A}\to\mathbb{R}_{\geq 0}^{N_B}$ *and* $T_{BA}^{tx/rx}:\mathbb{R}_{\geq 0}^{N_B}\to\mathbb{R}_{\geq 0}^{N_A}$ *such that*

$$R_B^* \triangleq T_{AB}^{tx/rx}(y_A^*), \qquad \text{and} \qquad R_A^* \triangleq T_{BA}^{tx/rx}(y_B^*). \tag{3.3}$$

The increasing property of these maps is meaningful, since a higher input of the autoinducer synthase leads to more production and, thus, more detection on the receiver side.

Next, we represent the blocks H_k^i, $i=1,...,N$ of type $k\in\{A,B\}$ with models of the form:

$$H_k^i:\left\{\begin{array}{rcl}\dot{x}_i &=& f_k(x_i,u_i)\\ y_i &=& h_k(x_i),\end{array}\right. \tag{3.4}$$

where $x_i\in\mathbb{R}_{\geq 0}^n$ describes the vector of reactant concentrations in compartment i, $y_i\in\mathbb{R}_{\geq 0}$ is the output of compartment i (in this context, the concentration of an autoinducer synthase), and $u_i\in\mathbb{R}_{\geq 0}$ is the input of compartment i (the concentration of the receiver complex). We denote $x_k=[x_1^\top,...,x_{N_k}^\top]^\top\in\mathbb{R}_{\geq 0}^{nN_k}$, $u_k=[u_1,...,u_{N_k}]^\top\in\mathbb{R}_{\geq 0}^{N_k}$, and $y_k=[y_1,...,y_{N_k}]^\top\in\mathbb{R}_{\geq 0}^{N_k}$, $k\in\{A,B\}$.

Similar to the cell dynamics in Chapter 2, we assume that $f_k(\cdot,\cdot)$ and $h_k(\cdot)$ are continuously differentiable and further satisfy the following properties:

Assumption 14. *For* $k\in\{A,B\}$ *and each constant input* $u^*\in\mathbb{R}_{\geq 0}$*, the system* (3.4) *has a globally asymptotically stable steady-state*

$$x^*\triangleq S_k(u^*), \tag{3.5}$$

which is a hyperbolic equilibrium. Furthermore, the maps $S_k:\mathbb{R}_{\geq 0}\to\mathbb{R}_{\geq 0}^n$ *and* $T_k:\mathbb{R}_{\geq 0}^n\to\mathbb{R}_{\geq 0}$*, defined as:*

$$T_k(\cdot)\triangleq h_k\left(S_k\left(\cdot\right)\right), \tag{3.6}$$

are continuously differentiable, and $T_k(\cdot)$ *is a positive, bounded and decreasing function.*

The decreasing property of $T_k(\cdot)$ is consistent with the lateral inhibition feature, since a higher input in one cell leads to lower output values.

When do Contrasting Patterns Emerge?

We now present a method to find steady-state patterns for the system defined by (3.4)-(3.2). Given Assumptions 13 and 14, the existence of variables $z_A\in\mathbb{R}_{\geq 0}^{N_A}$ and $z_B\in\mathbb{R}_{\geq 0}^{N_B}$ such that:

$$\left\{\begin{array}{rcl} z_A &=& \mathbf{T}_A\left(T_{BA}^{\text{tx/rx}}\left(\mathbf{T}_B\left(T_{AB}^{\text{tx/rx}}\left(z_A\right)\right)\right)\right)\\ z_B &=& \mathbf{T}_B\left(T_{AB}^{\text{tx/rx}}\left(\mathbf{T}_A\left(T_{BA}^{\text{tx/rx}}\left(z_B\right)\right)\right)\right)\end{array}\right. \tag{3.7}$$

where

$$\mathbf{T}_A(u_A) = [T_A(u_A^1), ..., T_A(u_A^{N_A})]^\top : \mathbb{R}_{\geq 0}^{N_A} \to \mathbb{R}_{\geq 0}^{N_A},$$
$$\mathbf{T}_B(u_B) = [T_B(u_B^1), ..., T_B(u_B^{N_B})]^\top : \mathbb{R}_{\geq 0}^{N_B} \to \mathbb{R}_{\geq 0}^{N_B}.$$

is sufficient to conclude the existence of a steady-state for the full system (3.2)-(3.4). Our goal is to determine when z_A and z_B exhibit sharply contrasting values, indicating an on/off pattern.

To reduce the dimension of the maps defined in (3.7), we use the notion of *equitable partition*. For the weighted and undirected graph $\mathcal{G}(V, E)$ represented by the Laplacian matrix L in (3.1), a partition of the vertex set V into classes $O_1, ..., O_r$ is *equitable* if there exists $\overline{d}_{ij}$ $i, j = 1, ..., r$, such that

$$\sum_{v \in O_j} d_{uv} = \overline{d}_{ij} \quad \forall u \in O_i,\ i \neq j. \tag{3.8}$$

We let the *quotient Laplacian* $\overline{L} \in \mathbb{R}^{r \times r}$ be formed by the off-diagonal entries $\overline{d}_{ij}$, and $\{\overline{L}\}_{ii} = -\sum_{j=1, j\neq i}^{r} \overline{d}_{ij}$.

Assumption 15. *The partition of the compartments V into the classes O_A and O_B of type A and B, respectively, is equitable, and the quotient Laplacian is given by*

$$\overline{L} = \begin{bmatrix} -\overline{d}_{AB} & \overline{d}_{AB} \\ \overline{d}_{BA} & -\overline{d}_{BA} \end{bmatrix}. \tag{3.9}$$

This assumption implies that the total incoming edge weight of the species X is the same for all the compartments of type B, and the total incoming edge weight of the species Y is the same for all the compartments of type A. For example, the network in Figure 3.1(left) is equitable with respect to the classes O_A and O_B when $d_{13} + d_{14} = d_{23} + d_{24}$ and $d_{13} + d_{23} = d_{14} + d_{24}$, which implies $d_{13} = d_{24}$ and $d_{23} = d_{14}$. Since the edge weights d_{ij} are inversely proportional to the square of the distance, this means that opposite channels must have the same length, thus exhibiting a parallelogram geometry, see Figure 3.3.

Assumption 15 allows us to search for solutions to (3.7) where the compartments of the same type have the same steady-state, *i.e.*,

$$z = [\overline{z}_A, ..., \overline{z}_A, \overline{z}_B, ..., \overline{z}_B]^\top = [\overline{z}_A \mathbf{1}_{N_A}^\top, \overline{z}_B \mathbf{1}_{N_B}^\top]^\top \tag{3.10}$$

where $\overline{z}_A \in \mathbb{R}_{\geq 0}$ and $\overline{z}_B \in \mathbb{R}_{\geq 0}$. This means that the transceiver input-output maps become decoupled and that

$$T_{AB}^{\text{tx/rx}}(\overline{z}_A \mathbf{1}_{N_A}) = T_{AB}(\overline{z}_A)\mathbf{1}_{N_B}, \tag{3.11}$$

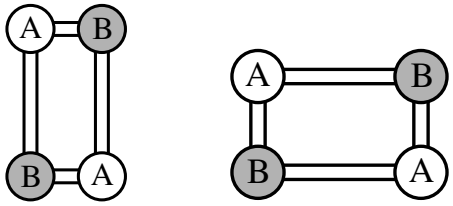

Figure 3.3: Examples of equitable partitions for the compartmental lateral inhibition system in Figure 3.1(left).

where $T_{AB} : \mathbb{R}_{\geq 0} \to \mathbb{R}_{\geq 0}$. The same holds for $T_{BA}^{\text{tx/rx}}(\cdot)$ with $T_{BA} : \mathbb{R}_{\geq 0} \to \mathbb{R}_{\geq 0}$. Note that the diffusion coefficients are implicit in the maps $T_{AB}(\cdot)$ and $T_{BA}(\cdot)$. Furthermore, $\overline{z}_A$ and $\overline{z}_B$ satisfy the following reduced system of equations:

$$\left\{ \begin{array}{rcl} \overline{z}_A & = & T_A\left(T_{BA}\left(T_B\left(T_{AB}\left(\overline{z}_A\right)\right)\right)\right) \triangleq \overline{T}_A\left(\overline{z}_A\right) \\ \overline{z}_B & = & T_B\left(T_{AB}\left(T_A\left(T_{BA}\left(\overline{z}_B\right)\right)\right)\right) \triangleq \overline{T}_B\left(\overline{z}_B\right) \end{array} \right. , \tag{3.12}$$

where $\overline{T}_A : \mathbb{R}_{\geq 0} \to \mathbb{R}_{\geq 0}$ and $\overline{T}_B : \mathbb{R}_{\geq 0} \to \mathbb{R}_{\geq 0}$ are a composition of scalar maps. The solutions of the scalar equations in (3.12) are solutions of the coupled system of N_A (and N_B) equations in (3.7). Note that it is sufficient to study the solution of one of the equations in (3.12): if $\tilde{z}_A$ is a solution to the top equation, then $\tilde{z}_B \triangleq T_B(T_{AB}(\tilde{z}_A))$ must be a solution to the bottom one. The derivative of these two functions at the fixed points $\tilde{z}_A$ and $\tilde{z}_B \triangleq T_B(T_{AB}(\tilde{z}_A))$ is the same and given by

$$\left.\frac{d\overline{T}_A}{dz_A}\right|_{\tilde{z}_A} = T'_{AB}(\tilde{z}_A)T'_B\left(T_{AB}(\tilde{z}_A)\right)T'_{BA}(\tilde{z}_B)T'_A\left(T_{BA}(\tilde{z}_B)\right) = \left.\frac{d\overline{T}_B}{dz_B}\right|_{\tilde{z}_B}, \tag{3.13}$$

where $T'(z_k) \triangleq \left.\frac{dT}{dz}\right|_{z=z_k}$.

From Assumptions 13 and 14, the input-output transfer maps $T_A(\cdot)$ and $T_B(\cdot)$ are decreasing and bounded, whereas $T_{BA}(\cdot)$ and $T_{AB}(\cdot)$ are increasing. Since $\overline{T}_A(\cdot)$ and $\overline{T}_B(\cdot)$ in (3.12) are compositions of these four maps, they are positive, increasing and bounded functions. Figure 3.4 illustrates typical shapes of the input-output maps $\overline{T}_A(\cdot)$ and $\overline{T}_B(\cdot)$. In Figure 3.4(a) there exists only one solution pair (orange circles). This is a near-homogeneous steady-state, where the discrepancy between $\tilde{z}_A$ and $\tilde{z}_B$ is due only to nonidentical $\overline{T}_A(\cdot)$ and $\overline{T}_B(\cdot)$. The map $\overline{T}_A(\cdot)$ in Figure 3.4(b) has three fixed points: a middle solution (near-homogenous steady-state), a large fixed point (blue triangle), and a small fixed point (green square). The latter two have a corresponding opposite fixed point pair in $\overline{T}_B(\cdot)$, specifically $\tilde{z}_B \triangleq T_B(T_{AB}(\tilde{z}_A))$, and therefore represent a contrasting steady-state pattern.

Note that a contrasting pattern emerges when the near-homogenous steady-state has a slope larger than 1, that is:

$$T'_{AB}(\tilde{z}_A)T'_B\left(T_{AB}(\tilde{z}_A)\right)T'_{BA}(\tilde{z}_B)T'_A\left(T_{BA}(\tilde{z}_B)\right) > 1. \tag{3.14}$$

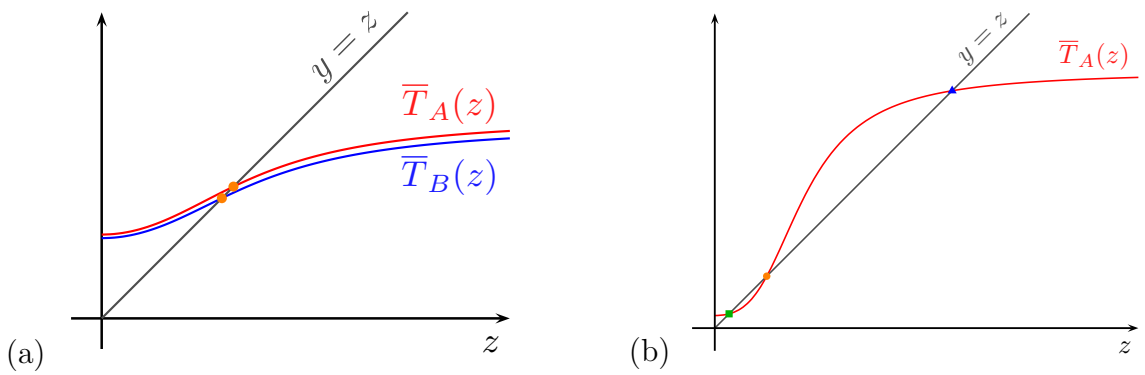

Figure 3.4: Typical shapes of input-output maps $\overline{T}_A(\cdot)$ and $\overline{T}_B(\cdot)$: (a) In this case, the unique pair of fixed points (orange circles) is near-homogenous and no contrasting patterns emerge; (b) In this case, there exist three pairs of fixed points (orange circle, green square, and blue triangle), and the two extra solutions represent contrasting steady-state patterns.

Indeed, due to the boundedness and strictly increasing properties of the map $\overline{T}_A(\cdot)$, if (3.14) holds for $(\tilde{z}_A, \tilde{}_B)$ then there must exist at least two other fixed point pairs of (3.12),

$$\left(z_A^*,\, z_B^* \triangleq T_B\left(T_{AB}\left(z_A^*\right)\right)\right) \quad \text{and} \quad \left(z_A^{**},\, z_B^{**}\right)$$

for which

$$\left(z_A^* > \tilde{z}_A \;\text{ and }\; z_B^* < \tilde{z}_B\right) \quad \left(z_A^{**} < \tilde{z}_A \;\text{ and }\; z_B^{**} > \tilde{z}_B\right). \tag{3.15}$$

In the next section, we show that (3.14) implies that the near-homogenous steady-state becomes unstable, setting the stage for contrasting patterns to emerge. Condition (3.14) provides a parameter tuning principle and is instrumental in characterizing the parameter ranges for patterning in Section 3.3.

3.2 Convergence to Contrasting Patterns

To analyze convergence to the steady-state patterns in (3.12), we employ the following monotonicity assumptions.

Assumption 16. *The system $tx/rx_{A\to B}$ in (3.2) is monotone with respect to $K^U = \mathbb{R}^{N_A}_{\geq 0}$, $K^Y = \mathbb{R}^{N_B}_{\geq 0}$, and $K^X = \mathbb{R}^{N+N_B}_{\geq 0}$. Similarly $tx/rx_{B\to A}$ is monotone with respect to $K^U = \mathbb{R}^{N_B}_{\geq 0}$, $K^Y = \mathbb{R}^{N_A}_{\geq 0}$, and $K^X = \mathbb{R}^{N+N_A}_{\geq 0}$.*

Assumption 17. *The systems H_A and H_B in (3.4) are monotone with respect to $K^U = -K^Y = \mathbb{R}_{\geq 0}$, and $K^X = K$, where K is some positivity cone in $\mathbb{R}$.*

These monotonicity assumptions are consistent with Assumptions 13 and 14, as they imply the increasing property of the input-output maps $T_{BA}^{\text{tx/rx}}(\cdot)$ and $T_{AB}^{\text{tx/rx}}(\cdot)$ and the decreasing behavior of $T_A(\cdot)$ and $T_B(\cdot)$. We now state a stability result for solutions restricted to the steady-state solutions described by (3.12).

Theorem 18. *Consider the network* (3.2)-(3.4) *and suppose Assumptions 13, 14, 16 and 17 hold. Let the partition of the compartments into the classes O_A and O_B be equitable. Then the steady-state described by* (3.12) *is asymptotically stable if*

$$T'_{AB}(\tilde{z}_A)T'_B\left(T_{AB}(\tilde{z}_A)\right)T'_{BA}(\tilde{z}_B)T'_A\left(T_{BA}(\tilde{z}_B)\right) < 1, \tag{3.16}$$

and unstable if (3.14) *holds.*

To prove Theorem 18, we first use the result that the compartmental network (3.2)-(3.4) is monotone.

Lemma 19. *If monotonicity Assumptions 16 and 17 hold, then the network* (3.2)-(3.4) *is monotone.*

Proof of Lemma 19. The main idea of the proof follows similarly to [8, Theorem 3], we can represent the network as a unitary positive feedback interconnection of a monotone system where the inputs and outputs are ordered with respect to the same positivity cone. Note the network is a cascade of an "anti-monotone" system (H_A composed with $\text{tx/rx}_{A\to B}$) with another "anti-monotone" system (H_B composed with $\text{tx/rx}_{B\to A}$), thus the composite system is monotone with the same input and output ordering, $K^U = K^Y = \mathbb{R}^{N_A}_{\geq 0}$ and $K^X = K^{N_A}\times\mathbb{R}^{N+N_B}_{\leq 0}\times\{-K\}^{N_B}\times\mathbb{R}^{N+N_A}_{\geq 0}$. □

Since the network is monotone, we know from [3, Lemma 6.4] that the linearized system around the steady-state is also monotone with respect to the same positivity cones. Furthermore, [39, Theorem 2] shows that for a linear system $\dot{x} = Ax + Bu$ and $y = Cx$ that is monotone with respect to the cones $K^U = K^Y$, K^X, and Hurwitz matrix A, the following equivalence holds: $A + BC$ is Hurwitz if and only if $-(I + CA^{-1}B)$ is Hurwitz. Therefore, we can prove stability of the positive feedback monotone system from the "dc-gain" of the open loop system.

Proof of Theorem 18. The linearization of the full network (3.2)-(3.4) about the steady-state is given by:

$$\begin{bmatrix} A_A\otimes I_{N_A} & 0 & 0 & (B_A\otimes I_{N_A})C_{BA} \\ B_{AB}(C_A\otimes I_{N_A}) & A_{AB} & 0 & 0 \\ 0 & (B_B\otimes I_{N_B})C_{AB} & A_B\otimes I_{N_B} & 0 \\ 0 & 0 & B_{BA}(C_B\otimes I_{N_B}) & A_{BA} \end{bmatrix}, \tag{3.17}$$

where matrices $A_A \in \mathbb{R}^{n\times n}$, $B_A \in \mathbb{R}^{n\times 1}$, $C_A \in \mathbb{R}^{1\times n}$ are associated with the linearization of H_A; and matrices $A_{AB} \in \mathbb{R}^{(N_A+2N_B)\times(N_A+2N_B)}$, $B_{AB} \in \mathbb{R}^{(N_A+2N_B)\times N_A}$, $C_{AB} \in \mathbb{R}^{N_B\times(N_A+2N_B)}$ are the linearization matrices of the transceiver $\mathrm{tx}/\mathrm{rx}_{A\to B}$. For the transceiver, the linearization matrices are of the form:

$$A_{AB} = \begin{bmatrix} & L_{AB} & & 0 \\ & & & 0 \\ 0 & 0 & & 0 \end{bmatrix} + \begin{bmatrix} \partial\Gamma_x & 0 & 0 \\ 0 & \partial\Phi_x & \partial\Phi_R \\ 0 & \partial\Psi_x & \partial\Psi_R \end{bmatrix},$$

and with

$$B_{AB} = \begin{bmatrix} \partial\Gamma_u & 0_{N_B\times N_A} & 0_{N_B\times N_A} \end{bmatrix}^\top, \quad C_{AB} = \begin{bmatrix} 0_{N_B\times N_A} & 0_{N_B\times N_B} & I_{N_B} \end{bmatrix},$$

where due to the structure of the steady-state, $\partial\Gamma_x = \partial\gamma_X I_{N_A}$ with $\partial\gamma_X \triangleq \frac{\partial\gamma_X^i}{\partial X_A^i}|_{\tilde{x}_A}$, and similarly the matrices $\partial\Phi_x$, $\partial\Phi_R$, $\partial\Psi_x$, $\partial\Psi_R$, and $\partial\Gamma_u$, are diagonal with constants $\partial\phi_x$, $\partial\phi_R$, $\partial\psi_x$, $\partial\psi_R$ and $\partial\gamma_u$, respectively. The matrix L_{AB} is the Laplacian matrix of the network when labeling first the nodes of type A.

Due to the monotonicity property of the network proved in Lemma 19, the proof follows as discussed above. We write (3.17) as a unitary positive feedback system: $\mathcal{A} + \mathcal{B}\mathcal{C}$ where $\mathcal{C} = [0\ 0\ 0\ C_{AB}]$, $B = \left[B_A \otimes I_{N_A}^\top\ 0\ 0\ 0\right]^\top$, and $\mathcal{A}$ is the block triangular matrix defined in (3.17) except for the block $(B_A \otimes I_{N_A})C_{BA}$, which is replaced by $0 \in \mathbb{R}^{nN_A\times(N_B+2N_A)}$. Then, since the network is monotone with respect to the same input and output cones, we conclude stability from $-(I + \mathcal{C}\mathcal{A}^{-1}\mathcal{B})$. First note that:

$$\begin{aligned} \mathcal{C}\mathcal{A}^{-1}\mathcal{B} &= -C_{BA}A_{BA}^{-1}B_{BA}(C_BA_B^{-1}B_B \otimes I_{N_B})C_{AB}A_{AB}^{-1}B_{AB}(C_AA_A^{-1}B_A \otimes I_{N_A}) \\ &= -T_A'(T_{BA}(\tilde{z}_B))T_B'(T_{AB}(\tilde{z}_A))(C_{BA}A_{BA}^{-1}B_{BA})(C_{AB}A_{AB}^{-1}B_{AB}), \end{aligned}$$

where the second equality follows from Claim 3 where $T_k'(\tilde{z}) = -C_k^{\tilde{z}}(A_k^{\tilde{z}})^{-1}B_k^{\tilde{z}}$ is the static input-output map for each block at steady-state $\tilde{z}$, and C_j, A_j, B_j are the linearization matrices of each block at $\tilde{z}$, we drop the superscripts $\tilde{z}$ to simplify the notation. Assumptions 13 and 14 guarantee that A_j^{-1} exists and that $\mathcal{A}$ is nonsingular.

For the final step, we use the equitability assumption on the partition defined by the classes O_A and O_B to derive the largest eigenvalue of the matrix $(C_{BA}A_{BA}^{-1}B_{BA}C_{AB}A_{AB}^{-1}B_{AB}) \in \mathbb{R}^{N_B\times N_B}$, and therefore the stability of the matrix $-(I + \mathcal{C}\mathcal{A}^{-1}\mathcal{B})$.

Claim 20. *The largest eigenvalue of the matrix $(C_{BA}A_{BA}^{-1}B_{BA}C_{AB}A_{AB}^{-1}B_{AB})$ is given by $(\overline{C}_{BA}\overline{A}_{BA}^{-1}\overline{B}_{BA}\overline{C}_{AB}\overline{A}_{AB}^{-1}\overline{B}_{AB})$ with eigenvector $\mathbf{1}_{N_A}$, where*

$$\overline{A}_{AB} = \begin{bmatrix} & \overline{L}_{AB} & & 0 \\ & & & 0 \\ 0 & 0 & & 0 \end{bmatrix} + \begin{bmatrix} \partial\gamma_x & 0 & 0 \\ 0 & \partial\phi_x & \partial\phi_R \\ 0 & \partial\psi_x & \partial\psi_R \end{bmatrix},$$

and with

$$\overline{B}_{AB} = \begin{bmatrix} \partial\gamma_u & 0 & 0 \end{bmatrix}^\top, \quad \overline{C}_{AB} = \begin{bmatrix} 0 & 0 & 1 \end{bmatrix},$$

where $\overline{A}_{AB} \in \mathbb{R}^{3\times 3}$, $\overline{L}_{AB} \in \mathbb{R}^{2\times 2}$ *is the quotient Laplacian,* $\overline{C}_{AB} \in \mathbb{R}^{1\times 3}$, *and* $\overline{B}_{AB} \in \mathbb{R}^{3\times 1}$; *and by appropriate change of subscripts the same follows for the matrices* $\overline{A}_{AB}$, $\overline{B}_{AB}$ *and* $\overline{C}_{AB}$.

The theorem follows from this claim because $T'_{AB}(\tilde{z}_A) = -\overline{C}_{AB}\overline{A}_{AB}^{-1}\overline{B}_{AB}$, and thus the largest eigenvalue of $\mathcal{C}\mathcal{A}^{-1}\mathcal{B}$ is given by $T'_A(T_{BA}(\tilde{z}_B))T'_B(T_{AB}(\tilde{z}_A))T'_{AB}(\tilde{z}_A)T'_{BA}(\tilde{z}_B)$. Therefore, when inequality (3.16) holds the matrix $-(I+\mathcal{C}\mathcal{A}^{-1}\mathcal{B})$ is Hurwitz and the steady-state is asymptotically stable. If the condition (3.14) holds, $-(I+\mathcal{C}\mathcal{A}^{-1}\mathcal{B})$ has a positive eigenvalue and the steady-state is unstable. □

Proof of Claim 20. First note that due to equitability of the compartmental network, we can construct matrices $Q_{AB} \in \mathbb{R}^{(N_A+2N_B)\times 3}$ where

$$Q_{AB} = \begin{bmatrix} \underbrace{1 \ldots 1}_{\times N_A} & \underbrace{0 \ldots 0}_{\times N_B} & \underbrace{0 \ldots 0}_{\times N_B} \\ 0 \ldots 0 & 1 \ldots 1 & 0 \ldots 0 \\ 0 \ldots 0 & 0 \ldots 0 & 1 \ldots 1 \end{bmatrix}^\top,$$

and similarly $Q_{BA} \in \mathbb{R}^{(N_B+2N_A)\times 3}$ with appropriate dimensions. Therefore, due to equitability $L_{AB}Q_{AB} = Q_{AB}\overline{L}_{AB}$ and $L_{BA}Q_{BA} = Q_{BA}\overline{L}_{BA}$. Let $P \triangleq [Q\ R]$ where R is a matrix in $\mathbb{R}^{(N_A+2N_B)\times(N_A+2N_B-3)}$ (or $R \in \mathbb{R}^{(N_B+2N_A)\times(N_B+2N_A-3)}$) such that its columns, together with those of Q, form a basis for $\mathbb{R}^{N_A+2N_B}$ (or $\mathbb{R}^{N_B+2N_A}$). We conclude that, there exist matrices N and M such that

$$P_{AB}^{-1}A_{AB}P_{AB} = \begin{bmatrix} \overline{A}_{AB} & N \\ 0 & M \end{bmatrix}, \tag{3.18}$$

and similarly for A_{BA}. Therefore,

$$\begin{aligned} C_{AB}A_{AB}^{-1}B_{AB}\mathbf{1}_{N_A} &= (C_{AB}P_{AB})(P_{AB}^{-1}A_{AB}P_{AB})^{-1}(P_{AB}^{-1}B_{AB}\mathbf{1}_{N_A}) \\ &= \begin{bmatrix} \overline{C}_{AB}\mathbf{1}_{N_B} & S \end{bmatrix} \begin{bmatrix} \overline{A}_{AB}^{-1} & U \\ 0 & V \end{bmatrix} \begin{bmatrix} \overline{B}_{AB} \\ 0 \end{bmatrix}, \\ &= \overline{C}_{AB}\overline{A}_{AB}^{-1}\overline{B}_{AB}\mathbf{1}_{N_B}. \end{aligned}$$

for some matrices S, U, and V with appropriate dimensions. This implies that

$$\begin{aligned} C_{BA}A_{BA}^{-1}B_{BA}C_{AB}A_{AB}^{-1}B_{AB}\mathbf{1}_{N_A} &= (\overline{C}_{AB}\overline{A}_{AB}^{-1}\overline{B}_{AB})C_{BA}A_{BA}^{-1}B_{BA}\mathbf{1}_{N_B} \\ &= (\overline{C}_{BA}\overline{A}_{BA}^{-1}\overline{B}_{BA}\overline{C}_{AB}\overline{A}_{AB}^{-1}\overline{B}_{AB})\mathbf{1}_{N_A} \end{aligned}$$

i.e., the scalar $\overline{C}_{BA}\overline{A}_{BA}^{-1}\overline{B}_{BA}\overline{C}_{AB}\overline{A}_{AB}^{-1}\overline{B}_{AB} = T'_{AB}(\tilde{z}_A)T'_{BA}(\tilde{z}_B)$ is an eigenvalue of the matrix $C_{BA}A_{BA}^{-1}B_{BA}C_{AB}A_{AB}^{-1}B_{AB}$, with associated eigenvector $\mathbf{1}_{N_A}$. Note that this eigenvalue is

positive since the static input-output maps of the transceivers have positive slope. Finally, we need to show that this is the largest eigenvalue. Note that due to Assumption 16, the transceivers' input-output maps $T_{AB}^{\text{tx/rx}\prime}(\tilde{z}_A \mathbf{1}_{N_A}) = -C_{AB}A_{AB}^{-1}B_{AB}$ and $T_{BA}^{\text{tx/rx}\prime}(\tilde{z}_B \mathbf{1}_{N_B}) = -C_{BA}A_{BA}^{-1}B_{BA}$ are nonnegative matrices [4], and thus so is $T_{AB}^{\text{tx/rx}\prime}(\tilde{z}_A \mathbf{1}_{N_A}) T_{BA}^{\text{tx/rx}\prime}(\tilde{z}_B \mathbf{1}_{N_B})$, with no zero rows. This concludes the proof of the claim since, by the Perron-Frobenius Theorem [14], the eigenvalue with associated positive eigenvector $\mathbf{1}_{N_A}$, must be the largest positive eigenvalue. □

3.3 Synthetic Lateral Inhibition Circuit

We propose a lateral inhibition circuit with two types of compartments as described above. The diffusible species are two acyl-homoserine lactones (AHL), namely 3-O-C12-HSL and 3-O-C6-HSL, while the two receiver proteins are LasR and LuxR, respectively. This choice guarantees that the LuxR-AHL and LasR-AHL pairs interact orthogonally with each other [27]. To keep the notation used in the previous section, we denote 3OC12HSL by X, 3OC6HSL by Y, and the complexes LasR-3OC12HSL by R_B, and LuxR-3OC6HSL by R_A.

In Figure 3.5 we represent the synthetic circuit for each cell of type A (left) and B (right). We use the *luxI*/*luxR* (and *lasI*/*lasR*) genes as autoinducer synthase and receptor, the autoinducer synthase *luxI* (*lasI*), which is transcribed by $P_{LtetO\text{-}1}$, translates LuxI (LasI) which is responsible for the production of X or Y. The receptor proteins, variants of LuxR, in each compartment, detect and bind to the X and Y received, forming the complexes R_B and R_A, respectively. The R_B (R_A) complex induces the production of the protein TetR and inhibition occurs when TetR represses the promoters $P_{LtetO\text{-}1}$, thus inhibiting the production of LuxI (LasI). We use red fluorescence protein (RFP) as reporters for each compartment, which are induced by R_A (or R_B).

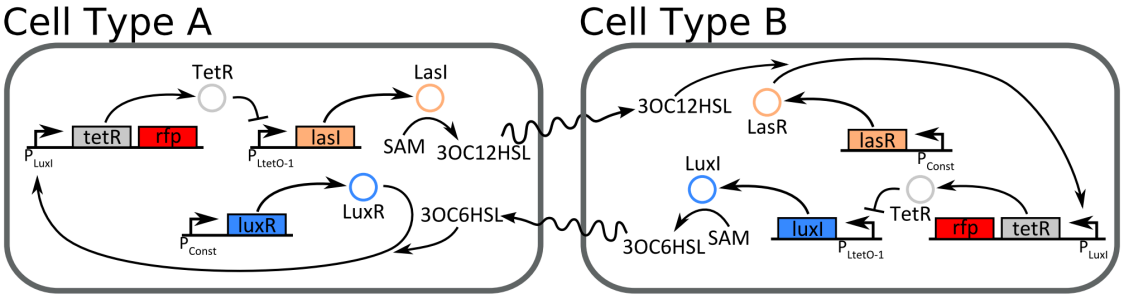

Figure 3.5: Diagram of the synthetic lateral inhibition circuit under implementation, using two orthogonal AHL/LuxR pairs: 3OC12HSL/LasR and 3OC6HSL/LuxR.

We study the following equations for this network, grouped into the transceiver blocks and the inhibitory cell circuits as defined in the Section 3.1. The model for the inhibitory

circuit of cell type A is:

$$H_A^i : \begin{cases} \frac{d}{dt}m^i_{T_Y} &= V_{\mathrm{P_{LuxI}}} N_{\mathrm{P_{LuxI}}} C \left(\frac{1}{1+(K_{RA}/R^i_A)^{n_{RA}}} + \ell_{\mathrm{P_{LuxI}}} \right) - \gamma_{m_T} m^i_{T_Y} \\ \frac{d}{dt}p^i_{T_Y} &= \epsilon_T m^i_{T_Y} - \gamma_T p^i_{T_Y} \\ \frac{d}{dt}m^i_{I_X} &= V_{\mathrm{P_{LtetO\text{-}1}}} N_{\mathrm{P_{LtetO\text{-}1}}} C \left(\frac{1}{1+(p^i_{T_Y}/K_T)^{n_T}} + \ell_{\mathrm{P_{LtetO\text{-}1}}} \right) - \gamma_{mI_X} m^i_{I_X} \\ \frac{d}{dt}p^i_{I_X} &= \epsilon_{I_X} m^i_{I_X} - \gamma_{I_X} p^i_{I_X} \end{cases} \tag{3.19}$$

where m_k is the $mRNA_k$ concentration and p_k the protein concentration (with subscripts T for TetR and I for LuxI); γ_k the degradation rate; ϵ_k the translation rate; V_k the transcriptional velocity rate; N_k the copy number; C the concentration (in M) of a single molecule in a cell; ℓ_k the leakage rate; K_k the dissociation constant; while n_{RA} and n_T represent the cooperativity.

For the dynamics of the transceiver of X, we consider X^i_A, $i = 1, ..., N_A$ to be the concentration of species X at compartment i of type A, and X^j_B, $j = 1, ..., N_B$ the concentration of species X at compartment j of type B. Let $[X^\top, R_B^\top]^\top$ be the transceiver state, with $X = [X_A^\top, X_B^\top]^\top = [X^1_A, ..., X^{N_A}_A, X^1_B, ..., X^{N_B}_B]^\top$ and $R_B = [R^1_B, ..., R^{N_B}_B]^\top$. The transceiver dynamics are:

$$\mathrm{tx/rx}_{A\to B} : \begin{cases} \frac{d}{dt}X^i_A &= \nu p^i_{I_X} - \gamma_X X^i_A + L_i X \\ \frac{d}{dt}X^j_B &= -k_{on} X^j_B (p_{R_X} - R^j_B) + k_{off} R^j_B - \gamma_X X^j_B + L_{j+N_A} X \\ \frac{d}{dt}R^j_B &= k_{on} X^j_B (p_{R_X} - R^j_B) - k_{off} R^j_B, \end{cases} \tag{3.20}$$

for $i = 1, ..., N_A$, $j = 1, ..., N_B$, where L_i corresponds to the row i of the Laplacian matrix, p_{R_k} is the constitutive concentration of total LuxR (bound and unbound), k_{on}/k_{off} are the binding rates, and ν is the generation rate of AHL. The dynamics for the inhibitory circuit of cell type B and for the transceiver $\mathrm{tx/rx}_{B\to A}$ are obtained similarly, by changing the indices appropriately.

Next, we analyze the range of parameters where patterning occurs. To analyze the steady-states of the network above, note that both H_A and $\mathrm{tx/rx}_{A\to B}$ (H_B and $\mathrm{tx/rx}_{B\to A}$) meet the Assumptions in 14, 17 and 13, 16, respectively. From (3.19), for each constant input R^{i*}_A, there is only one steady-state solution ($m^{i*}_{T_Y}$, $p^{i*}_{T_Y}$, $m^{i*}_{I_X}$, $p^{i*}_{I_X}$), which is a globally asymptotically stable hyperbolic equilibrium, due to the lower triangular structure of (3.19) with bounded nonlinearities. Furthermore, the static input-output map is decreasing:

$$T^i_A(R^{i*}_A) = K_1 \left(\frac{1}{1 + \left(\frac{K_2}{K_T} \left(\frac{1}{1+(K_{RA}/R^{i*}_A)^{n_{RA}}} + \ell_{\mathrm{P_{LuxI}}} \right) \right)^{n_T}} + \ell_{\mathrm{P_{LtetO\text{-}1}}} \right), \tag{3.21}$$

where

$$K_1 = \frac{\epsilon_{I_X}}{\gamma_{I_X}} \frac{V_{\mathrm{P_{LtetO\text{-}1}}} N_{\mathrm{P_{LtetO\text{-}1}}} C}{\gamma_{m_{I_X}}} \quad \text{and} \quad K_2 = \frac{\epsilon_T}{\gamma_T} \frac{V_{\mathrm{P_{LuxI}}} N_{\mathrm{P_{LuxI}}} C}{\gamma_{m_T}} \quad (\mathrm{M}).$$

The subsystem is monotone with respect to $K^U = -K^Y = \mathbb{R}_{\geq 0}$, $K = \{x \in \mathbb{R}^4 | x_1 \geq 0, x_2 \geq 0, x_3 \leq 0, x_4 \leq 0\}$ [8, Lemma 4].

As for the transceiver $\text{tx/rx}_{A\to B}$ in (3.20), we see that in steady-state, for a constant input $p^*_{I_X} \in \mathbb{R}^{N_A}$, the dynamic equations for R_B become zero, which implies that the first terms of the dynamical equations for X_B are also zero. Therefore, due to the linearity of the remainder terms, there exists a unique solution for $[X_A^{*T}, X_B^{*T}]^\top$:

$$\begin{bmatrix} X_A^* \\ X_B^* \end{bmatrix} = (-L + \gamma_X I_N)^{-1} \begin{bmatrix} \nu p^*_{I_X} \\ 0_{N_B} \end{bmatrix}. \tag{3.22}$$

The inverse of $(-L + \gamma_X I_N)$ exists since $-L$ is a positive semidefinite matrix (property of Laplacian matrices). The single solution for the steady-state of R_B^i is given by

$$R_B^{i*} = \frac{p_{R_X}}{1 + \frac{k_{off}}{k_{on}} \frac{1}{X_B^{i*}}}, \tag{3.23}$$

where X_B^{i*} is as in (3.22). Note that the static input-output map $T_{AB}^{tx/rx}(p_{I_X}^{i*})$ is positive and increasing, because $(-L + \gamma_X I_N)$ is a positive definite matrix with nonpositive off-diagonal elements, and thus its inverse is a positive matrix (*i.e.*, all elements are positive) [14, Theorem 6.2.3]. Finally, to conclude that these steady-states are asymptotically stable and hyperbolic, we write the Jacobian of the transceiver as:

$$J = \left[\begin{array}{cc|c} & & 0 \\ & L - \gamma_X I_N & 0 \\ & & \\ \hline 0 & 0 & 0 \end{array}\right] + \left[\begin{array}{c|cc} 0 & 0 & 0 \\ \hline 0 & -D_{R_B} & D_{X_B} \\ 0 & D_{R_B} & -D_{X_B} \end{array}\right], \tag{3.24}$$

where D_{R_B} and D_{X_B} are diagonal matrices with elements $\{D_{R_B}\}_{ii} = k_{on}(p_{R_X} - R_B^{i*})$ and $\{D_{X_B}\}_{ii} = k_{on} X_B^{i*} + k_{off}$, $i = 1, ..., N_B$. The matrix J has negative diagonal terms and nonnegative off-diagonal terms, and there exists a D such that the column sum of DJD^{-1} are all negative for all states in the nonnegative orthant[1]. Note that this implies that the *matrix measure* of DJD^{-1} with respect to the one-norm is negative [32, Chapter 2], and $\mu_D(J) = \mu_1(DJD^{-1}) < 0$. This is a *contraction* property with respect to the weighted one-norm; therefore, for each constant input, the steady-state is globally asymptotically stable [94]. Moreover, it is an hyperbolic equilibrium since $Re\{\lambda_k(J)\} \leq \mu(J) < 0$ [32]. The transceiver is monotone with respect to the cones in Assumption 16 since the Jacobian off-diagonal terms are all positive and the dependence on the input variable p_{I_X} is positive [4].

To find stable steady-state patterns where all the compartments of the same type have the same final value, let the network be an equitable graph $\mathcal{G}$ with respect to the compartment

[1] choose $D = \text{diag}(\underbrace{1, ..., 1}_{N\text{times}}, \underbrace{k, ..., k}_{N_B\text{times}})$, with $1 < k < 1 + \frac{\gamma_X}{k_{on} p_{R_X}}$

types. The transceiver input-output map decouples into the scalar maps,

$$T_{AB}(\tilde{z}_A) = \frac{1}{1 + \frac{k_{off}}{k_{on}} \frac{\gamma_X(\gamma_X + \overline{d}_{AB} + \overline{d}_{BA})}{\overline{d}_{BA}\nu} \frac{1}{\tilde{z}_A}}, \tag{3.25}$$

where $\overline{d}_{AB}$ and $\overline{d}_{BA}$ are as in (3.8). As discussed in the previous section, we look for the steady-states that are fixed points of $\overline{T}_A(\cdot)$ and $\overline{T}_B(\cdot)$.

Table 3.1: Parameters used in the simulations of the synthetic lateral inhibition circuit.

Parameter	**Description**	**Value**	**Units**
k_{on}	binding rate between LuxR and AHL	1e9	$s^{-1}M^{-1}$
k_{off}	dissociation rate between LuxR and AHL	50	s^{-1}
p_{R_i}	constitutive concentration of total LuxR	variable	M
d_{12}	diffusion rate of AHL	variable	s^{-1}
$V_{\mathrm{P_{LuxI}}}$	velocity rate of promoter $\mathrm{P_{LuxI}}$	0.26	s^{-1}
$N_{\mathrm{P_{LuxI}}}$	copy number of promoter $\mathrm{P_{LuxI}}$	5	1
C	concentration of a single molecule in a cell	1.5e-9	M
K_{RA}	dissociation constant between p_{R_A} and $\mathrm{P_{LuxI}}$	1.5e-9	M
n_{RA}	cooperativity	2	1
$\ell_{\mathrm{P_{LuxI}}}$	leakage of promoter $\mathrm{P_{LuxI}}$	1/167	1
$V_{\mathrm{P_{LtetO\text{-}1}}}$	velocity rate of promoter $\mathrm{P_{LtetO\text{-}1}}$	0.3	s^{-1}
$N_{\mathrm{P_{LtetO\text{-}1}}}$	copy number of promoter $\mathrm{P_{LtetO\text{-}1}}$	5	1
K_T	dissociation constant between TetR and $\mathrm{P_{LtetO\text{-}1}}$	1.786e-10	M
n_T	cooperativity	2	1
$\ell_{\mathrm{P_{LtetO\text{-}1}}}$	leakage of promoter $\mathrm{P_{P_{LtetO\text{-}1}}}$	1/5050	1
γ_A	rate of degradation of AHL	7.70e-4	s^{-1}
γ_{m_T}	degradation constant of mRNA TetR	5.78e-3	s^{-1}
γ_T	degradation constant of TetR	2.89e-4	s^{-1}
γ_{m_I}	degradation constant of mRNA LuxI/LasI	5.78e-3	s^{-1}
γ_I	degradation constant of LuxI/LasI	1.16e-3	s^{-1}
ϵ_T	translation rate TetR	6.224e-6	s^{-1}
ϵ_I	translation rate LuxI/LasI	2.655e-5	s^{-1}
ν	generation rate of AHL	0.0135	s^{-1}

The reaction parameters used for the analysis are displayed in Table 3.1, and are similar to the parameters suggested in [61]. We assume that the two orthogonal types of AHL have

similar induction and binding reception parameters, and thus consider both cell types to have the same parameter values. In this particular case, the maps $\overline{T}_A(\cdot)$ and $\overline{T}_B(\cdot)$ are identical, and when there exist three fixed points as in Figure 3.4(b), the middle solution pair is the same for A and B (*i.e.*, $\tilde{z}_A = \tilde{z}_B$). The slope of these maps at the fixed points depends, among others, on the edge weights d_{ij} and constitutive concentration of total LuxR/LasR p_{R_k}, which are tunable parameters. As discussed next, d_{ij} can be tuned by changing the channel lengths, and p_{R_k} can be tuned by changing the strength of the constitutive promoter.

When each compartment is a square of side w, and the channel connecting the compartments be of length l_{ij} and width w, the edge weight is, by [35]:

$$d_{ij} = \frac{D_{\text{AHL}}}{l_{ij} w} = k \frac{D_{\text{AHL}}}{l_{ij}^2}. \tag{3.26}$$

Here we let the width be a factor c of the length, *i.e.* $w = l/c$. In the laboratory, we laser cut acrylic sheets into the shape of the desired channels and then we fill these channels and compartments with agar (so that diffusion occurs mostly on the surface of the agar), and then pipettes one colony in each compartment. As the agar solidifies, a thin layer of water is formed on its surface. The AHL diffusion occurs on the agar surface. Although the cells remain on the agar surface, the AHL diffusion occurs through the agar as well, but we assume this to be negligible in comparison with the diffusion on the surface. We consider the diffusivity coefficient for AHL in water at $25°C$ [99]: $D_{\text{AHL},25°C} = 4.9 \times 10^{-10}\, m^2/s$.

As an illustration of the patterning condition (3.14), consider now two compartments connected by one channel, one compartment of type A and the other of type B. This is equivalent to considering any equitable network topology with the same $\overline{d}_{AB}$ and $\overline{d}_{BA}$. Figure 3.6 maps the regions over the pairs (p_{R_k}, l_{12}) where contrasting patterns emerge. We obtain patterning within a wide range of realistic values of p_{R_k}. At the extreme values, if the concentration of p_{R_k} is too low, the detection ability of each cell is affected, which leads to a low concentration of the receiver complexes LuxR-AHL and LasR-AHL. Thus, no cell is being inhibited (fluorescence reporters are low) and no contrasting patterning emerges. When p_{R_k} is too high, no contrasting patterning occurs, both compartments are inhibited since both cells are too sensitive to the received signal due to leakage production of AHL.

Further analysis using condition (3.14) reveals that the circuit, for this set of parameters, is fairly robust to parameter uncertainty. We introduced a variation of 10% in each parameter and the patterning range didn't suffer significant change. Patterning occurs when $n_T n_{RA} \geq 2$, greater n_T and n_{RA} implies stronger inhibition and in general increases the patterning region.

There is also a limit on the length of the channel for the emergence of contrasting patterns (Figure 3.6). In implementation, we expect a stricter limit on the length of the channel since

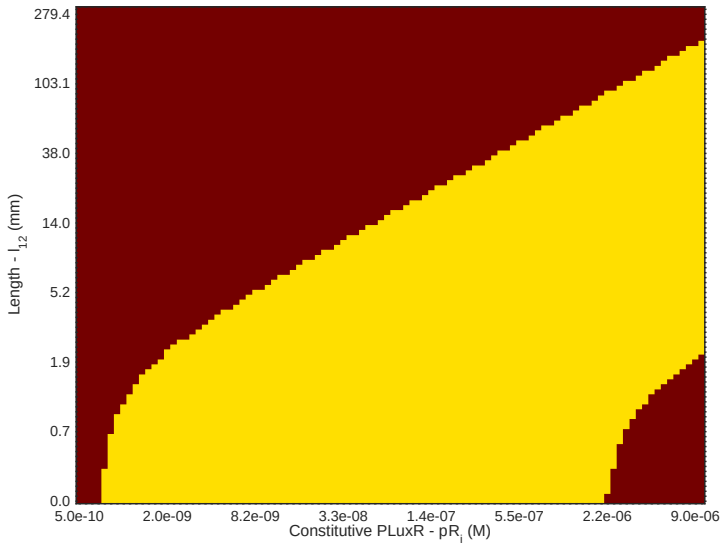

Figure 3.6: Patterning (yellow) vs. non-patterning (dark red) region, for varying p_{R_k} and l_{12}, with $c = 2$.

the compartmental model does not account for degradation of AHL along the channels. For validation, we have implemented the compartment network in COMSOL, a finite element analysis, solver and simulation software for multi-physics applications, which allows for coupled systems of partial differential equations (PDEs) with complex geometry. In COMSOL, we define the geometry of the channel and the compartments, and only allow AHL to diffuse through the channel. For the values of p_{R_i} studied, we have seen a cap on patterning for lengths no larger than 5 mm. Due to degradation along the channel, only a small portion of the AHL actually reaches the opposite compartment. Although the ODE model does not account for this, for shorter channels ($\leq 3\,mm$), we compute a degradation correction factor for the ODE compartmental model that compensates for the extra degradation along the channel. In these regimes, we obtain an accurate steady-state and dynamical match between the ODE model and the PDE COMSOL model, see Figure 3.7.

When the equitability condition is satisfied approximately rather than exactly, we treat the system as a perturbation of an equitable one. If the nonlinear system verifies Lipschitz continuity in x (uniformly in L, for small variations), which is true for the proposed circuit, the solutions are continuously dependent on the parameters of the Laplacian L, *i.e.*, weights of d_{ij}. We see such behavior in simulations on networks with approximately equitable topologies (by adding small random changes to d_{ij}), where the emergence of on/off patterning behavior doesn't get affected, and where there is only a small variation on the final values of cells with the same type.

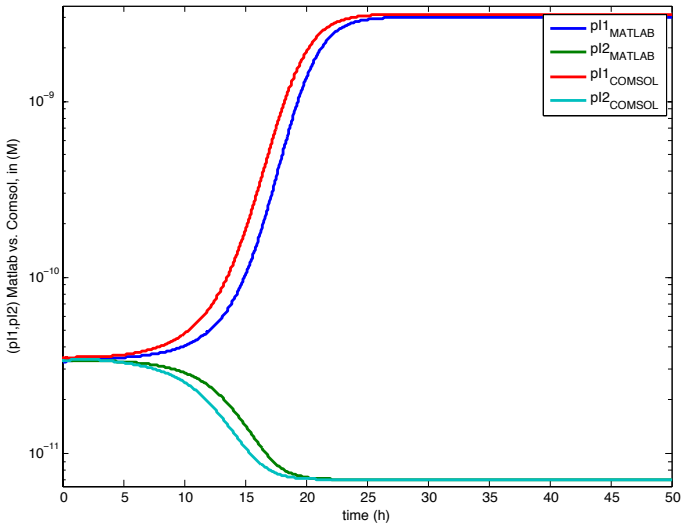

Figure 3.7: Result comparison between ODE model, in MATLAB, and PDE model, in COMSOL (with $p_{R_i} = 5 \times 10^{-7}$, $l_{12} = 500\mu m$, and $k = 2$). Note that both models converge to the same steady-state, with a similar time constant (∼22hrs vs. ∼19hrs, respectively).

3.4 Conclusions

In this chapter we proposed a synthetic lateral inhibition circuit where contrasting patterns between neighboring compartments emerge using diffusible molecules. For a generic network, we show that equitable partitions allow for a dimensionality reduction of the steady-state analysis into fixed points of a scalar map. Those solutions, represent steady-states where all the compartments of the same type have the same final value. For the synthetic circuit we propose, the emergence of contrasting patterns occurs within a realistic range of reaction parameters. We validate our analysis by simulating the compartmental ODE model agains the PDE model in COMSOL.

In addition to the current effort to implement this design in the laboratory, several analytical problems remain to be explored: i) due to the inherent stochastic nature of biochemical reactions and diffusion, it is of interest to investigate the stochastic patterning behavior of these networks; ii) in practice, one would expect to be hard to build an equitable network, it is important to further investigate perturbation analysis for the emerging patterns in networks where small variations to the channel lengths exist, resulting in quasi-equitable graphs.

Chapter 4

Symmetry Reduction for Performance Certification of Interconnected Systems

Consider the system in Figure 4.1 where H_i are subsystems mapping $u_i \to y_i$ and M is a static matrix characterizing the interconnection topology. In [80], certification of performance from a disturbance d to an exogenous output e is cast as a feasibility problem with local constraints guaranteeing dissipativity properties of the individual subsystems together with a global constraint that certifies the desired property of the interconnected system. The local constraints only depend on the dynamics of each subsystem, while the global constraint depends on the subsystem properties and M. In this chapter we take advantage of symmetry in the interconnection to reduce the complexity of the global constraint.

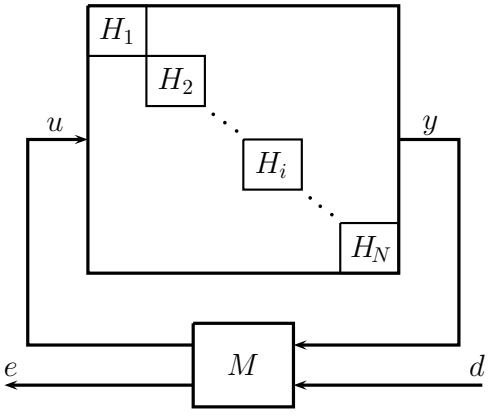

Figure 4.1: Interconnected System.

The global constraint is a linear matrix inequality (LMI) that becomes computationally intractable for large interconnections. Exploiting the symmetry of the interconnection, we

partition the subsystems into equivalence classes and reduce the number of decision variables and size of the global constraint. For this reduction the subsystems in each equivalence class are allowed to be different and only required to share dissipativity properties. These reductions significantly reduce the computational time required and allow the analysis of very large systems.

In general it may be difficult to determine symmetry from the matrix M, but it is readily apparent in many physical systems, like vehicle platoons or biological networks, *e.g.*, Chapters 2 and 3, where M can be interpreted as the adjacency matrix of a weighted directed graph. In some cases, the networks may have a symmetric structure but the weights in the interconnection M break the symmetry. We demonstrate that, in some cases, it is possible to diagonally scale M to recover this symmetry and then apply the symmetry reduction to the scaled system.

For large interconnections we use the symmetry reduction with distributed optimization techniques to decompose the problem into local and global subproblems that are solved iteratively. In this case the symmetry reduction is especially beneficial since the global constraint is solved multiple times. Often the subsystems in an interconnection are similar but have uncertain or slightly different parameters. For such cases, robust dissipativity is valuable, since it certify properties that are shared among the similar subsystems.

Symmetry reduction techniques have been widely applied. In [57] stability of large interconnections is inferred from the stability of a reduced, equivalent system under the assumptions that the subsystems are identical and the interconnection has a certain structure that implies symmetry. Symmetry reduction techniques were used in [48] to reduce the complexity of sum-of-squares (SOS) and semidefinite programming (SDP) problems. These results have been applied to many problems including controller synthesis for symmetric linear systems in [24] and the fastest mixing problem in reversible Markov chains with graph symmetries in [17]. Symmetries in the network topology have been associated in [88] to uncontrollability of networked consensus dynamics.

In this chapter we quantify local properties and global performance in the framework of dissipative systems with quadratic supply rates [110].

Definition 21. *A nonlinear system of the form*

$$\begin{aligned} \dot{x}(t) &= f(x(t), u(t)), \qquad f(0,0) = 0 \\ y(t) &= h(x(t), u(t)), \qquad h(0,0) = 0 \end{aligned} \tag{4.1}$$

with $x(t) \in \mathbb{R}^n$, $u(t) \in \mathbb{R}^m$, $y(t) \in \mathbb{R}^p$, is dissipative with respect to a quadratic supply rate defined by the symmetric matrix $X \in \mathbb{R}^{(m+p)\times(m+p)}$ if there exists a differentiable and

nonnegative storage function $V : \mathbb{R}^n \to \mathbb{R}_+$ *such that* $V(0) = 0$ *and*

$$\nabla V(x)^\top f(x,u) - \begin{bmatrix} u \\ h(x,u) \end{bmatrix}^\top X \begin{bmatrix} u \\ h(x,u) \end{bmatrix} \leq 0 \tag{4.2}$$

for all $x \in \mathbb{R}^n$, $u \in \mathbb{R}^m$.

The notion of dissipativity implies that $\int_0^T \begin{bmatrix} u(t) \\ y(t) \end{bmatrix}^\top X \begin{bmatrix} u(t) \\ y(t) \end{bmatrix} dt + V(x(0)) \geq 0$ for all T in the time interval where solutions to the system exist. The following section describes a compositional approach to dissipativity certification. We certify that an interconnected system is dissipative with respect to a global supply rate, specified by the analyst, by searching over supply rates for individual subsystems.

Later in the chapter we extend the symmetry reduction techniques to systems that satisfy integral quadratic constraints (IQCs), using a state-space approach. This is a generalization of the dissipativity framework that allows frequency dependent properties of a system to be certified.

In section 4.1, we introduce the performance certification problem using local and global constraints. In Section 4.2, we define symmetries in the interconnection matrix, which are used in Section 4.3 to reduce the dimensionality of the global constraint. We provide applications of the results in Section 4.4 and study examples in Section 4.5. We finalize with Sections 4.6 and 4.7, discussing how the results can be used to certify performance using IQCs and to certify stability.

4.1 Performance Certification via Dissipativity

In Figure 4.1 the dynamical systems H_i are given by:

$$H_i : \begin{cases} \dot{x}_i(t) = f_i(x_i(t), u_i(t)), & f_i(0,0) = 0 \\ y_i(t) = h_i(x_i(t), u_i(t)), & h_i(0,0) = 0 \end{cases} \tag{4.3}$$

with $x_i(t) \in \mathbb{R}^{n_i}$, $u_i(t) \in \mathbb{R}^{m_i}$, $y_i(t) \in \mathbb{R}^{p_i}$. The coupling of these systems is dictated by:

$$\begin{bmatrix} u \\ e \end{bmatrix} = M \begin{bmatrix} y \\ d \end{bmatrix} = \begin{bmatrix} M_{11} & M_{12} \\ M_{21} & M_{22} \end{bmatrix} \begin{bmatrix} y \\ d \end{bmatrix} \tag{4.4}$$

where M is a static matrix, $d(t) \in \mathbb{R}^{p_d}$ is a disturbance input, and $e(t) \in \mathbb{R}^{m_e}$ is a performance output. We assume well-posedness of the interconnection, *i.e.*, by substituting $y_i = h_i(x_i, u_i)$ in (4.4), u can be uniquely solved as a function of x and d.

Consider the interconnected system described by (4.3)-(4.4) and suppose that we wish to certify its dissipativity with respect to a global supply rate

$$\begin{bmatrix} d \\ e \end{bmatrix}^\top W \begin{bmatrix} d \\ e \end{bmatrix}, \tag{4.5}$$

where W is a real symmetric matrix specified by the analyst. For example, to certify an L_2-gain from $d(t)$ to $e(t)$ choose $W = \begin{bmatrix} \gamma^2 & 0 \\ 0 & -1 \end{bmatrix}$, which implies that $\|e\|_2^2 \leq \gamma^2 \|d\|_2^2 + V(x(0))$.

Using the dissipativity properties of the subsystems, we can certify dissipativity of the interconnected system. The problem is casted as a feasibility problem where the *local* constraint sets are

$$\mathcal{L}_i \triangleq \left\{ X_i \;\middle|\; \text{the } i\text{-th subsystem is dissipative w.r.t. the supply rate } \begin{bmatrix} u_i \\ y_i \end{bmatrix}^\top X_i \begin{bmatrix} u_i \\ y_i \end{bmatrix} \right\} \tag{4.6}$$

and the global constraint set is

$$\mathcal{G} \triangleq \left\{ X_1, ..., X_N \;\middle|\; \begin{bmatrix} M \\ I_p \end{bmatrix}^\top P_\pi^\top Q P_\pi \begin{bmatrix} M \\ I_p \end{bmatrix} \preceq 0 \right\} \tag{4.7}$$

where $Q = \text{blkdiag}(X_1, ..., X_N, -W)$ and the matrix P_π is defined such that

$$\begin{bmatrix} u_1 \\ y_1 \\ \vdots \\ u_N \\ y_N \\ d \\ e \end{bmatrix} = P_\pi \begin{bmatrix} u \\ e \\ y \\ d \end{bmatrix}. \tag{4.8}$$

It then follows from (4.4) and (4.8) that

$$\begin{bmatrix} y \\ d \end{bmatrix}^\top \begin{bmatrix} M \\ I_p \end{bmatrix}^\top P_\pi^\top Q P_\pi \begin{bmatrix} M \\ I_p \end{bmatrix} \begin{bmatrix} y \\ d \end{bmatrix} = \sum_{i=1}^{N} \begin{bmatrix} u_i \\ y_i \end{bmatrix}^\top X_i \begin{bmatrix} u_i \\ y_i \end{bmatrix} - \begin{bmatrix} d \\ e \end{bmatrix}^\top W \begin{bmatrix} d \\ e \end{bmatrix}. \tag{4.9}$$

Thus, if there exists $X_1, \dots X_N$ satisfying

$$\begin{aligned} &X_i \in \mathcal{L}_i \text{ for } i = 1, \dots, N \\ &(X_1, ..., X_N) \in \mathcal{G}, \end{aligned} \tag{4.10}$$

the interconnected system is dissipative with respect to the global supply rate (4.5). To see why, choose the storage function to be $V(x) = \sum_i V_i(x_i)$, where $V_i(\cdot)$ is a storage function

that guarantees (4.6) for the i-th subsystem.

For systems with linear or polynomial dynamics (4.10) can be cast as a SDP using SOS programming techniques. The local constraints depend only on the individual subsystems and their supply rates, but the global constraint depends on the supply rates for all the subsystems. Therefore, the resulting SDP becomes computationally intractable for large interconnections.

In this chapter, we explore the symmetries in the interconnection matrix M to reduce the number of variables of the LMI in the global constraint set (4.7), thus, reducing the number of decision variables. The next section introduces the necessary notions of symmetry for the interconnection matrix M. For simplicity of notation, we address the case where each subsystem is SISO (*i.e.*, $m_i = p_i = 1$, $i = 1, ..., N$) although the results are generalizable to MIMO systems (see Remark 29).

4.2 Interconnection Symmetries

To characterize the symmetry properties we adapt the notion of *automorphism* to the interconnection matrix M, which takes into account inputs and outputs.

Definition 22. *Consider the interconnection defined by the matrix M in (4.4). An automorphism is a tuple (R_N, R_D, R_E) where $R_N \in \mathbb{R}^{N\times N}$, $R_D \in \mathbb{R}^{p_d\times p_d}$, and $R_E \in \mathbb{R}^{m_e\times m_e}$ are permutation matrices, and the following equalities hold:*

$$\begin{aligned} R_N M_{11} &= M_{11} R_N \qquad & R_N M_{12} &= M_{12} R_D \\ R_E M_{21} &= M_{21} R_N \qquad & R_E M_{22} &= M_{22} R_D. \end{aligned} \tag{4.11}$$

The set of all automorphisms of the interconnection M forms a group, called the *automorphism group*:

$$Aut(M) = \{(R_N, R_D, R_E) \text{ such that (4.11) holds}\}. \tag{4.12}$$

Definition 23. *Given the automorphism group $Aut(M)$, the orbit of index $i \in V_N = \{1, ..., N\}$ is defined as:*

$$O_i = \left\{ j \in V_N \;\middle|\; R_N q_i = q_j \text{ for some } (R_N, R_D, R_E) \in Aut(M) \right\} \tag{4.13}$$

where $q_i \in \mathbb{R}^{N\times 1}$ is the i-th unit vector.

Hence, two indices i, j are in the same orbit if there exists a permutation in $Aut(M)$ that permutes subsystem H_i with H_j. The orbits form an *equivalence class* given by the *equivalence relation* $\sim$, where $i \sim j$ if $j \in O_i$. Let r be the number of distinct orbits,

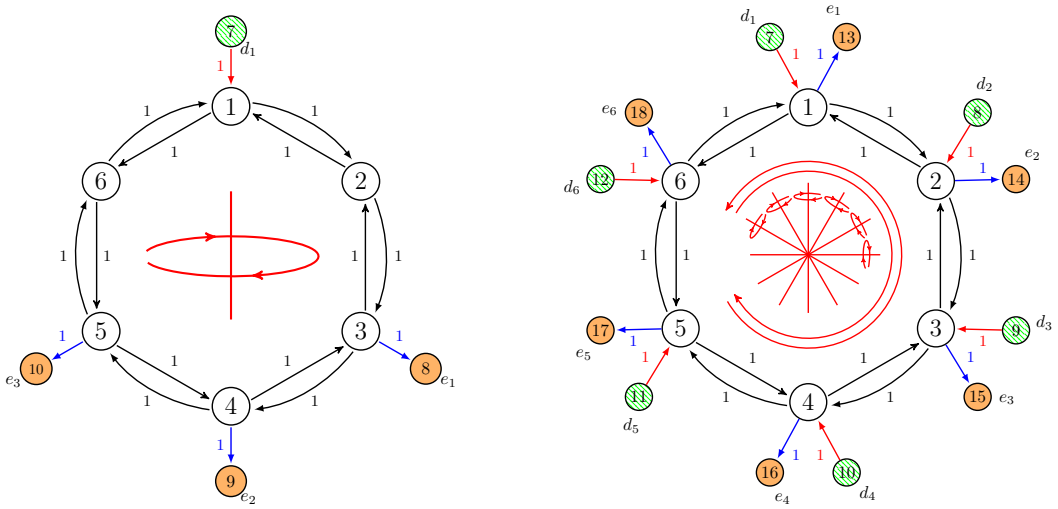

Figure 4.2: Graph representation of a cyclic network with six subsystems. White vertices represent the subsystems H_i, green dashed vertices represent the disturbances d_l, and orange filled vertices represent the outputs e_k. The network in (a) has one disturbance and three performance outputs. The network in (b) has one disturbance and one performance output per subsystem and exhibits a richer class of symmetries.

labeled as $\hat{O}_1, ..., \hat{O}_r$.

To recover the definition of automorphism in Chapter 1, we can view the interconnection matrix M as the adjacency matrix of graph $\mathcal{M}(V, E)$. The vertex set of $\mathcal{M}(V, E)$ is

$$V = V_N \cup V_D \cup V_E \tag{4.14}$$

where $V_N = \{1, ..., N\}$ corresponds to the subsystems H_i, $i = 1, ..., N$, and similarly, $V_D = \{N + 1, ..., N + p_d\}$ and $V_E = \{N + p_d + 1, ..., N + p_d + m_e\}$ correspond to the disturbance inputs d_l, $l = 1, ..., p_d$, and performance outputs e_k, $k = 1, ..., m_e$. The set of edges is

$$E = E_N \cup E_D \cup E_E \cup E_O, \tag{4.15}$$

where E_N includes the edges between H_i and H_j with weight $\{M_{11}\}_{ij}$; the edges E_D from V_D to V_N represent the effect of disturbance d_l in H_i with input weight $\{M_{12}\}_{il}$; the edges E_E from V_N to V_E represent the effect of H_i in the output e_k with weight $\{M_{21}\}_{ki}$; and the edges E_O from V_D to V_E represent the throughput of the disturbance d_k on the output e_l with weight $\{M_{22}\}_{kl}$.

As an illustration, consider the cyclic network with six subsystems $H_1, ..., H_6$, one disturbance d_1, and three performance outputs e_1, e_2, e_3, with incidence graph depicted in Figure

4.2a. Since the graph is symmetric with respect to the vertical axis, it remains unchanged when 2 permutes with 6, 3 with 5, and 8 with 10. The automorphism group is given by $R_i = (R_N^i, R_D^i, R_E^i)$, for $i = 1, 2$:

$$R_1 = (I_6, 1, I_3) \text{ and } R_2 = \left(\begin{bmatrix} 1&0&0&0&0&0 \\ 0&0&0&0&0&1 \\ 0&0&0&0&1&0 \\ 0&0&0&1&0&0 \\ 0&0&1&0&0&0 \\ 0&1&0&0&0&0 \end{bmatrix}, 1, \begin{bmatrix} 0&0&1 \\ 0&1&0 \\ 1&0&0 \end{bmatrix} \right).$$

The four distinct orbits are $\hat{O}_1 = \{1\}$, $\hat{O}_2 = \{2, 6\}$, $\hat{O}_3 = \{3, 5\}$, $\hat{O}_4 = \{4\}$.

In Figure 4.2b each subsystem has a disturbance input performance output pair, and $M_{12} = M_{21} = I_N$. Thus, definition (4.11) implies that $R_D = R_E = R_N$, and the automorphisms are determined by R_N alone. The graph now exhibits rotational symmetry as well as symmetry with respect to all axes that are angled by integer multiples of 30^o. Thus all subsystems permute with each other (as well as all disturbances and outputs) and there is only one orbit: $\hat{O}_1 = \{1, ..., 6\}$.

Remark 24. *The full automorphism group of the interconnection may be hard to compute [73]. However, we can still make use of subgroups corresponding to symmetries that are easy to identify. The reduction discussed in the next section is valid for subgroups of $Aut(M)$ although the reduction may not be as extensive.*

4.3 Main Result: Using Symmetries for Performance Certification

In this section, we use the automorphism group of the interconnection matrix M to reduce the dimensionality of the LMI in the global constraint set (4.7).

Lemma 25. *If the LMI in* (4.7) *is satisfied by* $(X_1, ..., X_N, W)$ *then it is also satisfied by* $(\tilde{X}_1, ..., \tilde{X}_N, \tilde{W})$*, where*

$$\tilde{X}_i \triangleq \frac{1}{|O_i|} \sum_{j \in O_i} X_j \quad \textit{and} \quad \tilde{W} \triangleq \frac{1}{k} \sum_{i=1}^{k} \begin{bmatrix} R_D^i & 0 \\ 0 & R_E^i \end{bmatrix}^\top W \begin{bmatrix} R_D^i & 0 \\ 0 & R_E^i \end{bmatrix} \tag{4.16}$$

with $k = |Aut(M)|$ and $(R_N^i, R_D^i, R_E^i) \in Aut(M)$.

Proof. Let $R_L \triangleq \text{blkdiag}(R_N, R_E)$ and $R_R \triangleq \text{blkdiag}(R_N, R_D)$ be constructed from an automorphism $(R_N, R_D, R_E) \in Aut(M)$, such that $R_L M = M R_R$. Since the matrices R_N, R_E, R_D are orthonormal, the following holds for M and P_π,

$$\begin{bmatrix} M \\ I \end{bmatrix} = \begin{bmatrix} R_L & 0 \\ 0 & R_R \end{bmatrix} \begin{bmatrix} M \\ I \end{bmatrix} R_R^\top \text{ and } P_\pi \begin{bmatrix} R_L & 0 \\ 0 & R_R \end{bmatrix} = S P_\pi \tag{4.17}$$

where

$$P_\pi = \left[\begin{array}{c|c|c|c} I_N \otimes \begin{bmatrix} 1 \\ 0 \end{bmatrix} & 0 & I_N \otimes \begin{bmatrix} 0 \\ 1 \end{bmatrix} & 0 \\ \hline 0 & 0 & 0 & I_{p_d} \\ 0 & I_{m_e} & 0 & 0 \end{array}\right] \quad \text{and} \quad S = \left[\begin{array}{c|c} R_N \otimes \begin{bmatrix} 1 & 0 \\ 0 & 1 \end{bmatrix} & 0 \\ \hline 0 & \begin{matrix} R_D & 0 \\ 0 & R_E \end{matrix} \end{array}\right]. \tag{4.18}$$

Then, the following LMI equivalence holds:

$$\begin{bmatrix} M \\ I \end{bmatrix}^\top P_\pi^\top Q P_\pi \begin{bmatrix} M \\ I \end{bmatrix} \preceq 0 \;\Leftrightarrow\; \begin{bmatrix} M \\ I \end{bmatrix}^\top P_\pi^\top S^\top Q S P_\pi \begin{bmatrix} M \\ I \end{bmatrix} \preceq 0. \tag{4.19}$$

Since Q is block diagonal we obtain

$$S^\top Q S = \left[\begin{array}{ccc|c} X_{R_N(1)} & & & \\ & \ddots & & 0 \\ & & X_{R_N(N)} & \\ \hline & 0 & & -\hat{W} \end{array}\right], \quad \text{with} \quad \hat{W} = \begin{bmatrix} R_D & 0 \\ 0 & R_E \end{bmatrix}^\top W \begin{bmatrix} R_D & 0 \\ 0 & R_E \end{bmatrix}, \tag{4.20}$$

and where the subscripts $R_N(i)$ represent the subsystem to which i gets permuted. Finally, since the equivalence in (4.19) holds for all automorphisms in $Aut(M)$, take the mean over all automorphisms to obtain:

$$\begin{bmatrix} M \\ I \end{bmatrix}^\top P_\pi^\top Q P_\pi \begin{bmatrix} M \\ I \end{bmatrix} \preceq 0 \;\Leftrightarrow\; \begin{bmatrix} M \\ I \end{bmatrix}^\top P_\pi^\top \underbrace{\frac{1}{k}\sum_{i=1}^{k} S_i^\top Q S_i}_{\triangleq \tilde{Q}} P_\pi \begin{bmatrix} M \\ I \end{bmatrix} \preceq 0, \tag{4.21}$$

where $|Aut(M)| = k$, and where each block in $\tilde{Q}$ becomes

$$\tilde{X}_i = \frac{1}{|O_i|}\sum_{j \in O_i} X_j, \quad \text{and} \quad \tilde{W} = \frac{1}{k}\sum_{i=1}^{m} \hat{W}_i. \tag{4.22}$$

Therefore, $\tilde{X}_i = \tilde{X}_j$ for $i \sim j$. □

This lemma implies that (4.7), when feasible, admits a solution satisfying

$$\tilde{X}_i = \tilde{X}_j \;\text{ if }\; i \sim j; \tag{4.23}$$

thus, we may search for one common variable for subsystems in the same orbit. In particular, when M is vertex-transitive (i.e., all the vertices in V_N, V_D and V_E permute with each other) there is only one orbit $\hat{O}_1 = V_N$ and the number of decision variables X_i reduces to one.

Note, however, that in this reduction W is replaced with $\tilde{W}$ in (4.16). Since W specifies the desired performance, and may not be altered, we ask that W be invariant under $Aut(M)$, so that $\tilde{W} = W$.

Assumption 26. *The matrix W is invariant under $Aut(M)$; that is,*

$$\begin{bmatrix} R_D & 0 \\ 0 & R_E \end{bmatrix} W = W \begin{bmatrix} R_D & 0 \\ 0 & R_E \end{bmatrix} \quad \text{for all} \quad (R_N, R_D, R_E) \in Aut(M). \tag{4.24}$$

As an example, suppose we want to certify an L_2-gain bound in the network of Figure 4.2a with the global supply rate $\|d_1\|^2 - \frac{1}{\gamma_1^2}\|e_1\|^2 - \frac{1}{\gamma_2^2}\|e_2\|^2 - \frac{1}{\gamma_3^2}\|e_3\|^2$. If we seek the same gain bound for e_1 and e_3, *i.e.*, $\gamma_1 = \gamma_3$, then the corresponding W is invariant under $Aut(M)$ because the global supply rate is unchanged under the automorphism that permutes e_1 and e_3.

The combination of Lemma 25 with Assumption 26 leads to the following main result:

Theorem 27. *If $(X_1, ..., X_N)$ is an element of the global set $\mathcal{G}$ in* (4.7) *and Assumption 26 holds, then $(\tilde{X}_1, ..., \tilde{X}_N)$ such that $\tilde{X}_i = \tilde{X}_j$ when $i \sim j$ is also an element of $\mathcal{G}$.*

Theorem 27 states that the feasibility of the LMI in (4.7) is not compromised if we reduce the search space to identical supply rates for subsystems in the same orbit. However, demanding a common supply rate in the local constraint sets (4.6) may introduce conservatism. Nevertheless, this conservatism is minimal for systems with near-identical dynamics or with similar dissipativity properties (see the robust dissipativity application in the next section).

In addition to this result, the contrapositive of Lemma 25 provides an infeasibility certificate for the supply rate desired.

Corollary 28. *If there is no solution $(\tilde{X}_1, ..., \tilde{X}_N, \tilde{W})$ to* (4.7) *such that $\tilde{X}_i = \tilde{X}_j$ for $i \sim j$, then no other solution $(X_1, ..., X_N, W)$ exists.*

Remark 29. *For MIMO systems, the definition of automorphism in* (4.11) *changes to the tuple (R_U, R_Y, R_D, R_E), such that $R_U M_{11} = M_{11} R_Y$, where $M_{11} \in \mathbb{R}^{\sum_i m_i \times \sum_i p_i}$, $R_U \in \mathbb{R}^{\sum_i m_i \times \sum_i m_i}$, and $R_Y \in \mathbb{R}^{\sum_i p_i \times \sum_i p_i}$. Instead of interpreting the automorphism as a permutation on the subsystems, we now look for permutations of inputs and outputs for each subsystem. In this case, the P_π matrix in* (4.7) *must be changed accordingly, in the blockwise sense, e.g., the top left block becomes* $\text{blkdiag}(I_{m_1}, O_{p_1}, ..., I_{m_N}, O_{p_N})$. *Moreover, note that $X_i \in \mathbb{R}^{(m_i+p_i)\times(m_i+p_i)}$ and that equality* (4.23) *still holds, but the labeling of u_i and y_i must be chosen appropriately in order to obtain $\tilde{X}_i$ as in Lemma 25.*

When considering the case where all MIMO systems have the same input and output dimensions, i.e., $p_i = m_i = m \ \forall i$, the permutations $R_U = R_Y = R_N \in \mathbb{R}^{mN \times mN}$ can be defined as $R_N = \tilde{R}_N \otimes I_m$, where $\tilde{R}_N \in \mathbb{R}^{N \times N}$, i.e., a permutation of systems.

Reducing the Global LMI to a Quotient LMI

In Lemma 25, we conclude that it is equivalent to analyze the problem as an "averaged" global constraint LMI given by

$$\mathcal{A} \triangleq \begin{bmatrix} M \\ I \end{bmatrix}^\top P_\pi^\top \tilde{Q} P_\pi \begin{bmatrix} M \\ I \end{bmatrix} \preceq 0, \tag{4.25}$$

where $\tilde{Q} = \frac{1}{k}\sum_{i=1}^{k} S_i^\top Q S_i$ for $S_i = \text{blkdiag}(R_N^i \otimes I_2,\, R_D^i,\, R_E^i)$ with $(R_N^i,\, R_D^i,\, R_E^i) \in Aut(M)$. We show that when $\mathcal{A}$ is quasi-positive, apart from reducing the number of decision variables in the global constraint LMI, we can also reduce its dimension.

To explore the symmetric structure of $\mathcal{A}$, we first let r_N, r_d, and r_e be the number of distinct orbits of the vertices V_N, V_D, and V_E, respectively. Then, we define

$$T_I \triangleq \text{blkdiag}(T_N, T_D) \quad \text{and} \quad T_O \triangleq \text{blkdiag}(T_N, T_E), \tag{4.26}$$

where $T_I \in \mathbb{R}^{(N+p_d)\times(r_N+r_d)}$, $T_O \in \mathbb{R}^{(N+m_e)\times(r_N+r_e)}$, with $\{T_N\}_{ij} = 1$ if vertex $i \in V_N$ is in orbit j, and $\{T_N\}_{ij} = 0$ otherwise; and T_D and T_E are defined similarly for vertices in V_D and V_E and their orbits.[1] The symmetry in the interconnection matrix implies that $MT_I = T_O\overline{M}$ where

$$\overline{M} \triangleq (T_O^\top T_O)^{-1} T_O^\top M T_I \tag{4.28}$$

is the *quotient* interconnection matrix. Moreover, due to the symmetry of $\tilde{Q}$, the matrix $\mathcal{A}$ in (4.25) is also symmetric and $\mathcal{A}T_I = T_I\overline{\mathcal{A}}$ where

$$\overline{\mathcal{A}} \triangleq (T_I^\top T_I)^{-1} T_I^\top \mathcal{A} T_I = (T_I^\top T_I)^{-1} \begin{bmatrix} \overline{M} \\ I \end{bmatrix}^\top \overline{P}_\pi^\top \overline{Q}\, \overline{P}_\pi \begin{bmatrix} \overline{M} \\ I \end{bmatrix} \tag{4.29}$$

and where $\overline{P}_\pi \triangleq (T_S^\top T_S)^{-1} T_S^\top P_\pi T$, $\overline{Q} \triangleq T_S^\top Q T_S$, with $T \triangleq \text{blkdiag}(T_O, T_I)$ and $T_S \triangleq \text{blkdiag}(T_N \otimes I_2, T_D, T_E)$. The symmetric property of the LMI condition in (4.25) allows for further reduction.

Proposition 30. *Consider the LMI* (4.25) *and assume that* $\mathcal{A}$ *is a quasi-positive matrix*[2]*. Then*

$$\mathcal{A} \preceq 0 \;\Leftrightarrow \lambda_{max}(\overline{\mathcal{A}}) \leq 0. \tag{4.30}$$

[1] For the example In Figure 4.2a, we have:

$$T_N = \begin{bmatrix} 1 & 0 & 0 & 0 \\ 0 & 1 & 0 & 0 \\ 0 & 0 & 1 & 0 \\ 0 & 0 & 0 & 1 \\ 0 & 0 & 1 & 0 \\ 0 & 1 & 0 & 0 \end{bmatrix} \quad T_D = 1 \quad T_E = \begin{bmatrix} 1 & 0 \\ 0 & 1 \\ 1 & 0 \end{bmatrix} \tag{4.27}$$

[2] A matrix N is said to be *quasi-positive* if $\{N\}_{ij} \geq 0$ for $i \neq j$.

Proof. Since $\mathcal{A}$ is symmetric, it is enough to show that its largest eigenvalue is nonpositive if and only if the largest eigenvalue of $\overline{\mathcal{A}}$ is also nonpositive. Thus, due to quasi-positiveness of $\mathcal{A}$, the proof follows from the claim:

Claim 31. *The largest eigenvalue of $\overline{\mathcal{A}}$ is the largest eigenvalue of $\mathcal{A}$.*

Proof of Claim: First we show that all the eigenvalues of $\overline{\mathcal{A}}$ are also eigenvalues of $\mathcal{A}$. Letting $\overline{\mathcal{A}}\overline{v} = \lambda\overline{v}$ and $v = T_I\overline{v}$ we have

$$\mathcal{A}v = \mathcal{A}T_I\overline{v} = T_I\overline{\mathcal{A}}\overline{v} = \lambda T_I\overline{v} = \lambda v. \tag{4.31}$$

Then, since $\mathcal{A}$ is quasi-positive, it follows from the Perron-Frobenius Theorem that $\lambda_{max}(\mathcal{A})$ has an associated eigenvector that is positive, *i.e.*, $v_M > 0$. Since v_M is positive, the vector $\overline{v}_M = (T_I^\top T_I)^{-1}T_I^\top v_M$ is nonzero and we can show it is an eigenvector of $\overline{\mathcal{A}}$:

$$\begin{aligned}\overline{\mathcal{A}}\overline{v}_M &= (T_I^\top T_I)^{-1}T_I^\top \mathcal{A}T_I\overline{v}_M = (T_I^\top T_I)^{-1}T_I^\top \mathcal{A}T_I(T_I^\top T_I)^{-1}T_I^\top v_M \\ &= (T_I^\top T_I)^{-1}\overline{\mathcal{A}}^\top T_I^\top v_M = \left((T_I^\top T_I)^{-1}T_I^\top\right)\lambda_{max}v_M = \lambda_{max}\overline{v}_M.\end{aligned} \tag{4.32}$$

The third and fourth equalities hold since $T_I^\top\mathcal{A} = T_T^\top\mathcal{A}^\top = \overline{\mathcal{A}}_I^\top T_I^\top$. We conclude that $\lambda_{max}(\mathcal{A}) = \lambda_{max}(\overline{\mathcal{A}})$. □

The following are sufficient conditions that guarantee $\mathcal{A}$ to be quasi-positive.

Claim 32. *Let the interconnection matrix M be nonnegative, with $M_{22} \equiv 0$, and consider quadratic supply rates $X_1, \ldots, X_N$ and W of the form:*

$$X_i = \begin{bmatrix} Q_i & S_i \\ S_i^\top & R_i \end{bmatrix}, \quad i = 1, ..., N \quad \textit{and} \quad W = \begin{bmatrix} Q_0 & S_0 \\ S_0^\top & R_0 \end{bmatrix}.$$

Then, the following conditions on X_i and W guarantee the quasi-positiveness of $\mathcal{A}$ in (4.25)*:*

- *For $k \neq l$, $\{R_i\}_{kl} \geq 0$ (i.e., diagonal elements can be negative);*
- *Q_i, S_i are nonnegative;*
- *For $k \neq l$, $\{Q_0\}_{kl} \leq 0$, $\{R_0\}_{kl} \leq 0$ (i.e. diagonal elements can be positive)[3];*
- *S_0 is nonpositive.*

For each specific interconnection, one can derive less restrictive quasi-positiveness conditions by inspecting the sign structure of $\mathcal{A}$.

[3]If $M_{22} \neq 0$ then R_0 needs to be nonpositive.

Recovering Symmetry with Weight Balancing

In practice the *unweighted* incidence graph of M may possess symmetries which are lost in the weighted graph because the edges are not compatibly weighted. An example is Figure 4.3a where the apparent rotational symmetry is broken unless the weights g_i are identical for each i, and the same holds for g_{d_i} and g_{e_i}. In this case symmetry can be recovered by transforming M into an interconnection $\hat{M}$ with weight redistributions on the edges of M. Indeed, our performance certificate remains valid under the transformation

$$\hat{M} \triangleq \begin{bmatrix} D_N & 0 \\ 0 & D_E \end{bmatrix}^{-1} M \begin{bmatrix} D_N & 0 \\ 0 & D_D \end{bmatrix}, \tag{4.33}$$

where $D_N \in \mathbb{C}^{N\times N}$, $D_D \in \mathbb{C}^{p_d\times p_d}$, and $D_E \in \mathbb{C}^{m_e\times m_e}$ are diagonal and invertible.

Lemma 33. *The LMI in* (4.7) *is satisfied by* $(X_1, ..., X_N, W)$ *with the interconnection matrix* M *if and only if it is satisfied by* $(\hat{X}_1, ..., \hat{X}_N, \hat{W})$ *with the interconnection matrix* $\hat{M}$*, where* $\hat{X}_i = |\{D_N\}_i|^2 X_i$ *and*

$$\hat{W} = \begin{bmatrix} D_D & 0 \\ 0 & D_E \end{bmatrix}^* W \begin{bmatrix} D_D & 0 \\ 0 & D_E \end{bmatrix}. \tag{4.34}$$

An application of Lemma 33 is illustrated in Figure 4.3 where the graph in Figure 4.3a is transformed into the vertex-transitive graph in Figure 4.3b with the weight balancing matrices:

$$\begin{aligned} D_N &= \operatorname{diag}\left(1, \frac{g_2 g_3}{r^2}, \frac{g_3}{r}\right), \\ D_D &= \operatorname{diag}\left(\frac{1}{g_{d_1}}, \frac{g_2 g_3}{g_{d_2} r^2}, \frac{g_3}{g_{d_3} r}\right), \\ D_E &= \operatorname{diag}\left(g_{e_1}, \frac{g_2 g_3 g_{e_2}}{r^2}, \frac{g_3 g_{e_3}}{r}\right), \end{aligned} \tag{4.35}$$

where $r = (g_1 g_2 g_3)^{\frac{1}{3}}$. The performance certification problem then reduces to a single decision variable. When $g_1 g_2 g_3 < 0$, these matrices are complex and the weights throughout the cycle can be balanced to $r = |g_1 g_2 g_3|^{\frac{1}{3}} e^{-i\frac{\pi}{3}}$.

4.4 Large-Scale Performance Certification

Distributed Optimization

In practice, the feasibility problem in (4.10) may be too large to solve directly. This is especially true for polynomial systems where certifying dissipativity requires SOS programming techniques. A more scalable approach to solving this problem is proposed in [80] using distributed optimization techniques to decompose the problem. In this section we demonstrate

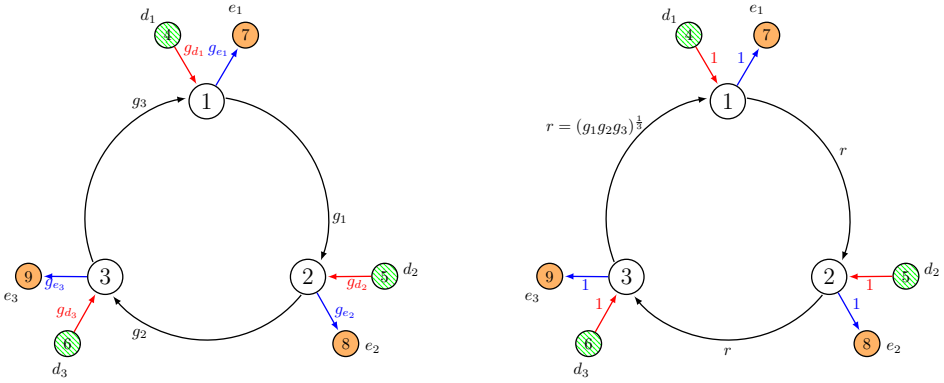

(a) Original interconnection with trivial $Aut(M)$.

(b) Balanced interconnection with a unique orbit $O_1 = V_N$

Figure 4.3: Balancing the weights of the original interconnection M as in (4.33), with (4.35).

that the symmetry reduction can be combined with this technique for further scalability.

Each local constraint in (4.10) depends only on X_i and the dynamics of the relevant subsystem, while the global constraint depends on $(X_1, \ldots, X_N)$. This structure allows the decomposition of the problem into smaller subproblems that are solved iteratively. To decouple the local and global constraints, the authors in [80] use auxiliary variables $(Z_1, \ldots, Z_N)$ to rewrite (4.10) as the following optimization problem

$$\begin{aligned} \underset{X_{1:N}, Z_{1:N}}{\text{minimize}} \quad & \sum_{i=1}^{N} \mathbb{I}_{\mathcal{L}_i}(X_i) + \mathbb{I}_{\mathcal{G}}(Z_1, \ldots, Z_N) \\ \text{subject to} \quad & X_i = Z_i \text{ for } i = 1, \ldots, N \end{aligned} \tag{4.36}$$

where $X_{1:N} \triangleq (X_1, \ldots, X_N)$, $Z_{1:N} \triangleq (Z_1, \ldots, Z_N)$, and the indicator functions $\mathbb{I}_{\mathcal{L}_i}$ and $\mathbb{I}_{\mathcal{G}}$ are defined as

$$\mathbb{I}_{\mathcal{L}_i}(X_i) \triangleq \begin{cases} 0 & X_i \in \mathcal{L}_i \\ \infty & \text{otherwise} \end{cases}, \quad \text{and} \quad \mathbb{I}_{\mathcal{G}}(Z_1, \ldots, Z_N) \triangleq \begin{cases} 0 & (Z_1, \ldots, Z_N) \in \mathcal{G} \\ \infty & \text{otherwise.} \end{cases}$$

We combine Theorem 27 with (4.36) and reduce the problem to

$$\begin{aligned} \underset{\{X_i, Z_i\}_{i=1}^{N}}{\text{minimize}} \quad & \sum_{i=1}^{N} \mathbb{I}_{\mathcal{L}_i}(X_i) + \mathbb{I}_{\mathcal{G}}(Z_1, \ldots, Z_N) \\ \text{subject to} \quad & Z_i = Z_j \text{ for } i \sim j \\ & X_i = Z_i \text{ for } i = 1, \ldots, N. \end{aligned} \tag{4.37}$$

Distributed optimization algorithms, like dual decomposition or the alternating direction method of multipliers (ADMM) [18], can be applied to (4.37). The ADMM algorithm is solved as follows:

1. X-updates: for each i, solve the subsystem problem:

$$X_i^{k+1} = \underset{X \in \mathcal{L}_i}{\arg\min} \left\| X - Z_i^k + U_i^k \right\|_F^2$$

2. Z-update: solve the global problem:

$$\begin{aligned} Z_{1:N}^{k+1} = \underset{Z_{1:N} \in \mathcal{G}}{\arg\min} & \sum_{i=1}^{N} \left\| (X_i^{k+1} - Z_i + U_i^k) \right\|_F^2 \\ \text{subject to} \quad & Z_i = Z_j \text{ for } i \sim j \end{aligned}$$

3. U-update: update U by

$$U_i^{k+1} = X_i^{k+1} - Z^{k+1} + U_i^k$$

   and return to step 1.

Once $(Z_1, \ldots, Z_N)$ satisfy the local constraints, the performance of the system is certified and the algorithm can be terminated. However, it becomes inefficient to check this condition for each subsystem at every iteration, when the number of subsystems is large. Instead, one could check the convergence of the primal and dual residuals, defined as $r_i^{k+1} \triangleq X_i^{k+1} - Z_i^{k+1}$ and $s_i^{k+1} \triangleq Z_i^{k+1} - Z_i^k$, respectively. Solving problem (4.37) using ADMM is guaranteed to converge as $k \to \infty$, if a feasible point exists, [80].

Robust Dissipativity

Local constraints (4.2) for systems with known linear or polynomial dynamics can be casted as SDPs. These formulations can be generalized to the case where the systems depend on uncertain or unknown parameters. For interconnections where the subsystems have the same structure but where their parameter values may vary, it is of interest to provide a certification approach that, given a bound on the range of the unknown parameters, can determine supply rates that satisfy the constraints for all values in the parameter range.

Consider a system of the form

$$\begin{aligned} \dot{x} &= f(x, u, \delta) \\ y &= h(x, u, \delta) \\ \delta &\in \Delta \end{aligned} \tag{4.38}$$

where $\Delta \triangleq \{\delta \in \mathbb{R}^d \mid q_i(\delta) \leq 0 \text{ for } i = 1, \ldots, n_q\}$ is a closed semialgebraic set and $q_i : \mathbb{R}^d \to \mathbb{R}$ are real polynomials. This system is *robustly dissipative* with respect to a quadratic supply

rate defined by the symmetric matrix $X \in \mathbb{R}^{(m+p)\times(m+p)}$ if it is dissipative with respect to this supply rate for all $\delta \in \Delta$. A sufficient condition for robust dissipativity is the existence of a differentiable and nonnegative storage function $V : \mathbb{R}^n \to \mathbb{R}_+$ and nonnegative functions $r_i : \mathbb{R}^{n+m+d} \to \mathbb{R}_+$ such that

$$\nabla V(x)^\top f(x,u,\delta) - \begin{bmatrix} u \\ y \end{bmatrix}^\top X \begin{bmatrix} u \\ y \end{bmatrix} - \sum_{i=1}^{n_q} r_i(x,u,\delta) q_i(\delta) \leq 0 \tag{4.39}$$

for all $x \in \mathbb{R}^n$, $u \in \mathbb{R}^m$, $\delta \in \mathbb{R}^d$, and $y = h(x,u,\delta)$.

The symmetry approach described above is particularly useful when certifying robust dissipativity. Consider the case where multiple subsystems are in the same orbit, under the action of $Aut(M)$. If such subsystems have identical structure but if their parameter values are distinct, or uncertain, then it is possible to search simultaneously for a supply rate and a storage function certifying robust dissipativity for all these subsystems. This, significantly reduces the size of the problem and is especially beneficial if there are many similar systems in the same orbit.

4.5 Examples

Vehicle Platoon We analyze the disturbance attenuation properties of a vehicle platoon [21, 28, 80], where each vehicle's control input depends on the relative distances between its position and that of its neighbors. The dynamics of the i^{th} vehicle is described by

$$\dot{v}_i(t) = -v_i(t) + v_i^{\text{nom}} + u_i(t)$$

where $v_i(t)$ is the vehicle velocity, v_i^{nom} the nominal velocity, and $u_i(t)$ the control input.

The interconnection of vehicles is represented by a connected, bidirectional, acyclic graph, where L links interconnect N vehicles. See the platoon example in Figure 4.4(top), where d_1 is an additive disturbance on u_3, and e_i are the performance outputs which correspond to the velocity of the respective vehicles.

Letting $p_\ell(t)$ be the relative displacement between the vehicles connected by link ℓ gives $\dot{p}_\ell(t) = v_i(t) - v_j(t)$ where i is the leading node and j is the trailing node. Define $D \in \mathbb{R}^{N\times L}$ as

$$D_{i\ell} \triangleq \begin{cases} 1 & \text{if } i \text{ is the leading node of edge } \ell \\ -1 & \text{if } i \text{ is the trailing node of edge } \ell \\ 0 & \text{otherwise,} \end{cases}$$

so that D maps the vehicles velocities to the relative velocities of each link which we define as η:

$$\eta(t) \triangleq \dot{p}(t) = D^\top v(t). \tag{4.40}$$

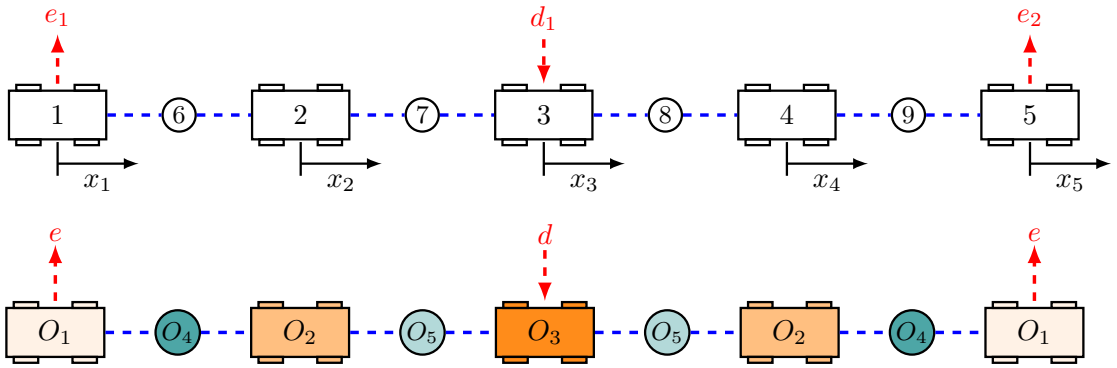

Figure 4.4: Vehicle platoon with linear topology. Each vehicle measures the relative distance of all vehicles connected to it by a link (dotted line) (top). Reduction due to the symmetry along the middle vehicle (bottom).

Consider a class of control laws that encompass those presented in [21, 28]:

$$u_i(t) = -\sum_{\ell=1}^{L} D_{i\ell}\phi_\ell(p_\ell(t))$$

where $\phi_\ell : \mathbb{R} \to \mathbb{R}$ is increasing and surjective, but otherwise unknown. This assumption guarantees the existence of an equilibrium point $p_\ell = p_\ell^\star$, $v_i = v^\star$ for the interconnected system [21]. Letting $\tilde{p}_\ell \triangleq p_\ell - p_\ell^\star$, the dynamics of the ℓ^{th} link Λ_ℓ is then given by

$$\Lambda_\ell : \begin{cases} \dot{\tilde{p}}_\ell(t) = \eta_\ell(t) \\ z_\ell(t) = \phi_\ell(\tilde{p}_\ell(t) + p_\ell^\star) + \phi_\ell(p_\ell^\star) \end{cases} \qquad \ell = 1, \dots, L$$

with input $\eta_\ell(t)$ and output $z_\ell(t)$. Note that, each Λ_ℓ subsystem is dissipative with supply rate matrix $X = \left[\begin{smallmatrix} 0 & 1 \\ 1 & 0 \end{smallmatrix}\right]$. Similarly, we let $\tilde{v}_i(t) \triangleq v_i(t) - v^\star$ and $\tilde{u}_i(t) \triangleq u_i(t) - u_i^\star$ where $u^\star = D\phi(p^\star)$ so that the vehicle dynamics are

$$\Sigma_i : \begin{cases} \dot{\tilde{v}}_i(t) = -v_i(t) + \tilde{u}_i(t) \\ y_i(t) = \tilde{v}_i(t) \end{cases} \qquad i = 1, \dots, N$$

with input $\tilde{u}_i(t)$ and output $y_i(t)$. In the following computations the supply rates of each Λ_ℓ are fixed and the supply rates of each Σ_i are decision variables.

The interconnected system can then be represented as in the block diagram in Figure 4.5 where $\Sigma = \text{blkdiag}(\Sigma_1, \dots, \Sigma_N)$ and $\Lambda = \text{blkdiag}(\Lambda_1, \dots, \Lambda_L)$.

We now exploit the symmetric topology of the vehicle platoon using the results of the previous sections. Consider a platoon of $N = 101$ vehicles with the interconnection depicted

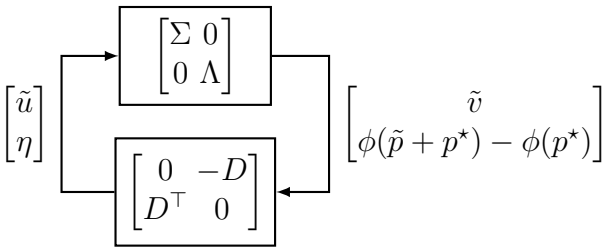

Figure 4.5: Block diagram of the vehicle platoon dynamics.

in Figure 4.4 and where the nominal velocity of each vehicle is randomly chosen. To numerically test our reduction algorithm we apply a disturbance d to the 51-st vehicle and investigate the L_2-gain from disturbance d to the velocity output of the first and last vehicles, designated as the performance variables e_1 and e_2. This configuration allows us to exploit the symmetry of the interconnection about the center vehicle (Figure 4.4) reducing the number of unique supply rates in the global LMI constraint from 101 to 51. Since the supply rate X_i for each vehicle has three unique entries, the number of decision variables reduces from 303 to 153.

Using the ADMM algorithm and the symmetry reduction we certify that the L_2-gain from d to e is not greater than 1. In fact, the original ADMM algorithm cannot certify a smaller gain; hence, for this example the symmetry reduction does not add extra conservatism.

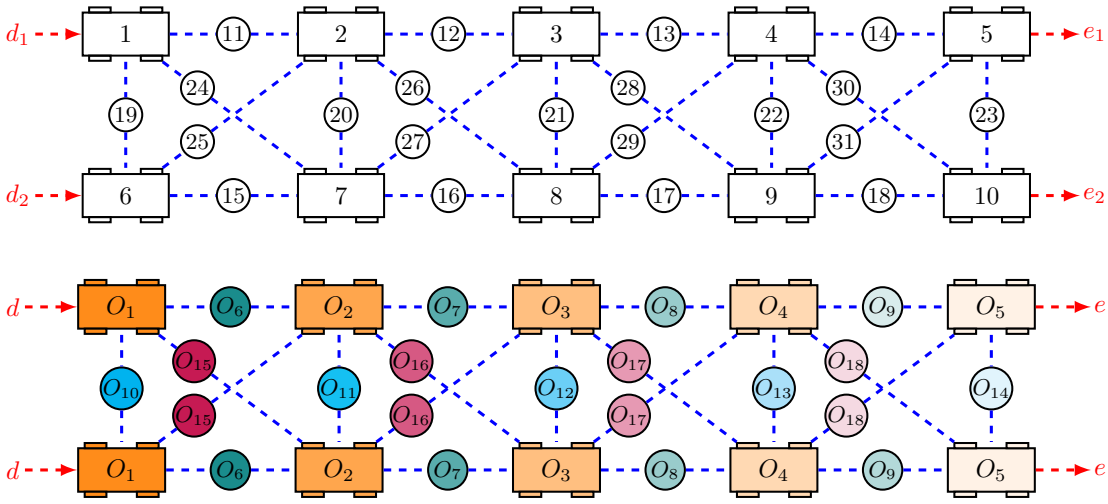

Figure 4.6: Two-lane vehicle platoon (top), and respective symmetry reduction (bottom).

Another interesting example of a symmetric topology is a two-lane interconnection where, in addition to communicating with the vehicles in front and behind, each vehicle also communicates with the three vehicles on the other lane, Figure 4.6. In this example, there exists

a symmetry along the longitudinal line that divides the two lanes. This allows the reduction of the problem to a single lane linear platoon topology, *i.e.*, 1 and 6 are in O_1, 2 and 7 are in O_2, 3 and 8 are in O_3, and so on.

Large-Scale Polynomial Example Consider a cyclically interconnected system, as in Figure 4.2b, where each subsystem has a disturbance input and performance output. The N subsystems are described by

$$H_i : \begin{cases} \dot{x}_1(t) = x_2(t) \\ \dot{x}_2(t) = \dfrac{-a_i x_2(t) - b_i x_1(t)^3 + u_i(t) + d_i(t)}{1 + c_i x_2(t)^2} \\ y_i(t) = e_i(t) = x_2(t) \end{cases}$$

where $a_i, b_i, c_i > 0$ are parameters, $d_i(t)$ is the input disturbance, and $e_i(t)$ the exogenous output. For $N = 100$ subsystems we certified an L_2-gain bound from d to e using three different methods: (1) ADMM without symmetry reduction; (2) ADMM with symmetry reduction; and (3) robust analysis with symmetry reduction.

The parameters a_i, b_i, and c_i are chosen uniformly from the interval $[1.1,\ 1.2]$ so that the subsystems are all different. For each method we certify subsystem dissipativity using SOS programming with a quartic storage function.

Without symmetry reduction, the ADMM algorithm certifies that the system has an L_2-gain less than 0.58. By taking advantage of the interconnection symmetry, the number of supply rate matrices reduces from 100 to 1, thus reducing the number of decision variables in the global constraint from 300 to 3, one for each unique entry in the symmetric matrix $X_i \in \mathbb{R}^{2\times 2}$. In this case, ADMM certifies that the system has an L_2-gain less than 0.64. While this bound is more conservative, solving the global constraint takes $25-30\%$ less time, specifically, 5.0 seconds on average compared to 7.1 seconds [4]. This reduction is especially beneficial since the global constraint must be solved multiple times (in this case, the ADMM algorithm ran in 12 iterations).

For the robust analysis, the subsystems parameters a_i, b_i, and c_i are uncertain but contained in the interval $[1.1,\ 1.2]$. This method also certifies that the system has an L_2-gain less than 0.64. Since, in this case, there is only one local constraint, the problem can be solved directly without decomposing the problem. Therefore, it takes less then 10 seconds to solve both the local and global constraints simultaneously.

Computational Considerations

In the previous examples, we see that the symmetry reduction provides a modest reduction in the solution time of the global constraint. The reason for this is because the computa-

[4] computations were performed on a desktop computer with a 2.8 GHz Intel i7-860 processor. The problem was formulated in MATLAB and the SDP was solved with SDPT3 [102].

tional complexity for solving a semidefinite program (SDP) depends not only on the number of decision variables v, but also on the dimension of the semidefinite cone s and the sparsity of the problem. For the global constraint (4.7) we have $v = \frac{1}{2}\sum_{i=1}^{N}(p_i + m_i + 1)(p_i + m_i)$ and $s = p_d + \sum_{i=1}^{N} p_i$. The symmetry reduction applied greatly reduces v but s is unchanged.

However, as discussed in the second part of Section 4.3, under certain conditions, it is possible to reduce the global LMI to a quotient LMI, which effectively implies a reduction in the dimension of the SDP cone, s. It is shown in Proposition 30 that, since the LMI has the same symmetric structure as the interconnection matrix M, when the left hand side of the LMI is quasi-positive, the certification of the LMI (4.7) with original dimension $s = p_d + \sum_{i=1}^{N} p_i$ reduces to $r_d + \sum_{i=1}^{r_N} p_i$, where r_d and r_N are the number of distinct orbits in V_D and V_N, respectively.

Even though the primal-dual interior point methods used to solve SDPs have polynomial complexity [103], they can still become computationally intractable for large problems. In fact, these algorithms are guaranteed to converge to an ϵ-suboptimal solution in $\mathcal{O}\left(\sqrt{s}\log\left(\frac{1}{\epsilon}\right)\right)$ iterations and for each iteration the computational complexity is given by $\alpha v^2 s^2 + \beta v s^3 + \gamma v^3 + \mathcal{O}(vs^2 + v^2 s + s^3)$, where $\alpha, \beta, \gamma > 0$ are constants that depend on the search direction of the specific algorithm [83]. The dimensionality reduction on both v and s are of particular interest for an actual fast certification of large scale interconnections.

Examples

Polynomial: Consider again the polynomial example in Section 4.5 and note that the left hand side of the LMI in (4.7) is quasi-positive for this interconnection if the local supply rate matrices are of the form $\left[\begin{smallmatrix} x^i_{11} & x^i_{12} \\ x^i_{12} & -x^i_{22} \end{smallmatrix}\right]$ where $x^i_{11}, x^i_{12}, x^i_{22} \geq 0$. Therefore, by constraining the local supply rates to be of this form the dimension of the LMI in the global constraint can be reduced from 200 to 2. Combining this reduction with the ADMM algorithm allows the global problem to be solved in less than 0.1 seconds. For the robust analysis the local and global problem can be solved simultaneously in less than 0.5 seconds.

Table 4.1 compares the size of the problem for each certification method used. Specifically, N is the number of local problems that must be solved, v is the number of decision variables in the global constraint LMI, and s is the size of this LMI.

Platoon: This LMI reduction can also be applied to the vehicle platoon example with interconnection as in Figure 4.4. For this case, we consider supply rates X_i of the form $\left[\begin{smallmatrix} 0 & x^i_{12} \\ x^i_{12} & -x^i_{22} \end{smallmatrix}\right]$, where $x^i_{12}, x^i_{22} \geq 0$, which guarantee quasi-positiveness for the left hand side of the LMI in (4.7). Then, in addition to the reduction in the number of decision variables, the dimension of the global LMI is reduced from 202 (101 vehicles, 100 links, and 1 disturbance) to 102 (51 vehicles, 50 links, and 1 disturbance) without introducing additional conservatism.

Table 4.1: Dimensionality comparison for various performance certification methods.

Method	N	v	s	Gain Bound
ADMM	100	300	200	0.58
ADMM + Sym. Reduction	100	3	200	0.64
ADMM + Quotient Reduction	100	3	2	0.64
Robust Analysis + Sym. Reduction	1	3	200	0.64
Robust Analysis + Quotient Reduction	1	3	2	0.64

4.6 Extension to Integral Quadratic Constraints (IQCs)

IQCs are a generalization of the dissipativity framework that capture frequency dependent properties of a system. Here we employ a state-space variant of IQCs [104, 91] and let $(\hat{A}, \hat{B}, \hat{C}, \hat{D})$ be the realization of a stable LTI system Ψ with input $\left[\begin{smallmatrix} u \\ y \end{smallmatrix}\right]$, state η, and output z, and let X be a real symmetric matrix. The system of the form (4.3) satisfies the IQC defined by $\Pi = \Psi^* X \Psi$ if there exists a positive semidefinite storage function $V(x, \eta)$ such that

$$\begin{aligned} \nabla_x V(x,\eta)^\top f(x,u) + \nabla_\eta V(x,\eta)^\top \left(\hat{A}\eta + \hat{B} \begin{bmatrix} u \\ h(x,u) \end{bmatrix} \right) \leq \\ \leq \left(\hat{C}\eta + \hat{D} \begin{bmatrix} u \\ h(x,u) \end{bmatrix} \right)^\top X \left(\hat{C}\eta + \hat{D} \begin{bmatrix} u \\ h(x,u) \end{bmatrix} \right) \end{aligned} \tag{4.41}$$

for all $x \in \mathbb{R}^n$ and $u \in \mathbb{R}^m$. Dissipativity is recovered when $\Psi = I_{m+p}$.

The approach in the previous subsection can be extended to the performance certification of an interconnected system with respect to a global IQC of the form $\Pi_W \triangleq \Psi_W^* W \Psi_W$, where Ψ_W is a stable linear system with realization $(\hat{A}_W, \hat{B}_W, \hat{C}_W, \hat{D}_W)$, and W is a real symmetric matrix, both specified by the user.

First redefine the local constraint sets as

$$\mathcal{L}_i \triangleq \{ X_i \mid \exists V_i(x_i, \eta_i) \succeq 0 \ \text{ such that (4.41) holds} \} \tag{4.42}$$

where η_i is the state of a stable linear system Ψ_i specified by the analyst and the symmetric matrix X_i is a decision variable. Next let $(\hat{A}_i, \hat{B}_i, \hat{C}_i, \hat{D}_i)$ be a state-space realization of Ψ_i, and redefine the global constraint set as:

$$\mathcal{G} = \left\{ X_1, ..., X_N \;\middle|\; \exists P \succeq 0 \ \text{ s.t. } \begin{bmatrix} \hat{A}^\top P + P\hat{A} & P\hat{B} \\ \hat{B}^\top P & 0 \end{bmatrix} + \begin{bmatrix} \hat{C}^\top \\ \hat{D}^\top \end{bmatrix} Q \begin{bmatrix} \hat{C}^\top \\ \hat{D}^\top \end{bmatrix}^\top \preceq 0 \right\} \tag{4.43}$$

where $Q = \text{blkdiag}(X_1, ..., X_N, -W)$ and

$$\begin{aligned}
\hat{A} &\triangleq \text{blkdiag}(\hat{A}_1, ..., \hat{A}_N, \hat{A}_W) \\
\hat{B} &\triangleq \text{blkdiag}(\hat{B}_1, ..., \hat{B}_N, \hat{B}_W) P_\pi \begin{bmatrix} M \\ I \end{bmatrix} \\
\hat{C} &\triangleq \text{blkdiag}(\hat{C}_1, ..., \hat{C}_N, \hat{C}_W) \\
\hat{D} &\triangleq \text{blkdiag}(\hat{D}_1, ..., \hat{D}_N, \hat{D}_W) P_\pi \begin{bmatrix} M \\ I \end{bmatrix}
\end{aligned} \tag{4.44}$$

form a state-space realization of the stable linear system Ψ with input $\left[\begin{smallmatrix} u \\ d \end{smallmatrix}\right]$. Note that if the IQCs are static (*i.e.*, $\hat{A}$, $\hat{B}$, $\hat{C}$ have dimension 0) and $\hat{D} = P_\pi \left[\begin{smallmatrix} M \\ I \end{smallmatrix}\right]$, then the local and global constraints simplify to (4.6) and (4.7), respectively.

Under the following assumptions, the automorphisms of the interconnection matrix M provide a dimensionality reduction in the number of variables of the global constraint (4.43).

Assumption 34. *The state-space realizations for the stable linear system Ψ_i, $i = 1, ..., N$, used in the IQCs $\Psi_i^* X_i \Psi_i$, and given by $(\hat{A}_i, \hat{B}_i, \hat{C}_i, \hat{D}_i)$ are identical for systems in the same orbit, under the action of $Aut(M)$.*

Assumption 35. *The state-space realization for the stable linear system Ψ_W given by $(\hat{A}_W, \hat{B}_W, \hat{C}_W, \hat{D}_W)$ is symmetric with respect to the input permutations $R_U = \text{blkdiag}(R_D, R_E)$, i.e., there exist permutation matrices R_X and R_Y such that*

$$\hat{A}_W R_X = R_X \hat{A}_W, \quad \hat{B}_W R_U = R_X \hat{B}_W, \quad \hat{C}_W R_X = R_Y \hat{C}_W, \quad \hat{D}_W R_U = R_Y \hat{D}_W. \tag{4.45}$$

The next Corollary is the IQC counterpart of Lemma 25. To simplify the notation, we assume that the state-space realizations of each Ψ_i, $i = 1, ..., N$ have the same dimension, where $\hat{A}_i \in \mathbb{R}^{q \times q}$, $\hat{B}_i \in \mathbb{R}^{q \times 2}$, $\hat{C}_i \in \mathbb{R}^{l \times q}$, and $\hat{D}_i \in \mathbb{R}^{l \times 2}$. The Corollary still holds when the dimensions are different but the matrices S_X and S_Y need to be appropriately modified.

Corollary 36. *Let the Assumptions (34) and (35) hold. If the LMI defined in (4.43) is satisfied by $(X_1, ..., X_N, W)$ with $P \succeq 0$ then it is also satisfied by $(\tilde{X}_1, ..., \tilde{X}_N, \tilde{W})$, with $\tilde{X}_i = \tilde{X}_j$ if $i \sim j$, and $\overline{P} = \frac{1}{k} \sum_{i=1}^{m} S_X^{iT} P S_X^i$, where $S_X^i = \text{blkdiag}(R_N^i \otimes I_q, R_X^i)$, $(R_N^i, R_U^i) \in Aut(M)$, and R_X^i is as in (4.45).*

Remark 37. *The size of P depends on the dimension of the state-space realization of the IQCs and therefore can be very large. Corollary 36 shows that $\overline{P}$ and $\overline{Q}$ are also solutions of the LMI in (4.43) that have repeated elements. The reduction on the number of variables for the block diagonal matrix $\overline{Q}$ is the same as before. The diagonal variables of $\overline{P}$ repeat in a similar way, i.e., $\{\overline{P}\}_{kk} = \{\overline{P}\}_{ll}$ if elements $k, l \in (V_N, V_D, V_E)$ are in the same orbit. The off-diagonal elements of $\overline{P}$ repeat with the following pattern: $\{\overline{P}\}_{ij} = \{\overline{P}\}_{kl}$ if there exists a permutation $R \triangleq (R_N, R_X)$ consistent with $Aut(M)$ such that $Re_i = e_k$ and $Re_j = e_l$ or such that $Re_i = e_l$ and $Re_j = e_k$.*

Corollary 36. First note that due to the Assumptions above, the following holds for each automorphism in $Aut(M)$:

$$\begin{bmatrix} \hat{C}^\top \\ \hat{D}^\top \end{bmatrix}^\top = S_Y \begin{bmatrix} \hat{C}^\top \\ \hat{D}^\top \end{bmatrix}^\top \begin{bmatrix} S_X^\top & 0 \\ 0 & R_R^\top \end{bmatrix}$$

where $S_Y \triangleq \text{blkdiag}(R_N \otimes I_l, R_Y)$ and

$$\begin{bmatrix} A^\top P + PA & PB \\ B^\top P & 0 \end{bmatrix} = \begin{bmatrix} S_X & 0 \\ 0 & R_R \end{bmatrix} \begin{bmatrix} \hat{A}^\top \overline{P} + \overline{P}\hat{A} & \overline{P}\hat{B} \\ \hat{B}^\top \overline{P} & 0 \end{bmatrix} \begin{bmatrix} S_X^\top & 0 \\ 0 & R_R^\top \end{bmatrix}$$

where $R_R \triangleq \text{blkdiag}(R_N \otimes 2, R_U)$. Then, the proof follows from the equivalence

$$\begin{bmatrix} \hat{A}^\top P + P\hat{A} & P\hat{B} \\ \hat{B}^\top P & 0 \end{bmatrix} + \begin{bmatrix} \hat{C}^\top \\ \hat{D}^\top \end{bmatrix} Q \begin{bmatrix} \hat{C}^\top \\ \hat{D}^\top \end{bmatrix}^\top \preceq 0 \Leftrightarrow \begin{bmatrix} \hat{A}^\top \overline{P} + \overline{P}\hat{A} & \overline{P}\hat{B} \\ \hat{B}^\top \overline{P} & 0 \end{bmatrix} + \begin{bmatrix} \hat{C}^\top \\ \hat{D}^\top \end{bmatrix} \overline{Q} \begin{bmatrix} \hat{C}^\top \\ \hat{D}^\top \end{bmatrix}^\top \preceq 0 \tag{4.46}$$

with $\overline{Q} = S_Y^\top Q S_Y$. □

4.7 Stability Certification

We can certify stability of the interconnected system with a modification of the local and global constraints sets. In this case, since we don't consider the effect of the exogenous inputs d and outputs e, the performance supply rate term W in (4.7) vanishes, and the global LMI reduces to

$$\mathcal{G} \triangleq \left\{ X_1, ..., X_N \;\middle|\; \begin{bmatrix} M_{11} \\ I_p \end{bmatrix}^\top \tilde{P}_\pi^\top Q_X \tilde{P}_\pi \begin{bmatrix} M_{11} \\ I_p \end{bmatrix} \preceq 0 \right\} \tag{4.47}$$

where $Q_X = \text{blkdiag}(X_1, ..., X_N)$ and $\tilde{P}_\pi$ maps (u, y) to $(u_1, y_1, \ldots, u_N, y_N)$. Since the global Lyapunov function needs to be positive definite, the local storage functions V_i that verify the local constraint in (4.6) must also be positive definite.

Similarly, for the IQC case the matrices $\hat{A}$, $\hat{B}$, $\hat{C}$, and $\hat{D}$ in (4.44) drop the terms $\hat{A}_W$, $\hat{B}_W$, $\hat{C}_W$, and $\hat{D}_W$ of the state-space realization of Ψ_W, M reduces to M_{11}, and P_π to $\tilde{P}_\pi$. The local constraint sets in (4.42) also need to hold for positive definite storage functions.

As discussed in Section 4.3, we may also look for weight redistributions of M to search for interconnections with a richer set of automorphisms. For stability certification, we only require the invertible diagonal matrices D_N and the interconnection becomes $\hat{M} = D_N^{-1} M D_N$.

For example a cyclic interconnection with weights $g_1, \ldots, g_N$ (as in Figure 4.3 but with no inputs or outputs) can be transformed into a vertex-transitive graph. By choosing $D_N = \text{diag}\left(1, \frac{g_2 \cdots g_N}{r^{(N-1)}}, \ldots, \frac{g_N}{r}\right)$ the cyclic interconnection $\hat{M}$ becomes balanced and all weights

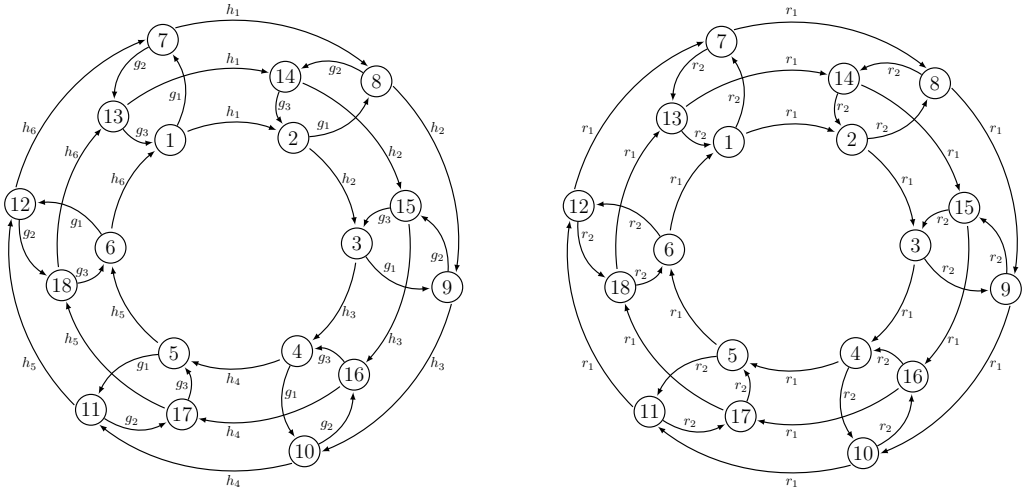

(a) (b)

Figure 4.7: Balancing a torus network (a) into a vertex-invariant interconnection (b).

equal to $r = (g_1 \dots g_N)^{\frac{1}{N}}$.

This can also be applied to a torus graph, as in Figure 4.7a, with $M = I_{n_1} \otimes M_{n_2} + M_{n_1} \otimes I_{n_2}$. The matrices M_{n_1} and Mn_2 are as in the cyclic case with n_1 and n_2 elements, and weights $h_1, ..., h_{n_1}$ and $g_1, ..., g_{n_2}$, respectively. Let $D_1 = \text{diag}\left(1, \frac{h_2 \dots h_{n_1}}{r_1^{(n_1-1)}}, ..., \frac{h_{n_1}}{r_1}\right)$ and $D_2 = \text{diag}\left(1, \frac{g_2 \dots g_{n_2}}{r_2^{(n_2-1)}}, ..., \frac{g_{n_2}}{r_2}\right)$ to obtain $\hat{M} = (D_1 \otimes D_2)^{-1} M (D_1 \otimes D_2) = (I_{n_1} \otimes \hat{M}_{n_2} + \hat{M}_{n_1} \otimes I_{n_1})$ which is also vertex-transitive.

4.8 Conclusions

Symmetry reduction techniques were applied to stability and performance certification of interconnected systems. The reduction decreases the number of decision variables and the size of the global constraint to greatly improve the computational performance of the certification method. We demonstrated that this reduction, when combined with distributed optimization and robust dissipativity, can be used in the analysis of very large interconnections without introducing excessive conservatism. In some graph interconnections, symmetry can be recovered through weight balancing (diagonal similarity transformation), which can be used together with the certification method proposed.

Chapter 5

Stability Certification of Large-Scale Stochastic Systems using Dissipativity

In this chapter, we represent large-scale nonlinear stochastic systems as an interconnection of lower-order stochastic dynamical subsystems. We then certify stability based on appropriate stochastic passivity properties of the subsystems and the structure of their interactions.

Previous studies have shown the effectiveness of this approach for deterministic models of biological networks, [10, 9, 62]. In [10], global asymptotic stability of a cyclic interconnection structure is established from the diagonal stability of a dissipativity matrix that incorporates information about the passivity properties of the subsystems and the interconnection structure of the network. The results are extended in [9] to a more general interconnection structure. Both [10, 9] exploit output strict passivity (OSP) properties and corresponding storage functions of the subsystems, and construct a composite Lyapunov function for the interconnection using these storage functions.

Deterministic models of biochemical reaction may be inadequate, particularly when the copy numbers of the species are small. Stochasticity appears as external noise (due to cell-to-cell variability of external signals) and as intrinsic noise (since chemical reactions depend on random motion). While external noise can be incorporated in noise-driven deterministic models, *i.e.* stochastic differential equations (SDEs), internal noise is accounted for by a Chemical Master Equation models (CME). Under appropriate assumptions, [54], it is common to perform a diffusion approximation of the CME, leading to the Chemical Langevin Equation (CLE), which is a particular type of SDE. Thus, both internal and external noise can be treated jointly with SDEs.

In this chapter, we explore large-scale nonlinear stochastic models described by SDEs. We extend the passivity approach in [10, 9] to the stochastic framework, by using an expansion of the definitions of passivity, [16, 45]. We prove stability in probability for an interconnection of stochastic OSP (sOSP) subsystems, if an appropriate diagonal stability condition

holds for a dissipativity matrix similar to the one in [10]. Early references, such as [81, 82], constructed composite Lyapunov functions for stochastic stability. However, as is common in the classical large-scale systems literature, these references restrict the magnitude of the coupling terms without regard to their sign structure. The passivity-based approach in the present chapter takes advantage of the negative feedback loops in the network to obtain less restrictive stability criteria.

We next investigate the notion of Noise-to-State stability (NSS), defined in [67], which is a stochastic counterpart of deterministic input-to-state stability, [95]. NSS implies that if there exists a bound in the noise variance, the state of a NSS system is also bounded in probability. This notion is less restrictive than stochastic stability in the sense that it accommodates systems with nonvanishing noise at the equilibrium, and unknown noise intensity. First, we provide a new sufficient condition for NSS that is easy to verify. We then introduce a new input-output definition that combines NSS and OSP properties, referred to as NSS$\oplus$OSP. We show that the interconnected system is NSS if the diagonal stability of a similar dissipativity matrix is ascertained.

Since passivity properties are defined in reference to the equilibrium, which depends on the full network, the verification of the sOSP and NSS$\oplus$OSP properties of the subsystems is a major difficulty encountered in the methodology presented. In [10], equilibrium-independent results for the verification of OSP properties are provided. In this chapter, we derive stochastic passivity conditions for sOSP and NSS$\oplus$OSP that do not rely on the knowledge of the equilibrium, which are not considered in the classical literature.

In Section 5.1, we provide the necessary notation and definitions, and derive sufficient conditions for NSS. The main results for stochastic stability of interconnected systems are presented in Section 5.2, where stability in probability and noise-to-state stability are achieved. In Section 5.3, we focus on the input/output passivity properties of the systems, by deriving equilibrium-independent conditions that guarantee sOSP and NSS$\oplus$OSP. Finally, in Section 5.4, we illustrate the application of the results obtained to classes of biological reaction networks.

5.1 Preliminaries

Consider the following nonlinear stochastic system

$$dx = f(x)dt + l(x)\Sigma dw \tag{5.1}$$

where $x(t) \in \mathbb{R}^n$ is the state vector, $w(t)$ is an r-dimensional independent standard Wiener process, $\Sigma = \{\sigma_{ij}\}$ is an $r \times r$ nonnegative-definite matrix, and σ_{ij} represents the intensity with which the j^{th} source of uncertainty influences the i^{th} state. Assume that the vector field and matrix function $f : \mathbb{R}^n \to \mathbb{R}^n$ and $l : \mathbb{R}^n \to \mathbb{R}^{n\times r}$ are locally Lipschitz continuous.

For the notions of stochastic stability and passivity, defined in Sections 5.1 and 5.1, we assume $\Sigma = I$ because $l(x)$ can be redefined to incorporate the constant Σ. Moreover, we also assume $f(0) = 0$ and $l(0) = 0$, so that $x(t) \equiv 0$ is a solution for the system. However, for the notion of noise-to-state stability, defined in Section 5.1, where Σ is treated as an unknown, the assumption $\Sigma = I$ is dropped, and also $l(x)$ is not necessarily required to be vanishing at the origin ($l(0) \neq 0$).

Notation and definitions: For a matrix $A \in \mathbb{R}^{p\times q}$, the *Frobenius Norm*, $|\cdot|_F : \mathbb{R}^{p\times q} \to \mathbb{R}_{\geq 0}$, is defined as $|A|_F = \sqrt{\mathrm{Tr}\{A^\top A\}} = \sqrt{\sum_{i=1}^{p}\sum_{j=1}^{q}|a_{ij}|^2}$. A scalar continuous function $\alpha : \mathbb{R}_{\geq 0} \to \mathbb{R}_{\geq 0}$ is said to be *class* $\mathcal{K}$ if it is strictly increasing and $\alpha(0) = 0$. It is *class* $\mathcal{K}_\infty$ if, in addition, $\lim_{s\to\infty}\alpha(s) = \infty$. A scalar continuous function $\beta : \mathbb{R}_{\geq 0} \times \mathbb{R}_{\geq 0} \to \mathbb{R}_{\geq 0}$ is *class* $\mathcal{KL}$ if, for each fixed t, function $\beta(\cdot, t)$ is class $\mathcal{K}$ and, for each fixed s, function $\beta(s, \cdot)$ is decreasing and $\lim_{t\to\infty}\beta(s, t) = 0$. Given functions $a : \mathbb{R} \to \mathbb{R}$ and $b : \mathbb{R} \to \mathbb{R}$, the expression $a(s) = O(b(s))$ as $s \to \infty$ means that $\exists K > 0 \in \mathbb{R}$ and $\exists x_0 \in \mathbb{R}$ such that $|a(x)| \leq K|b(x)|$ $\forall x > x_0$. Analogously, the expression $a(s) = o(b(s))$ as $s \to \infty$ means that $\forall K > 0 \in \mathbb{R}$, $\exists x_0 \in \mathbb{R}$ such that $|a(x)| \leq K|b(x)|$ $\forall x > x_0$, or equivalently, $\lim_{s\to\infty}|a(s)/b(s)| = 0$. Given a continuous function $f : \mathbb{R} \to \mathbb{R}_{\geq 0}$, we denote by:

$$\overline{f}(x) = \sup_{|s|\leq|x|} f(s) \quad \text{and} \quad \underline{f}(x) = \inf_{|s|\geq|x|} f(s). \tag{5.2}$$

Clearly, $\overline{f}$ and $\underline{f}$ are nondecreasing functions. Note that, $f^2(x) : x \to f(x)f(x)$, and so $\overline{f^2}(x) : x \to \overline{f(x)f(x)}$.

Stochastic Stability

An extensive coverage of stochastic stability and stochastic Lyapunov theorems exists in the literature, [59, 70]. In what follows, we refer to [31] where a notation based on class $\mathcal{K}$ functions is used, instead of the classical $\epsilon - \delta$.

Definition 38. *The equilibrium $x = 0$ of system (5.1) is:*
(i) Globally Stable in Probability if $\forall\epsilon > 0$, $\exists\gamma \in \mathcal{K}$ such that

$$P\{|x(t)| \leq \gamma(|x_0|)\} \geq 1 - \epsilon, \qquad \forall t \geq 0, \forall x_0 \in \mathbb{R}^n. \tag{5.3}$$

(ii) Globally Asymptotically Stable in Probability if it is globally stable in probability and

$$P\left\{\lim_{t\to\infty}|x(t)| = 0\right\} = 1, \qquad \forall x_0 \in \mathbb{R}^n. \tag{5.4}$$

Proposition 39. *For system (5.1), with $\Sigma = I$, suppose there exists a $\mathcal{C}^2$ function $V : \mathbb{R}^n \to \mathbb{R}_{\geq 0}$, class $\mathcal{K}_\infty$ functions α_1, α_2, and a continuous nonnegative function $S : \mathbb{R}^n \to \mathbb{R}_{\geq 0}$, such that for all $x \in \mathbb{R}^n$,*

$$\alpha_1(|x|) \leq V(x) \leq \alpha_2(|x|) \tag{5.5}$$

$$\mathcal{L}V(x) \triangleq \frac{\partial V}{\partial x} f(x) + \frac{1}{2} Tr\left\{ l(x)^\top \frac{\partial^2 V}{\partial x^2} l(x) \right\} \leq -S(x). \tag{5.6}$$

Then, the equilibrium $x = 0$ is globally stable in probability. If S is a positive definite function, the equilibrium $x = 0$ is globally asymptotically stable in probability, [66].

Stochastic Passivity and Output Strict Passivity

Consider now the controlled stochastic nonlinear system

$$\begin{cases} dx = (f(x) + g(x)u)\, dt + l(x)\Sigma dw \\ \quad y = h(x) \end{cases} \tag{5.7}$$

where $x(t) \in \mathbb{R}^n$ is the state, $u(t) \in \mathbb{R}^m$ is the control input, and $y(t) \in \mathbb{R}^m$ is the output. The control input u may be seen as a function of t that satisfies appropriate regularity properties so as to obtain existence and uniqueness of solutions. However, we do not need to specify these regularity properties in this chapter, since the only place were inputs are used is in defining passivity and other stability properties. These properties are defined in terms of algebraic inequalities involving Lyapunov-like functions and only pointwise values of x and u, so that regularity of $u(t)$ as a function of t is not relevant. On the other hand, when interconnecting several systems, $u(t)$ becomes a function of the subsystems' state variables, and the closed-loop system is assumed to satisfy the conditions assumed for (5.1). Next, we use the notion of stochastic passivity, discussed in Chapter 1.

Definition 40. *The system (5.7), with $\Sigma = I$, is said to be stochastic passive, [45], if there exists a $\mathcal{C}^2$ positive definite function $V : \mathbb{R}^n \to \mathbb{R}_{\geq 0}$, such that $\forall x \in \mathbb{R}^n$, and $\forall u \in \mathbb{R}^m$,*

$$EV(x(t)) - V(x(s)) \leq E \int_s^t h(x(\tau))^\top u(\tau) d\tau - E \int_s^t S(x(\tau)) d\tau \tag{5.8}$$

where $S : \mathbb{R}^n \to \mathbb{R}_{\geq 0}$ is a positive semidefinite function. Equivalently,

$$\begin{aligned} \mathcal{L}V(x) &= \frac{\partial V}{\partial x}^\top (f(x) + g(x)u) + \frac{1}{2} Tr\left\{ l(x)^\top \frac{\partial^2 V}{\partial x^2} l(x) \right\} \\ &\leq h(x)^\top u - S(x). \end{aligned} \tag{5.9}$$

The system is said to be stochastic strictly passive if the function S can be picked positive definite, [71], and stochastic output strictly passive (sOSP) if

$$S(x) = \frac{1}{\gamma} h(x)^\top h(x), \tag{5.10}$$

for some constant $\gamma > 0$, which we refer to as a "gain".

When $l(x) \equiv 0$, Definition 40 recovers the deterministic notions of passivity, strict passivity, and output strict passivity (OSP). From Dynkin's formula, [36], we conclude that the notion of sOSP is similar, in terms of expectation, to the notion of OSP, since

$$E\int_0^t h(x(\tau))^\top u(\tau)d\tau \geq E\int_0^t \mathcal{L}\mathcal{V}(x(\tau))d\tau = E(V(x(t))) - V(x(0)) \geq -V(x(0)). \quad (5.11)$$

Proposition 41 (Stochastic Kalman-Yakubovich-Popov)**.** *The system is passive (or strictly passive) if and only if the following holds:*

$$\begin{cases} \dfrac{\partial V}{\partial x}^\top f(x) + \dfrac{1}{2}Tr\left\{l(x)^\top \dfrac{\partial^2 V}{\partial x^2} l(x)\right\} \leq 0 \quad \left(-\dfrac{1}{\gamma}h(x)^\top h(x)\right) \\ \dfrac{\partial V}{\partial x}^\top g(x) = h(x)^\top. \end{cases} \quad (5.12)$$

Note that with $u \equiv 0$, Equation 5.9 implies asymptotic stability in probability of the sOSP system. Further results have been provided in the stochastic framework relating passivity with stability and feedback stabilization, see [45, 71].

Noise-To-State Stability

In this section, we discuss systems that may have nonvanishing noise ($l(0) \neq 0$) and unknown noise intensity Σ. We use the notion of noise-to-state stability (NSS) which guarantees that for any noise covariance, there exists a probability bound on the system's state, [67]. To accommodate unknown noise intensity, we drop the assumption $\Sigma = I$ used in the previous sections.

Definition 42. *(adapted[1] from [31]) For the nonlinear stochastic system* (5.1)*, suppose there exists a $\mathcal{C}^2$ function $V : \mathbb{R}^n \to \mathbb{R}_{\geq 0}$, and class $\mathcal{K}_\infty$ functions α_1, α_2, α_3 and ρ such that*

$$\alpha_1(|x|) \leq V(x) \leq \alpha_2(|x|) \quad (5.13)$$

and, for all nonnegative definite matrices $\Sigma \in \mathbb{R}^{r\times r}$,

$$\begin{aligned} \mathcal{L}V(x,\Sigma) &= \frac{\partial V}{\partial x}f(x) + \frac{1}{2}Tr\left\{\Sigma^\top l(x)^\top \frac{\partial^2 V}{\partial x^2} l(x)\Sigma\right\} \\ &\leq -\alpha_3(|x|) + \rho(|\Sigma\Sigma^\top|_F). \end{aligned} \quad (5.14)$$

Then, the system is said to be noise-to-state stable (NSS) and $V(x)$ is called a noise-to-state Lyapunov function.

[1] In [31], inequality (5.14) is equivalently stated as: $|x| \geq \rho(|\Sigma\Sigma^\top|_F) \Rightarrow \mathcal{L}V(x,\Sigma) \leq -\alpha(x)$, where ρ, $\alpha \in \mathcal{K}_\infty$.

In the special case that $\alpha_3(|x|) \geq cV(x)$ for some constant $c > 0$, the following inequality holds from [31, Thm4.1]:

$$E[V(x(t))] \leq e^{-ct}V(x_0) + c^{-1}\rho\left(|\Sigma\Sigma^\top|_F\right). \tag{5.15}$$

Therefore, from the Markov inequality[2], and from inequality (5.13) it is easy to conclude that, for any $\epsilon > 0$, there exists a $\mathcal{KL}$ function β, and a $\mathcal{K}_\infty$ function δ, such that:

$$P\left\{|x| < \beta(|x_0|, t) + \delta\left(|\Sigma\Sigma^\top|_F\right)\right\} \geq 1 - \epsilon \quad \forall t \geq 0. \tag{5.16}$$

This shows that the state of the system is bounded in probability. In the next Proposition we derive an easy to verify sufficient condition for NSS.

Proposition 43. *The nonlinear stochastic system* (5.1) *is noise-to-state stable if there exists a $\mathcal{C}^2$ function $V : \mathbb{R}^n \to \mathbb{R}_{\geq 0}$ satisfying* (5.13)*, a continuous strictly increasing function $\eta : \mathbb{R}_{\geq 0} \to \mathbb{R}_{\geq 0}$, and a class $\mathcal{K}_\infty$ function α, such that:*

$$\frac{\partial V(x)}{\partial x} f(x) \leq -\alpha(|x|), \quad \left| l(x)^\top \frac{\partial^2 V(x)}{\partial x^2} l(x) \right|_F \leq \eta(|x|) \tag{5.17}$$

and

$$\eta(s) = o(\alpha(s)) \text{ as } s \to \infty. \tag{5.18}$$

Proof. From the assumptions, $\mathcal{L}V(x, \Sigma)$ satisfies

$$\begin{aligned}
\mathcal{L}V(x,\Sigma) &= \frac{\partial V(x)}{\partial x} f(x) + \frac{1}{2}\mathrm{Tr}\left\{\Sigma^\top l(x)^\top \frac{\partial^2 V(x)}{\partial x^2} l(x)\Sigma\right\} \\
&= \frac{\partial V(x)}{\partial x} f(x) + \frac{1}{2}\mathrm{Tr}\left\{\Sigma\Sigma^\top l(x)^\top \frac{\partial^2 V(x)}{\partial x^2} l(x)\right\} \\
&\leq \frac{\partial V(x)}{\partial x} f(x) + \frac{1}{2}\left|\Sigma\Sigma^\top\right|_F \left| l(x)^\top \frac{\partial^2 V(x)}{\partial x^2} l(x) \right|_F \\
&\leq -\alpha(|x|) + \eta(|x|)|z|
\end{aligned}$$

where $z = \frac{1}{2}|\Sigma\Sigma^\top|_F$, and the first inequality follows from the matrix Cauchy-Schwarz inequality, [75] (*i.e.*, for any two real matrices A, B of the same order, $(\mathrm{Tr}\{A^\top B\})^2 \leq \mathrm{Tr}\{A^\top A\}\mathrm{Tr}\{B^\top B\}$).
If $\lim_{s\to\infty} \eta(s) = c < \infty$, the proof is straightforward, since $\mathcal{L}V \leq -\alpha(|x|) + c|z|$. When $\lim_{s\to\infty} \eta(s) = \infty$, define $\tilde{\eta}(\cdot) = \eta(\cdot) - \eta(0)$. Clearly, $\tilde{\eta}$ is a class $\mathcal{K}_\infty$ function. Therefore, $\mathcal{L}V(x, \Sigma)$ is upper bounded by

$$\begin{aligned}
\mathcal{L}V(x,\Sigma) &\leq -\alpha(|x|) + \eta(0)|z| + \tilde{\eta}(|x|)|z| \\
&\leq -\alpha(|x|) + (\eta(0) + \theta^{-1}(|z|))|z| + \tilde{\eta}(|x|)\theta(\tilde{\eta}(|x|))
\end{aligned}$$

[2]The Markov inequality states that for any random variable X and any constant $a > 0$, $P(|X| \geq a) \leq E|X|/a$.

where θ is a class $\mathcal{K}_\infty$ function to be selected.
Now, let $q_0(s) = \inf_{r \geq s} \frac{\alpha(r)}{\tilde{\eta}(r)}$ for $s > 0$. Since α and $\tilde{\eta}$ are positive and continuous, $q_0(s)$ is well-defined and continuous for $s > 0$. Moreover, by construction, $q_0(s)$ is non-decreasing and positive. From the definition of $\tilde{\eta}$, $\lim_{s\to\infty} \frac{\alpha(s)}{\tilde{\eta}(s)} = \lim_{s\to\infty} \frac{\alpha(s)}{\eta(s)-\eta(0)} \geq \lim_{s\to\infty} \frac{\alpha(s)}{\eta(s)}$. Given that $\eta(s) = o(\alpha(s))$ as $s \to \infty$, $\lim_{s\to\infty} \frac{\alpha(s)}{\tilde{\eta}(s)} = \infty$ which means that $q_0(s) \to \infty$ as $s \to \infty$.
Since $q_0(s)$ is non-decreasing and goes to infinity with s, there exists a class $\mathcal{K}_\infty$ function $q(s)$ such that $q(s) \leq q_0(s)\ \forall s > 0$. Since $q_0(s) = \inf_{r \geq s} \frac{\alpha(r)}{\tilde{\eta}(r)} \leq \frac{\alpha(s)}{\tilde{\eta}(s)}\ \forall s > 0$, then $q(s)\tilde{\eta}(s) \leq \alpha(s)$ $\forall s \in [0, \infty)$.
Finally, choose $\theta \in \mathcal{K}_\infty$ to be $\theta(\cdot) = \frac{1}{2}q(\tilde{\eta}^{-1}(\cdot))$, so that $\theta(\tilde{\eta}(\cdot)) = q(\cdot)/2$. The inequality becomes:

$$\begin{aligned} \mathcal{L}V(x, \Sigma) &\leq -\tfrac{1}{2}\alpha(|x|) + |z|(\theta^{-1}(|z|) + \eta(0)) \\ &= -\tfrac{1}{2}\alpha(|x|) + \rho(|\Sigma\Sigma^\top|_F), \end{aligned} \tag{5.19}$$

with $\mathcal{K}_\infty$ function $\rho(s) = \frac{1}{2}s\left(\theta^{-1}(\frac{1}{2}s\right) + \eta(0))$. The system is thus noise-to-state stable as in (5.14). □

The proposition above provides a new tool that simplifies the verification of NSS. Note that in the definition of NSS, the second term in condition (5.14) has Σ and x coupled, while Proposition 43 is only dependent on x.

5.2 Stochastic and Noise-to-State Stability of Interconnected Systems

Consider an interconnection of stochastic dynamical *"subsystems"* H_i, $i = 1, ..., N$, given by

$$H_i : \begin{cases} dx_i &= (f_i(x_i) + g_i(x_i)u_i)\, dt + l_i(x_i)\Sigma_i dw_i \\ y_i &= h_i(x_i) \end{cases} \tag{5.20}$$

where, for each subsystem H_i, $x_i \in \mathbb{R}^{n_i}$ is the state vector, $u_i \in \mathbb{R}^m$ the input, $y_i \in \mathbb{R}^m$ the output, and Σ_i a $r_i \times r_i$ nonnegative definite matrix. The coupling of the subsystems is described by:

$$u = (M \otimes I_m)y \tag{5.21}$$

where $u = [u_1^\top, ..., u_N^\top]^\top$, $y = [y_1^\top, ..., y_N^\top]^\top$, and $M \in \mathbb{R}^{N\times N}$. In the same manner, let $x = [x_1^\top, ..., x_N^\top]^\top$. Furthermore, assume $f_i(0) = 0$ and $h_i(0) = 0$, so that the resulting interconnected system has an equilibrium at the origin.

Stochastic Stability of Interconnected Systems

In the following theorem, we give a matrix condition that guarantees stochastic stability for an interconnection of sOSP subsystems:

Theorem 44. *For the interconnected system described in* (5.20)-(5.21)*, with* $\Sigma_i = I_{r_i}$ $i = 1, ..., N$*, assume that each dynamical subsystem* H_i *is stochastic output strictly passive, as in Definition 40, with gain* γ_i*, and storage function satisfying* (5.5)*. If there exists a diagonal matrix* $D = \text{diag}(d_1, ..., d_N) > 0$ *such that:*

$$D(M - \Gamma) + (M - \Gamma)^\top D \leq 0 \tag{5.22}$$

where $\Gamma = \text{diag}(\gamma_1^{-1}, ..., \gamma_N^{-1})$*, then the interconnected system is globally stable in probability.*

Proof. Let $V(x) = \sum_{i=1}^N d_i V_i(x_i)$, where V_i is as in (5.9) for each H_i. Then,

$$\begin{aligned}
\mathcal{L}V(x) &= \sum_{i=1}^N d_i \frac{\partial V_i}{\partial x_i}\left(f_i(x_i) + g_i(x_i)u_i\right) + \frac{1}{2} d_i \Sigma_i^\top l_i(x_i)^\top \frac{\partial^2 V_i}{\partial x_i^2} l_i(x_i)\Sigma_i^\top \\
&\leq \sum_{i=1}^N -\frac{1}{\gamma_i} d_i y_i^\top y_i + d_i y_i^\top u_i \\
&= -y^\top \left(\begin{bmatrix} d_1\gamma_1^{-1} & & \\ & \ddots & \\ & & d_N\gamma_N^{-1} \end{bmatrix} \otimes I_m \right) y + y^\top \left(\begin{bmatrix} d_1 & & \\ & \ddots & \\ & & d_N \end{bmatrix} M \otimes I_m \right) y
\end{aligned}$$

and,

$$\begin{aligned}
\mathcal{L}V(x) &\leq -\frac{1}{2} y^\top [(D\Gamma + \Gamma D) \otimes I_m] y + \frac{1}{2} y^\top [(DM + M^\top D) \otimes I_m] y \\
&= y^\top \left[\left(D(M - \Gamma) + (M - \Gamma)^\top D \right) \otimes I_m \right] y.
\end{aligned}$$

Thus, from assumption (5.22), $\mathcal{L}V(x) \leq 0$ $\forall x \in \mathbb{R}^{n_1 + ... n_N}$, the origin is globally stable in probability. □

Note that, since $\mathcal{L}V$ is bounded by a quadratic form in $y = h(x)$, we can only conclude that $\mathcal{L}V$ is negative semidefinite. A stochastic version of LaSalle's principle is available [76] and proves, under additional assumptions, convergence in probability to the largest invariant set where $\mathcal{L}V(x) = 0$. However, without resorting to LaSalle's principle, negative definiteness of $\mathcal{L}V$ follows under additional conditions.

Corollary 45. *For the interconnected system described in* (5.20)-(5.21) *assume that the conditions of Theorem 44 hold. The interconnected system is globally asymptotic stable in probability if either one of the following conditions holds: (i)* $h_i(s) = 0 \implies s = 0$ *for* $i = 1, ..., n$*, and* (5.22) *holds with strict inequality; (ii)* (5.22) *is not necessarily strict but, for each subsystem* H_i*, the inequality in* (5.12) *holds with* $S_i(s) = \frac{1}{\gamma_i} h_i(s)^\top h_i(s) + W_i(s)$*, where* W_i *is a positive definite function.*

The classical Passivity Theorem [114] proves stability (and passivity, when exogenous inputs are present) for a negative feedback interconnection of two passive systems. A stochastic version of this result follows from Theorem 44.

Corollary 46. *Let H_1 and H_2 be stochastic output strictly passive dynamical systems with gains γ_1, γ_2, described by the stochastic differential equation in* (5.20)*. If (i) $u_1 = -y_2$ and $u_2 = y_1$ then, for the interconnected system, the origin is stable in probability. If (ii) $u_1 = v_1 - y_2$ and $u_2 = v_2 + y_1$, the interconnected system is passive with respect to the input-output pair (v, y).*

Proof. For case (i), note that for $D = I_2$,

$$M = \begin{bmatrix} 0 & -1 \\ 1 & 0 \end{bmatrix} \Rightarrow D(M-\Gamma) + (M-\Gamma)^\top D = \begin{bmatrix} -2\gamma_1^{-1} & 0 \\ 0 & -2\gamma_2^{-1} \end{bmatrix} < 0.$$

For case (ii), the interconnection is given instead by:

$$u = \begin{bmatrix} 0 & -1 \\ 1 & 0 \end{bmatrix} y + v$$

where $v = [v_1\ v_2]^\top$. Therefore, by choosing D as before, $D(M-\Gamma) + (M-\Gamma)^\top D < 0$. From the proof of Theorem 44 we get $\mathcal{L}V \leq y^\top v$. □

Noise-To-State Stability of Interconnected Systems

In this section, we deal with an interconnection of stochastic subsystems with unknown noise intensity. We show that (5.22) guarantees NSS for an interconnection of subsystems which satisfy the following property:

Definition 47. *The stochastic dynamical system* (5.7) *is called NSS⊕OSP if it has a storage function $V : \mathbb{R}^n \to \mathbb{R}_{\geq 0}$ satisfying* (5.13) *and:*

$$\begin{aligned} \frac{\partial V}{\partial x} f(x) &\leq -\alpha(|x|) - \frac{1}{\gamma} h(x)^\top h(x), \\ \frac{\partial V}{\partial x} g(x) = h(x)^\top \quad &\text{and} \quad \left| l(x)^\top \frac{\partial^2 V}{\partial x^2} l(x) \right|_F \leq \eta(|x|) \end{aligned} \tag{5.23}$$

where $\gamma > 0$ is a constant, referred to as "gain", $\alpha \in \mathcal{K}_\infty$, and $\eta : \mathbb{R}_{\geq 0} \to \mathbb{R}_{\geq 0}$ is a strictly increasing continuous function, satisfying $\eta(s) = o(\alpha(s))$ as $s \to \infty$.

To see why we refer to this property as NSS⊕OSP, note that the first and third conditions in (5.23) guarantee NSS for the uncontrolled system (*cf.*, Proposition 43). Likewise, the first and second conditions imply OSP for the deterministic part of the system.

Remark 48. *To illustrate the distinction between sOSP and NSS⊕OSP we analyze the following scalar system:*

$$\begin{cases} dx &= (-x+u)dt + l(x)\sigma dw \\ y &= x. \end{cases}$$

NSS⊕OSP ⇏ sOSP: Let $l(x) = \sqrt{|x|}$. The storage function $V(x) = \frac{1}{2}x^2$ satisfies (5.23) with $\alpha(|x|) = \frac{1}{2}x^2$, and $\eta(|x|) = |x|$. Since $\eta(s) = o(\alpha(s))$ as $s \to \infty$, the system is NSS⊕OSP. However, the system is not sOSP since, the second condition in (5.12) prohibits a different choice of $V(x)$, for which the first condition fails when $|x| < \frac{\sigma^2}{2}$.
sOSP ⇏ NSS⊕OSP: Let $l(x) = x$. It is easy to verify that the system is sOSP. However, it is not NSS⊕OSP since, for $V(x) = \frac{1}{2}x^2$, we have $\alpha(x) \leq (1 - \frac{1}{\gamma})x^2$ with $\gamma > 1$, and $\eta \geq x^2$. This implies that $\eta(s) \neq o(\alpha(s))$ as $s \to \infty$.
This elucidates the differences between sOSP and NSS⊕OSP. While sOSP requires $\eta(x) \leq \alpha(x)$ in the entire domain, NSS⊕OSP only requires $\eta(x) \leq \alpha(x)$ for large enough x. On the other hand, NSS⊕OSP requires $\alpha(\cdot)$ to grow asymptotically faster than $\eta(\cdot)$, while sOSP may hold when $\alpha(\cdot)$ and $\eta(\cdot)$ are of the same order.

Theorem 49. *For the interconnected system described in (5.20)-(5.21), assume that each dynamical subsystem H_i is NSS⊕OSP, as in Definition 47, with gain γ_i. If there exists a diagonal matrix $D = \mathrm{diag}(d_1, ..., d_N) > 0$ satisfying inequality (5.22), where $\Gamma = \mathrm{diag}(\gamma_1^{-1}, ..., \gamma_N^{-1})$, then the interconnected system is noise-to-state stable.*

Proof. Let $V(x) = \sum d_i V_i(x_i)$, then

$$\begin{aligned}
\mathcal{L}V(x,\Sigma) &= \sum_{i=1}^{N} d_i \mathcal{L}V_i \\
&\leq \sum_{i=1}^{N} d_i \left(-\alpha_i(|x_i|) - \frac{1}{\gamma_i} h_i(x_i)^\top h_i(x_i) \right) + \sum_{i=1}^{N} d_i \left(h_i(x_i)^\top u_i + \frac{1}{2}\eta_i(|x_i|)|\Sigma_i \Sigma_i^\top|_F \right) \\
&= \sum_{i=1}^{N} d_i \left(-\alpha_i(|x_i|) + \frac{1}{2}\eta_i(|x_i|)|\Sigma_i \Sigma_i^\top|_F \right) + \frac{1}{2} y^\top \left[(D(M-\Gamma) + (M-\Gamma)^\top D) \otimes I_m \right] y \\
&\leq \sum_{i=1}^{N} d_i \left(-\alpha_i(|x_i|) + \eta_i(|x_i|)|z_i| \right) \qquad (5.24)
\end{aligned}$$

where $z_i = \frac{1}{2}|\Sigma_i \Sigma_i|_F$, and the last inequality follows from assumptions on D,M, and Γ.
Let, $J, I \subset \{1, ..., N\}$ be such that $J = \{j \in \{1, ..., N\} |\ \lim_{s\to\infty} \eta_j(s) = c_j < \infty\}$ and $I = J^c = \{i \in \{1, ..., N\} |\ \lim_{s\to\infty} \eta_i(s) = \infty\}$. Since $\eta_i(s) = o(\alpha_i(s))$ as $s \to \infty$, there exist $\theta_i \in \mathcal{K}_\infty$, $i \in I$, such that the next inequality follows as in the derivations leading to (5.19):

$$\mathcal{L}V \leq -\frac{1}{2}\sum_{i=1}^{N} d_i \alpha_i(|x_i|) + \sum_{j\in J} d_j c_j |z_j| + \sum_{i\in I} d_i |z_i| \left(\theta_i^{-1}(|z_i|) + \eta_i(0) \right).$$

Let

$$\tilde{\alpha}(r) = \min_{|x|\geq r} \sum_{i=1}^{N} d_i \alpha_i(|x_i|).$$

Clearly, $\tilde{\alpha}(|x|) \leq \sum d_i \alpha_i(|x_i|)$, $\tilde{\alpha}$ is nondecreasing, and $\tilde{\alpha}(0) = 0$. As $|x| \to \infty$, $|x_i| \to \infty$ for at least one i, which implies that $\tilde{\alpha}(r) \to \infty$. Therefore, $\exists \alpha \in \mathcal{K}_\infty$ such that $\alpha(r) \leq \tilde{\alpha}(r)\ \forall r \in \mathbb{R}_{\geq 0}$.
Now, choose

$$\rho_i(s) = \begin{cases} \frac{c_i}{2} s, & i \in J \\ (\theta_i^{-1}(\frac{1}{2}s) + \eta_i(0))\frac{1}{2}s, & i \in I \end{cases}$$

where, since $|z_i| \leq |z|$ and $\theta_i^{-1} \in \mathcal{K}_\infty$, we know that $\rho_i(|z|) \geq \rho_i(|z_i|)$. Let $\rho(|z|) = \sum_{i=1}^N d_i \rho_i(|z|) \geq \sum_{i=1}^N d_i \rho_i(|z_i|)$, and $\rho \in \mathcal{K}_\infty$. The inequality becomes,

$$\mathcal{L}V \leq -\frac{1}{2}\alpha(|x|) + \rho(|\Sigma\Sigma^\top|_F), \tag{5.25}$$

and thus the interconnected system is noise-to-state stable as in (5.14). □

Theorems 44 and 49 divide the problem of certifying stability properties of a large-sscale nonlinear system into two tractable steps. Step one is to identify dissipativity properties, such as sOSP or NSS⊕OSP, as an abstraction of the detailed dynamical model of the subsystems. Step two is to establish the feasibility of the linear matrix inequality (5.22), for which various computational methods exist [20, 58]. Tools for the verification of dissipation properties, for step one, are provided in the next section.

5.3 Verifying sOSP and NSS⊕OSP

Sufficient Conditions for One-Dimensional Systems with Nonzero Equilibrium

We now present conditions that guarantee the sOSP and the NSS⊕OSP properties for a scalar stochastic dynamical system. The goal is to apply such results to interconnected systems as in the previous section. As a simplifying assumption, we assume $g(x) = g$ is a constant, and without loss of generality $g = 1$ because the interconnection matrix M can be modified to incorporate a different value of g.
Consider again H_i, one of the nonlinear stochastic subsystems defined in (5.20), with $x_i \in \mathbb{R}$, $y_i \in \mathbb{R}$, $u_i \in \mathbb{R}$, $g_i(x_i) \equiv 1$, and where the inputs u_i are given by the feedback relation in (5.21). We drop the assumption that $f_i(0) = 0$, $h_i(0) = 0$, and assume instead that the deterministic part of (5.20) has an unique equilibrium point at x^*. This means that

$$0 = f_i(x_i^*) + u_i^*,$$

where u_i^* is the i^{th} entry of $u^* = My^*$. By taking the coordinate change $\tilde{(.)} = (.) - (.)^*$, we obtain:

$$\begin{cases} d\tilde{x}_i &= (\tilde{f}_i(\tilde{x}_i) + \tilde{u}_i)dt + \tilde{l}_i(\tilde{x}_i)\Sigma_i dw_i \\ \tilde{y}_i &= \tilde{h}_i(\tilde{x}_i) \end{cases} \tag{5.26}$$

where $\tilde{h}_i(\tilde{x}_i) = h_i(\tilde{x}_i + x_i^*) - h_i(x_i^*)$, $\tilde{l}_i(\tilde{x}_i) = l_i(\tilde{x}_i + x_i^*)$, $\tilde{f}_i(\tilde{x}_i) = f_i(\tilde{x}_i + x_i^*) - f_i(x_i^*)$, and, hence, $\tilde{f}_i(0) = 0$ and $\tilde{h}_i(0) = 0$. In what follows, we drop the subscript i to simplify the notation.

Corollary 50. ***(sOSP)*** *For each stochastic subsystem in* (5.26)*, with* $x, y, u \in \mathbb{R}$*,* $\Sigma = 1$*,* $l(x^*) = 0$*, and* h *differentiable, assume that* $\forall x \neq x^*$*:*

(A1) $(x - x^*)(h(x) - h(x^*)) > 0$ *and* $(x - x^*)(f(x) - f(x^*)) < 0$*;*

(A2) *There exists a constant* $\gamma > 0$ *such that*

$$\frac{f(x) - f(x^*)}{h(x) - h(x^*)} + \frac{1}{2}h'(x)\left(\frac{\|l(x)\|_2}{h(x) - h(x^*)}\right)^2 \leq -\frac{1}{\gamma}, \tag{5.27}$$

where $h'(x) \triangleq \frac{\partial h}{\partial x}$*.*

Then, the system is stochastic output strictly passive.

Proof. Let

$$V(x) = \int_{x^*}^{x} (h(s) - h(x^*))\, ds \tag{5.28}$$

which is positive definite, from (A1). Therefore, $\frac{\partial V}{\partial x} = h(x) - h(x^*)$ and $\frac{\partial^2 V}{\partial x^2} = \frac{\partial h(x)}{\partial x}$. Hence, from assumption (A2), inequality (5.9) holds, and the system is sOSP. □

Corollary 51. ***(NSS⊕OSP)*** *Consider a stochastic subsystem as described in* (5.26)*, with* $x, y, u \in \mathbb{R}$*,* $g(x) = 1$*, and* $h \in \mathcal{C}^1$*. Assume the following holds:*

(B1) $f(\cdot)$ *and* $h(\cdot)$ *are such that*

$$(x - x^*)(h(x) - h(x^*)) > 0 \text{ and } (x - x^*)(f(x) - f(x^*)) < 0,\ \forall x \neq x^*; \tag{5.29}$$

(B2) *There exists a constant* $\hat{\gamma} > 0$ *such that*

$$\frac{f(x) - f(x^*)}{h(x) - h(x^*)} \leq -\frac{1}{\hat{\gamma}} \quad \forall x \neq x^*; \tag{5.30}$$

(B3) $l(\cdot)$*,* $h(\cdot)$*, and* $f(.)$ *are such that*

$$|(h(x) - h(x^*))(f(x) - f(x^*))| \to \infty \text{ as } |x| \to \infty, \tag{5.31}$$

and that $\forall i, j = 1, ..., r$*,*

$$\overline{|h'(x)l_i(x)l_j(x)|} = o\left(\underline{|(h(x) - h(x^*))(f(x) - f(x^*))|}\right) \text{ as } |x| \to \infty. \tag{5.32}$$

Then, the system is NSS⊕OSP for any $\gamma > \hat{\gamma}$*.*

Proof. Without loss of generality, assume that $x^* = 0$. Let $V(x)$ be given as in (5.28), so that the equality condition in (5.23) holds, and $\frac{\partial V}{\partial x} f + \frac{1}{\hat{\gamma}} h^\top h = hf + \frac{1}{\hat{\gamma}} h^2$. Choose some constant $\gamma > \hat{\gamma}$ so that, from assumption (B2),

$$hf + \frac{1}{\gamma} h^2 < 0 \quad \forall x \neq 0. \tag{5.33}$$

Moreover, from (B2) and (B1), we know that, $hf + \frac{1}{\gamma} h^2 = \frac{\hat{\gamma}+(\gamma-\hat{\gamma})}{\gamma} hf + \frac{1}{\gamma} h^2 \leq \frac{\gamma-\hat{\gamma}}{\gamma} hf \leq 0$, *i.e.*,

$$|hf + \frac{1}{\gamma} h^2| \geq \frac{\gamma - \hat{\gamma}}{\gamma} |hf|. \tag{5.34}$$

Then, $\underline{|hf + \frac{1}{\gamma} h^2|} \geq \frac{\gamma-\hat{\gamma}}{\gamma} \underline{|hf|}$, and from assumption (B3), $\forall i, j = 1, ...r$,

$$\overline{|h'(x) l_i(x) l_j(x)|} = o\left(\underline{|h(x)f(x) + \tfrac{1}{\gamma} h^2(x)|}\right) \text{ as } |x| \to \infty. \tag{5.35}$$

Using relation (5.35) we will show that there exist functions α and η as defined in (5.23) such that $\eta(s) = o(\alpha(s))$ as $s \to \infty$. The following lemmas construct such functions.

Lemma 52. *Consider a continuous function $m : \mathbb{R} \to \mathbb{R}$ such that $m(x) < 0$ $\forall x \neq 0$, and $m(x) \to -\infty$ as $|x| \to \infty$. Then, there exists a $\mathcal{K}_\infty$ function α such that $m(x) \leq -\alpha(|x|)$ and $\underline{|m(x)|} = O(\alpha(|x|))$ as $|x| \to \infty$.*

Lemma 53. *Consider a continuous function $f : \mathbb{R} \to \mathbb{R}_{\geq 0}$. There exists a strictly increasing function $\eta : \mathbb{R}_{\geq 0} \to \mathbb{R}_{\geq 0}$ such that $f(x) \leq \eta(|x|)$ and $\eta(|x|) = O(\overline{f(x)})$ as $|x| \to \infty$.*

From Lemma 53, consider

$$\eta(|x|) \geq \sum_{i,j=1}^{r} |h'(x) l_i(x) l_j(x)| \geq |h'(x)| \sqrt{\sum_{i,j=1}^{r} |l_i(x) l_j(x)|^2} = \left| l(x)^\top \frac{\partial^2 V}{\partial x^2} l(x) \right|_F,$$

and $\eta(|x|) = O(\overline{\sum_{i,j=1}^{r} |h'(x) l_i(x) l_j(x)|})$ as $|x| \to \infty$. Likewise, we can choose α from Lemma 52 with $m(x) = h(x)f(x) + \frac{1}{\gamma} h(x)^2$. Note that function $hf + \frac{1}{\gamma} h^2$ satisfies conditions of Lemma 52, from (5.33)-(5.34) and the assumption that $|hf| \to \infty$. Finally, from (5.35) and properties of α and η we conclude that, as $|x| \to \infty$,

$$\eta(|x|) = O(\sum_{i,j=1}^{r} \overline{|h'(x)||l_i(x) l_j(x)|}) = o\left(\underline{|h(x)f(x) + \tfrac{1}{\gamma} h^2(x)|}\right) = o(\alpha(|x|)).$$

The system is thus NSS$\oplus$OSP, with constant $\gamma > \hat{\gamma}$, as in Definition 47. □

Proof of Lemma 53. Let (a_i, b_i) be the intervals where $\overline{f}$ is not increasing. Choose a constant $K > 0$. For each interval i, let ϵ_i be such that $0 < \epsilon_i < a_{i+1} - b_i$, $\overline{f}(b_i + \epsilon_i) - \overline{f}(a_i) \leq K$, and such that the intersection between the function $\overline{f}$ and the straight line passing through

$(a_i, \overline{f}(a_i))$ and $(b_i + \epsilon_i, \overline{f}(b_i + \epsilon_i))$ is empty for $a_i < x < b_i + \epsilon_i$. Note that, from continuity assumption of $\overline{f}$, such ϵ_i is guaranteed to exist. Define

$$\tilde{\eta}(x) = \begin{cases} \frac{\overline{f}(b_i+\epsilon_i)-\overline{f}(a_i)}{b_i+\epsilon_i-a_i}(x-a_i) + \overline{f}(a_i) & , \ x \in [a_i, b_i + \epsilon_i) \\ \overline{f}(x) & , \text{ otherwise} \end{cases}.$$

If $\overline{f}$ is such that there exists $b_i = \infty$ (*i.e.*, $\overline{f} = C \ \forall x \geq a_i$), let $\tilde{\eta} = \overline{f}(a_i) + K - e^{-(x-a_i)^2}$ for $x \geq a_i$.
Set $\eta = a\tilde{\eta}$. Then, $\eta = a\tilde{\eta} \geq a\overline{f} \geq af$ and also $\tilde{\eta} - \overline{f} \leq K$. Therefore, if we select a constant $c > 0$ such that $\overline{f} \geq c$ for $x > x_0$, and

$$\frac{\eta}{\overline{f}} \leq a\left(\frac{K}{\overline{f}} + 1\right) \leq a\left(\frac{K}{c} + 1\right) \text{ for } x > x_0.$$

Thus, $\eta = O(\overline{f})$. □

Proof of Lemma 52. Since $m(x) < 0 \ \forall x \neq 0$ and $m(x) \to -\infty$ as $|x| \to \infty$, then $\underline{|m(x)|} > 0$ $\forall x \neq 0$ and $\underline{|m(x)|} \to \infty$ as $|x| \to \infty$. Hence, there exists a $\mathcal{K}_\infty$ function α such that $\alpha \leq \underline{|m|}$. Using a construction similar to the proof of Lemma 53, we can define the $\mathcal{K}_\infty$ function α such that $\alpha \leq \underline{|m|} \leq |m|$, and $\underline{|m|} - \alpha \leq K$, for some constant $K > 0$. Therefore, $\underline{|m|} = O(\alpha)$, concluding the proof. □

Sufficient Conditions for One-Dimensional Systems with Unknown Equilibrium

The equilibrium point of an interconnected system becomes harder to determine as the system dimension increases. The following results give conditions for sOSP and NSS⊕OSP which are equilibrium-independent.

Corollary 54. ***(sOSP)*** *For the stochastic subsystem in* (5.26)*, with* $x, y, u \in \mathbb{R}$*,* $\Sigma = 1$*, and* $l(x^*) = 0$*, assume that* h*,* f*, and* l *are differentiable and satisfy the following, for all* $x \in \mathbb{R}$*:*

(A1*) *f is strictly decreasing, h is strictly increasing;*

(A2*) *There exist constants $a, b_k > 0$, $k = 1, ..., r$, such that*

$$\frac{\partial h(x)}{\partial x} \in [0, a] \quad \textit{and} \quad \left|\frac{\partial l_k(x)}{\partial x}\right| \leq \sqrt{b_k}\frac{\partial h(x)}{\partial x}, \tag{5.36}$$

and there exists a constant $\gamma > 0$ such that

$$\frac{\partial f(x)}{\partial x} \leq \left(-\frac{1}{\gamma} - \frac{1}{2}ab\right)\frac{\partial h(x)}{\partial x}, \tag{5.37}$$

where $b = \sum_{k=1}^{r} b_k$.

Then, the system is stochastic output strictly passive.

Proof. Given inequality (5.36), and the fact that $l_k(x^*) = 0$, we have $|l_k(x)| \leq \sqrt{b_k}|h(x) - h(x^*)|$. Thus, $\|l(x)\|_2^2 = \sum_{k=1}^r l_k(x)^2 \leq b(h(x) - h(x^*))^2$. Moreover, from (5.37), and since $\frac{\partial h(x)}{\partial x} \in [0, a]$, it is easy to see from Theorem 50 that the system is sOSP. □

Corollary 55. ***(NSS⊕OSP)*** *Consider a stochastic subsystem described by* (5.26)*, with* $x, y, u \in \mathbb{R}$*,* $g(x) = 1$*,* $h \in \mathcal{C}^1$*, and where* f *is differentiable. Assume the following holds:*

(B1*) f *is strictly decreasing,* h *is strictly increasing;*

(B2*) *There exists a constant* $\hat{\gamma} > 0$ *such that*

$$\frac{\partial f(x)}{\partial x} \leq -\frac{1}{\hat{\gamma}} \frac{\partial h(x)}{\partial x}; \tag{5.38}$$

(B3*) $l(\cdot)$*,* $h(\cdot)$*, and* $f(.)$ *are such that* $|h(x)f(x)| \to \infty$ *as* $|x| \to \infty$ *and* $\forall i, j = 1, ...r$

$$\overline{|h'(x)l_i(x)l_j(x)|} = o\left(\underline{|h(x)f(x)|}\right) \text{ as } |x| \to \infty. \tag{5.39}$$

Then, the system is NSS⊕OSP for any $\gamma > \hat{\gamma}$*.*

Proof. It is clear that (B1*)-(B2*) imply (B1)-(B2) in Theorem 51. Since $h(x^*)$ and $f(x^*)$ are constants, and since h and f are strictly monotone functions, we conclude that $|h(x)f(x)| \to \infty$ as $|x| \to \infty$ implies that $|\tilde{h}(\tilde{x})\tilde{f}(\tilde{x})| \to \infty$ as $|\tilde{x}| \to \infty$. Furthermore, such conditions imply that $\underline{|h(x)f(x)|} = O(\underline{|(h(x) - h(x^*))(f(x) - f(x^*))|})$. Hence, assumption (B3*) implies (B3) in Theorem 51. The subsystem is thus NSS⊕OSP with constant $\gamma > \hat{\gamma}$. □

5.4 Application to Biological Reaction Networks

Chemical reactions are dependent on random thermal motion, and are inherently stochastic. Several classic chemistry examples can be accurately described by their mean deterministic behavior when the number of species is high. Such processes are described by the laws of mass-action of the distinct chemical reactions, which yield a set of ordinary differential equations, [37]. However, it is often the case in molecular biology, where the number of species is very small, that fluctuations in the molecule number of species lead to large variability in the cell's response to a signal, [100].

Stochastic models are typically described by a Markov jump process $X(t)$, where $X_i(t)$ represents the number of species i at time t. This process is usually defined by the Chemical Master Equation (CME), a system of coupled ordinary differential equations describing the probability transition function of every reaction over time, [63]. However, since the CME

involves, in most cases, an infinite-dimensional probability transition vector, it is computationally expensive to obtain the exact solution. A common approach is to simulate sample paths of the process, [52, 53], but the simulation of every reaction event is also expensive, [37].

The Chemical Langevin Equation (CLE), replaces the large dimensional CME with a small stochastic differential equation (SDE) that is easier to compute. The solution of such an equation is now a continuous random process instead of the discrete Markov jump process $X(t)$, and thus, the solutions are not exactly the same. Nonetheless, one can derive a CLE[3], from the CME, such that the solution provides an approximation of $X(t)$ when the system is sufficiently large that the discrete character of the stochastic process becomes secondary, [54, 65]. This approximation is particularly useful for system sizes that are not so large that stochastic effects are averaged out.

Below we study a class of SDEs, that can be seen as an interconnection of stochastic subsystems as described by (5.20)-(5.21):

$$\begin{cases} dx_i = (-c_i x_i + u_i)dt + \sqrt{c_i|x_i|}\sigma_{i1}dw_{i1} \\ \qquad\qquad + \sum_{j=1}^{N} \sqrt{k_{ij}|y_j|}\sigma_{i1(j+1)}dw_{i(j+1)}, \\ y_i = h_i(x_i) \\ u = My \end{cases} \tag{5.40}$$

where $x_i, y_i, u_i \in \mathbb{R}$, and dw_{ij} are independent. The structure of these equations is motivated by the Chemical Langevin Equation. Since the regularity assumptions impose local Lipschitz continuity, there is a technical issue that arises from the square root terms of the CLE. We may view the results as applying to a slightly perturbed system with nonlinearities $\sqrt{\epsilon + c_i|x_i|}$, and similarly for y, where $0 < \epsilon \ll 1$. As long as trajectories stay away from the origin, this approximation is reasonable. In this class, for each subsystem i, the vector $l_i : \mathbb{R}^N \to \mathbb{R}^{1\times(N+1)}$ depends not only on x_i but also on other entries of x. However, when there exists $l_i^u : \mathbb{R} \to \mathbb{R}^{1\times(N+1)}$ so that

$$l_i(x) \le l_i^u(x_i) \quad \forall x \in \mathbb{R}^N,$$

where the inequality is elementwise, a result similar to Theorems 49 and 51 holds by using $l_i^u(x_i)$ instead of $l_i(x)$. The proof follows similarly since

$$\left| l_i(x)^\top \frac{\partial^2 V_i}{\partial x_i^2} l_i(x) \right|_F = \sqrt{\left|\frac{\partial^2 V}{\partial x^2}\right|^2 \sum_{j=1}^{N+1}\sum_{k=1}^{N+1} |l_{ij}(x)l_{ik}(x)|^2} \le \left| l_i^u(x_i)^\top \frac{\partial^2 V_i}{\partial x_i^2} l_i^u(x_i) \right|_F .$$

[3]This SDE is to be interpreted in the Itô sense, because, under appropriate assumptions, [69], a density dependent Markov Chain can be approximated by an Itô diffusion process.

Proposition 56. *For a stochastic system as described in* (5.40)*, assume that each h_i is: (i) strictly increasing; (ii) upper and lower bounded; (iii) has bounded derivative; and (iv) does not converge to zero at infinity. Then, each subsystem $i = 1, \ldots, N$ is NSS⊕OSP.*

Proof. It is sufficient to show that conditions in Corollary 55 hold. Since function h_i is strictly increasing, and $f_i = -c_i x_i$ is linearly decreasing, (B1*) holds. Moreover, since h_i has bounded derivative, we know that $0 \leq h_i'(x_i) \leq a_i$ for some $a_i > 0$. Therefore, for $\hat{\gamma}_i \geq \frac{a_i}{c_i}$, assumption (B2*) holds because:

$$\frac{\partial f_i}{\partial x_i} = -c_i \leq -\frac{1}{\hat{\gamma}_i} a_i \leq -\frac{1}{\hat{\gamma}_i} \frac{\partial h_i}{\partial x_i}.$$

Clearly, $|h_i(x_i) f_i(x_i)| \to \infty$ as $|x_i| \to \infty$. Since every h_i is bounded, then there exists some constant $b_{ij} \geq 0$ such that the corresponding diffusion coefficients $\sqrt{k_{ij} y_j} \leq b_{ij}$. Note that

$$l_i(x) = \left[\sqrt{c_i|x_i|}, \sqrt{k_{i1}|h_1(x_1)|}, ..., \sqrt{k_{iN}|h_N(x_N)|}\right]^\top \leq l_i^u(x_i) = \left[\sqrt{c_i|x_i|}, b_{i1}, ..., b_{i,N}\right]^\top.$$

We thus need to show that l_i^u verifies (5.39). Since $h_i'(x_i) \leq a_i$, for $j, k = 2, ..., N+1$ we obtain $\overline{h_i'(x_i) l_{ij}^u(x_i) l_{ik}^u(x_i)} \leq a_i b_{ij} b_{ik} = o(x_i) = O(\underline{|h_i(x_i) f_i(x_i)|})$ as $|x_i| \to \infty$, and also, $\overline{h_i'(x_i) l_{i1}^u(x_i) l_{ik}^u(x_i)} \leq a_i b_{ik} \sqrt{c_i|x_i|} = o(x_i)$ as $|x_i| \to \infty$. Additionally, $\lim_{|x_i|\to\infty} h_i'(x_i) = 0$, because h_i is a strictly increasing and bounded. Therefore, $\lim_{|x_i|\to\infty} |\overline{h_i'(x_i) l_{11}^u(x_i)^2}/x_i| = \lim_{|x_i|\to\infty} h_i'(x_i) c_i = 0$, which implies that $\overline{h_i'(x_i) l_{11}^u(x_i)^2} = o(x_i)$ as $|x_i| \to \infty$. Since (B3*) also holds, the system is NSS⊕OSP. □

The conditions imposed on h_i in Proposition 56 are satisfied by standard activation models in enzyme kinetics, such as Hill equations of the form $h(s) = \frac{k_1 s^p}{1+s^p}$. Likewise, inhibition terms, such as $h(s) = \frac{k_1}{1+s^p}$, can be encompassed by Proposition 56, by defining $\hat{h}(s) = -h(s)$, and incorporating the negative sign in the interconnection matrix M.

As a special case of (5.40), consider a cycle of three genes, each repressing the expression of the next one in the cycle, as in [38]:

$$\begin{aligned}
dx_1 &= \left(-c_1 x_1 + k_{32} + \tfrac{k_{31}}{1+x_3^p}\right) dt + \sqrt{c_1 x_1}\Sigma_{11} dw_{11} + \sqrt{k_{32}}\Sigma_{12} dw_{12} + \sqrt{\tfrac{k_{31}}{1+x_3^p}}\Sigma_{13} dw_{13} \\
dx_2 &= \left(-c_2 x_2 + k_{12} + \tfrac{k_{11}}{1+x_1^p}\right) dt + \sqrt{c_2 x_2}\Sigma_{21} dw_{21} + \sqrt{k_{12}}\Sigma_{22} dw_{22} + \sqrt{\tfrac{k_{11}}{1+x_1^p}}\Sigma_{23} dw_{23} \\
dx_3 &= \left(-c_3 x_3 + k_{22} + \tfrac{k_{21}}{1+x_2^p}\right) dt + \sqrt{c_3 x_3}\Sigma_{31} dw_{31} + \sqrt{k_{22}}\Sigma_{32} dw_{32} + \sqrt{\tfrac{k_{21}}{1+x_2^p}}\Sigma_{33} dw_{33}
\end{aligned} \tag{5.41}$$

where c_i and k_{jl}, for $i, j, l = 1, 2, 3$, are positive constants, and dw_{ij}'s are independent standard Brownian processes. Although, biologically, the system variables only make physical sense in the positive quadrant, we view the system as evolving on $\mathbb{R}^3$. Therefore, we let $h_i(x_i) = -k_{i2} - \frac{k_{i1}}{1+x_i^p}$ for $x_i \geq 0$, and define it to be $h_i(x_i) = -h_i(-x_i) + 2h_i(0)$ for $x_i < 0$,

so that the system is well-defined for negative values of x_i. Then, it can be written as in (5.20)-(5.21), for $x \in \mathbb{R}^3$:

$$\begin{cases} dx_i = (-c_i x_i + u_i)\, dt + \sqrt{c_i |x_i|}\Sigma_{i1} dw_{i1} \\ \qquad\qquad + \sqrt{k_{i2}}\Sigma_{i2} dw_{i2} + \sqrt{u_i}\Sigma_{i3} dw_{i3}, \quad i = 1,2,3, \\ y_i = h_i(x_i) \end{cases}$$

where

$$\begin{bmatrix} u_1 \\ u_2 \\ u_3 \end{bmatrix} = \begin{bmatrix} 0 & 0 & -1 \\ -1 & 0 & 0 \\ 0 & -1 & 0 \end{bmatrix} \begin{bmatrix} y_1 \\ y_2 \\ y_3 \end{bmatrix}.$$

From the proof of Proposition 56, each subsystem i is NSS$\oplus$OSP with $\gamma_i > a_i/c_i$, where

$$a_i \geq \max_{s \in \mathbb{R}_{\geq 0}} h_i'(s) = \frac{k_{i1}}{4p}(p-1)^{\frac{p-1}{p}}(p+1)^{\frac{p+1}{p}}.$$

In order to conclude NSS for the interconnected system, we need to verify the matrix inequality (5.22). Let $\Gamma = \mathrm{diag}(\gamma_1^{-1}, \gamma_2^{-1}, \gamma_3^{-1})$, and note that

$$(M - \Gamma) = \begin{bmatrix} -\gamma_1^{-1} & 0 & -1 \\ -1 & -\gamma_2^{-1} & 0 \\ 0 & -1 & -\gamma_3^{-1} \end{bmatrix}.$$

For matrices of this cyclic form, it was shown in [10] that a diagonal matrix $D > 0$ satisfying $D(M-\Gamma) + (M-\Gamma)^\top D < 0$ exists if and only if $\gamma_1\gamma_2\gamma_3 < sec(\frac{\pi}{3})^3 = 8$. Thus, we conclude that the interconnected system (5.41) is NSS if

$$\frac{k_{11}k_{21}k_{31}}{c_1c_2c_3} < \frac{8 \cdot 4^3}{(p-1)^{3\frac{p-1}{p}}(p+1)^{3\frac{p+1}{p}}}. \tag{5.42}$$

We simulated the system with two different sets of parameters and several noise levels (*i.e.*, $|\Sigma\Sigma^\top|_F$). Figure 5.1 shows the behavior of a system that is not NSS. In the absence of noise ($\Sigma_{ij} = 0$), the system converges to a steady-state oscillation, and therefore it is not asymptotically stable. Note that NSS implies asymptotic stability of the deterministic part of the system (*cf.* (5.14) with $\Sigma_{ij} = 0$). For the second case, we selected a set of parameters that satisfy the condition for NSS derived in (5.42). Indeed, in Figure 5.2 we see that the system is asymptotically stable when $\Sigma_{ij} = 0$ and, in the presence of noise, its sample paths are bounded in probability (as seen from the 99.5% confidence level plots).

5.5 Conclusions

We use stochastic Lyapunov theory to provide a technique to certify stability in probability and NSS using passivity of subsystems and a matrix diagonal stability condition. This technique is different from the classical large-scale literature, since it takes into account the sign

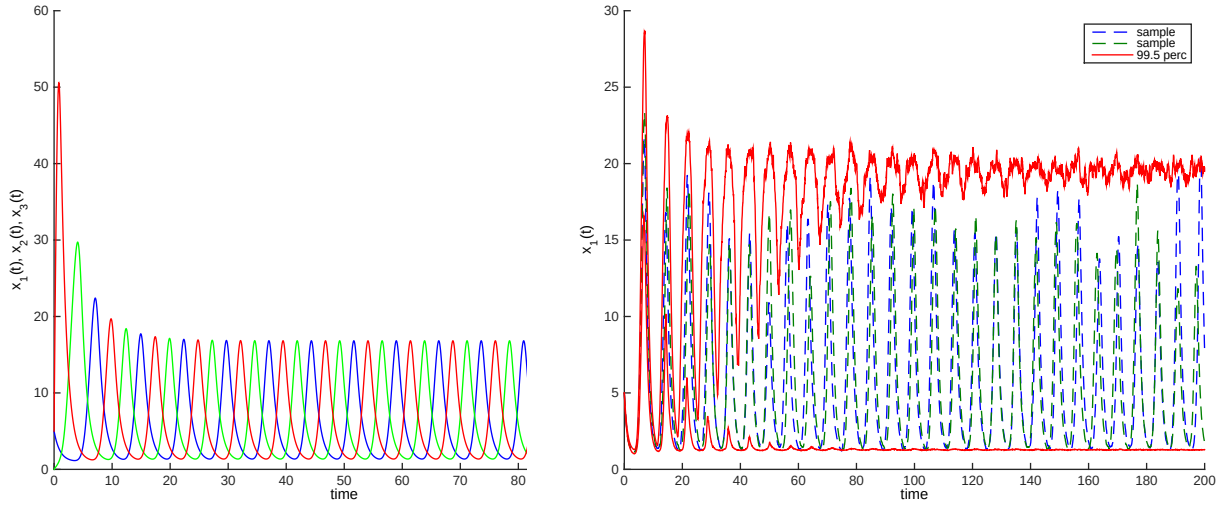

Figure 5.1: Simulation of system (5.41) with parameters $p = 4$, $c_i = 1$, $k_{i1} = 100$, $k_{i2} = 1$, for $i = \{1, 2, 3\}$, and $(x_1(0), x_2(0), x_3(0)) = (5, 0, 5)$. (Top) Plots of $x_1(t)$ (blue), $x_2(t)$ (green), and $x_3(t)$ (red) for $\Sigma_{ij} = 0$. (Bottom) Plots of two sample paths of $x_1(t)$ (dashed), and 99.5% confidence levels of 2000 samples paths of $x_1(t)$ (line), for $\Sigma_{ij} = 0.05$.

structure of the interconnection. We prove a sufficient condition for NSS that is only dependent on the state space x, and not on the noise Σ, thus providing a new tool that simplifies the verification of NSS. Moreover, we demonstrated that, under appropriate assumptions, sOSP and NSS$\oplus$OSP can be easily verifiable by equilibrium independent conditions. Literature results typically rely on the calculation of such equilibrium, which can be intractable as the dimension of the system increases. The NSS notion is appropriate for the stability analysis of biological reaction networks, as it admits systems with nonvanishing noise and unknown noise intensity. In the future, it is of interest to provide extensions of the NSS results to broader classes of biological models than the ones studied here. However, the unbounded tails in the noise process is one drawback in the use of diffusion approximations to obtain SDEs for reaction networks, since the invariance of the nonnegative orthant is not guaranteed and physical relevance may be lost.

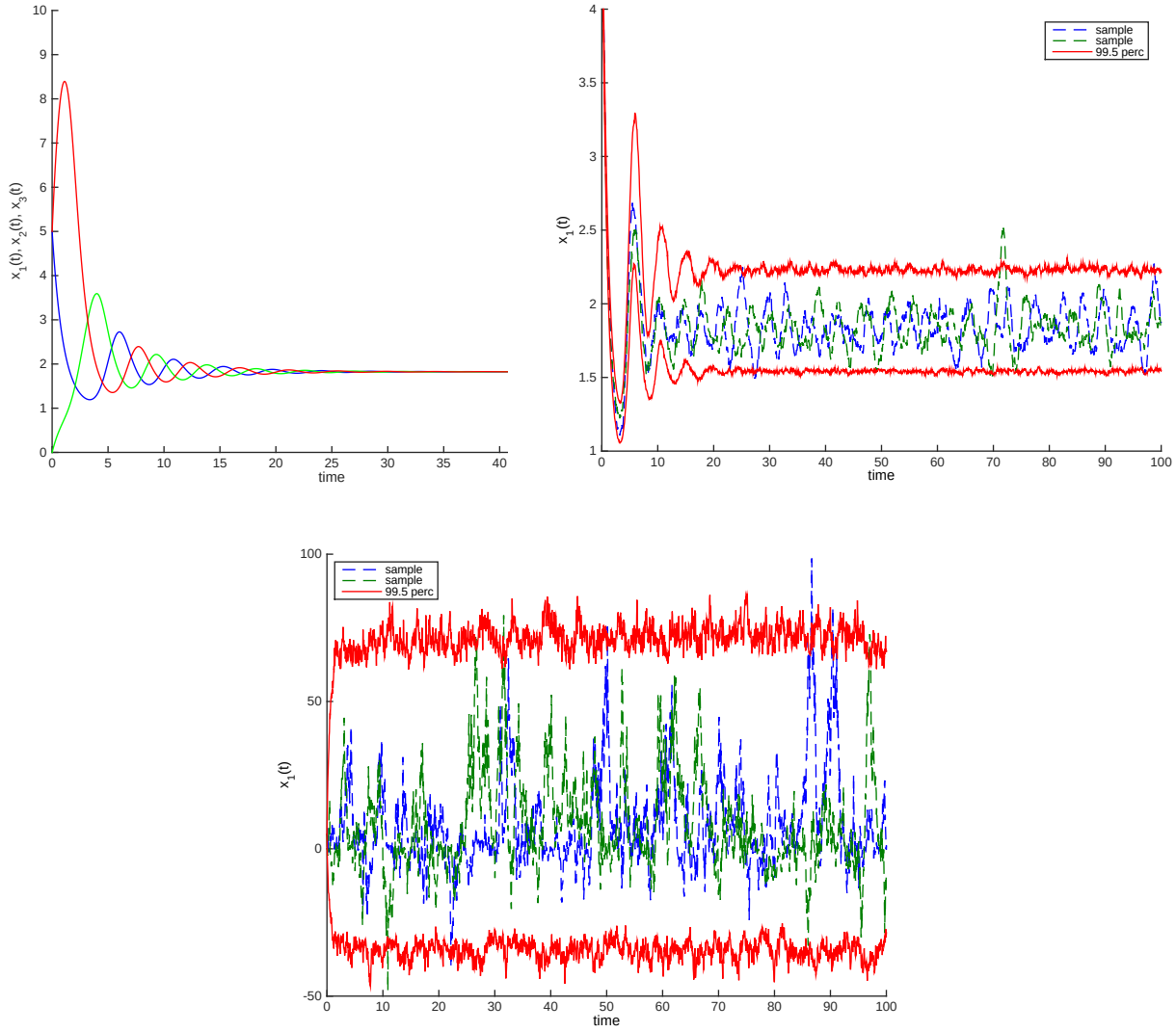

Figure 5.2: Behavior of system (5.41) with parameters: $p = 4$, $c_i = 1$, $k_{i1} = 10$, $k_{i2} = 1$ for $i = \{1, 2, 3\}$, and $(x_1(0), x_2(0), x_3(0)) = (5, 0, 5)$. (Top) Plots of $x_1(t)$ (blue), $x_2(t)$ (green), and $x_3(t)$ (red) for $\Sigma_{ij} = 0$. (Middle-Bottom) Plots of two sample path of $x_1(t)$ (dashed), and 99.5% confidence levels of 2000 samples paths of $x_1(t)$ (line), for $\Sigma_{ij} = 0.05$ and $\Sigma_{ij} = 5$, respectively.

Bibliography

[1] M. A. D. Aguiar and A. P. S. Dias. "The lattice of synchrony subspaces of a coupled cell network: characterization and computation algorithm". In: *Journal of Nonlinear Science* 24.6 (2014), pp. 946–996.

[2] Alkiviadis G. Akritas, Evgenia K. Akritas, and Genadii I. Malaschonok. "Various proofs of Sylvester's (determinant) identity". In: *Mathematics and Computers in Simulation* 42.4-6 (Jan. 1996), pp. 585–593.

[3] D. Angeli and E. Sontag. "Multi-stability in monotone input/output systems". In: *Systems & Control Letters* 51.3-4 (Mar. 2004), pp. 185–202.

[4] D. Angeli and E.D. Sontag. "Monotone control systems". In: *IEEE Transactions on Automatic Control* 48.10 (Oct. 2003), pp. 1684–1698.

[5] S. K. Aoki et al. "A widespread family of polymorphic contact-dependent toxin delivery systems in bacteria". In: *Nature* 468.7322 (2010), pp. 439–442.

[6] SK Aoki et al. "Contact-dependent growth inhibition causes reversible metabolic downregulation in Escherichia coli". In: *Journal of Bacteriology* 191.6 (2009), pp. 1777–1786.

[7] Mituhiko Araki. "Application of M-matrices to the stability problems of composite dynamical systems". In: *Journal of Mathematical Analysis and Applications* 52.2 (1975), pp. 309–321.

[8] M. Arcak. "Pattern formation by lateral inhibition in large-scale networks of cells". In: *IEEE Transactions on Automatic Control* 58.5 (May 2013), pp. 1250–1262.

[9] Murat Arcak and Eduardo D. Sontag. "A passivity-based stability criterion for a class of interconnected systems and applications to biochemical reaction networks". In: *Mathematical Biosciences and Engineering* 5(1) (2008), pp. 1–19.

[10] Murat Arcak and Eduardo D. Sontag. "Diagonal stability of a class of cyclic systems and its connection with the secant criterion". In: *Automatica* 42.9 (2006), pp. 1531–1537.

[11] Frederick K Balagadde et al. "A synthetic Escherichia coli predator–prey ecosystem". In: *Molecular Systems Biology* 4.1 (2008), p. 187.

[12] Subhayu Basu et al. "A synthetic multicellular system for programmed pattern formation". In: *Nature* 434.7037 (2005), pp. 1130–1134.

[13] Subhayu Basu et al. "Spatiotemporal control of gene expression with pulse-generation networks". In: *Proceedings of the National Academy of Sciences USA* 101.17 (2004), pp. 6355–6360.

[14] A. Berman and R. J. Plemmons. *Nonnegative matrices in the mathematical sciences*. (revised reprint of the 1979 original). Philadelphia, PA: Society for Industrial and Applied Mathematics (SIAM), 1994, pp. xx+340.

[15] Tommaso Biancalani, Duccio Fanelli, and Francesca Di Patti. "Stochastic Turing patterns in the Brusselator model". In: *Physical Review E* 81 (4 Apr. 2010), p. 046215.

[16] Vivek Borkar and Sanjoy Mitter. "A note on stochastic dissipativeness". In: *Directions in Mathematical Systems Theory and Optimization*. Ed. by Anders Rantzer and Christopher Byrnes. Vol. 286. Lecture Notes in Control and Information Sciences. Springer Berlin / Heidelberg, 2003, pp. 41–49.

[17] Stephen P. Boyd et al. "Symmetry analysis of reversible Markov chains." In: *Internet Mathematics* 2.1 (2005), pp. 31–71.

[18] Stephen Boyd et al. "Distributed optimization and statistical learning via the alternating direction method of multipliers." In: *Foundations and Trends in Machine Learning* 3.1 (2011), pp. 1–122.

[19] Stephen Boyd et al. "Fastest mixing Markov chain on graphs with symmetries". In: *SIAM Journal on Optimization* 20.2 (June 2009), pp. 792–819.

[20] Stephen Boyd et al. *Linear matrix inequalities in system & control theory*. Vol. 15. Society for Industrial and Applied Mathematics (SIAM), 1994.

[21] Mathias Burger, Daniel Zelazo, and Frank Allgower. "Duality and network theory in passivity-based cooperative control". In: *Automatica* 50.8 (2014), pp. 2051–2061.

[22] Thomas Butler and Nigel Goldenfeld. "Fluctuation-driven Turing patterns". In: *Physical Review E* 84 (1 July 2011), p. 011112.

[23] Frank M. Callier and Charles A. Desoer. *Linear system theory*. London, UK, UK: Springer-Verlag, 1991.

[24] Randy Cogill, Sanjay Lall, and Pablo A. Parrilo. "Structured semidefinite programs for the control of symmetric systems". In: *Automatica* 44.5 (2008), pp. 1411–1417.

[25] Daniel J. Cohen, Roberto C. Morfino, and Michel M. Maharbiz. "A modified consumer inkjet for spatiotemporal control of gene expression". In: *PLoS ONE* 4.9 (Sept. 2009), e7086.

[26] JR Collier et al. "Pattern formation by lateral inhibition with feedback: a mathematical model of Delta-Notch intercellular signalling." In: *Journal of Theoretical Biology* 183.4 (Dec. 1996), pp. 429–446.

[27] C. H. Collins, J. R. Leadbetter, and F. H. Arnold. "Dual selection enhances the signaling specificity of a variant of the quorum-sensing transcriptional activator LuxR". In: *Nature Biotechnology* 24.6 (June 2006), pp. 708–712.

[28] S. Coogan and M. Arcak. "A dissipativity approach to safety verification for interconnected systems". In: *IEEE Transactions on Automatic Control* 60.6 (June 2015), pp. 1722–1727.

[29] D.M. Cvetkovic, M. Doob, and H. Sachs. *Spectra of graphs: theory and application*. Pure and applied mathematics. Academic Press, 1980.

[30] Tal Danino et al. "A synchronized quorum of genetic clocks". In: *Nature* 463.7279 (Jan. 2010), pp. 326–330.

[31] Hua Deng, M. Krstic, and R.J. Williams. "Stabilization of stochastic nonlinear systems driven by noise of unknown covariance". In: *IEEE Transactions on Automatic Control* 46.8 (Aug. 2001), pp. 1237–1253.

[32] Charles A. Desoer and M. Vidyasagar. *Feedback systems: Input-output properties*. Society for Industrial and Applied Mathematics, 2009.

[33] R. Dillon, P. K. Maini, and H. G. Othmer. "Pattern formation in generalized Turing systems". In: *Journal of Mathematical Biology* 32 (4 1994), pp. 345–393.

[34] J.C. Doyle et al. "State-space solutions to standard $\mathcal{H}_2$ and $\mathcal{H}_\infty$ control problems". In: *IEEE Transactions on Automatic Control* 34.8 (Aug. 1989), pp. 831–847.

[35] Kristian Dreij et al. "A method for efficient calculation of diffusion and reactions of Lipophilic compounds in complex cell geometry". In: *PLoS ONE* 6.8 (Aug. 2011), e23128.

[36] E.B. Dynkin. *Markov processes*. Vol. I. Springer-Verlag, 1965.

[37] Hana El Samad et al. "Stochastic modelling of gene regulatory networks". In: *International Journal of Robust and Nonlinear Control* 15.15 (2005), pp. 691–711.

[38] M. B. Elowitz and S. Leibler. "A synthetic oscillatory network of transcriptional regulators". In: *Nature* 403.6767 (Jan. 2000), pp. 335–338.

[39] German A. Enciso and Eduardo D. Sontag. "Monotone systems under positive feedback: multistability and a reduction theorem". In: *Systems & Control Letters* 51.2 (2005), pp. 185–202.

[40] Ana Sofia Rufino Ferreira and Murat Arcak. "A graph partitioning approach to predicting patterns in lateral inhibition systems". In: *SIAM Journal on Applied Dynamical Systems* 12.4 (2013), pp. 2012–2031.

[41] Ana Sofia Rufino Ferreira, Murat Arcak, and Eduardo D. Sontag. "Stability certification of large scale stochastic systems using dissipativity". In: *Automatica* 48.11 (2012), pp. 2956–2964.

[42] Ana Sofia Rufino Ferreira, Justin Hsia, and Murat Arcak. "A compartmental lateral inhibition system to generate contrasting patterns". In: *IEEE Life Sciences Letters* 1.1 (June 2015), pp. 7–10.

[43] Ana Sofia Rufino Ferreira et al. "Pattern formation with a compartmental lateral inhibition system". In: *IEEE 53rd Annual Conference on Decision and Control (CDC)*. Dec. 2014, pp. 5413–5418.

[44] Ana Sofia Rufino Ferreira et al. "Symmetry reduction for performance certification of interconnected systems". In: *Submitted to IEEE Transactions on Control of Network Systems* (2015).

[45] Patrick Florchinger. "A passive system approach to feedback stabilization of nonlinear control stochastic systems". In: *SIAM Journal on Control and Optimization* 37.6 (Nov. 1999), pp. 1848–1864.

[46] *GAP – Groups, algorithms, and programming, version 4.4.12*. The GAP Group. 2008. URL: `http://www.gap-system.org`.

[47] C W Gardiner. *Handbook of stochastic methods for physics, chemistry, and the natural sciences*. Ed. by HermannEditor Haken. Springer-Verlag, 1985, p. 226.

[48] Karin Gatermann and Pablo A. Parrilo. "Symmetry groups, semidefinite programs, and sums of squares". In: *Journal of Pure and Applied Algebra* 192.1–3 (2004), pp. 95–128.

[49] R. Ghosh and J.C. Tomlin. "Symbolic reachable set computation of piecewise affine hybrid automata and its application to biological modeling: Delta-Notch protein signaling". In: *IET Systems Biology* 1 (2004), pp. 170–183.

[50] A. Gierer and H. Meinhardt. "A theory of biological pattern formation." In: *Biological Cybernetics* 12.1 (Dec. 1972), pp. 30–39.

[51] S.F. Gilbert. *Developmental biology*. 9th. Sinauer Associates, Inc., 2010.

[52] D. Gillespie. "A general method for numerically simulating the stochastic time evolution of coupled chemical reactions". In: *Journal of Computational Physics* 22.4 (Dec. 1976), pp. 403–434.

[53] Daniel T. Gillespie. "Exact stochastic simulation of coupled chemical reactions". In: *Journal of Physical Chemistry* 81.25 (1977), pp. 2340–2361.

[54] Daniel T. Gillespie. "The chemical Langevin equations". In: *Journal of Chemical Physics* 113.1 (2000), pp. 297–306.

[55] Chris Godsil and Gordon Royle. *Algebraic graph theory*. Springer, Apr. 20, 2001.

[56] Martin Golubitsky and Ian Stewart. "Nonlinear dynamics of networks: the groupoid formalism". In: *Bulletin of the American Mathematical Society* 43 (2006), pp. 305–364.

[57] Bill Goodwine and Panos Antsaklis. "Multi-agent compositional stability exploiting system symmetries". In: *Automatica* 49.11 (2013), pp. 3158–3166.

[58] M. Grant and S. Boyd. *CVX: Matlab software for disciplined convex programming, version 1.21*. Apr. 2011.

[59] Hasminskii. *Stochastic stability of differential equations*. Sijthoff and Noordhoff, Maryland, 1980.

[60] Yutaka Hori and Hara Shinji. "Noise-induced spatial pattern formation in stochastic reaction-diffusion systems". In: *Proceedings of the 51st IEEE Conference on Decision and Control (CDC)*. Dec. 2012.

[61] Justin Hsia et al. "A feedback quenched oscillator produces Turing patterning with one diffuser". In: *PLoS Computational Biology* 8.1 (Jan. 2012), e1002331.

[62] M.R. Jovanovic, M. Arcak, and E.D. Sontag. "A passivity-based approach to stability of spatially distributed systems with a cyclic interconnection structure". In: *IEEE Transactions on Automatic Control* 53.Special Issue (Jan. 2008), pp. 75–86.

[63] N. G. Van Kampen. *Stochastic processes in physics and chemistry*. North-Holland personal library. Elsevier, 2007.

[64] H.K. Khalil. *Nonlinear systems (3rd Edition)*. Englewood Cliffs, NJ: Prentice Hall, 2002.

[65] Raya Khanin and Desmond J. Higham. "Chemical master equation and Langevin regimes for a gene transcription model". In: *Proceeding of 2007 International Conference on Computational Methods in Systems Biology*. CMSB'07. Edinburgh, Scotland: Springer-Verlag, 2007, pp. 1–14.

[66] R. Khasminskii and G.N. Milstein. *Stochastic stability of differencial equations*. Stochastic Modelling and Applied Probability. Springer Berlin Heidelberg, 2011.

[67] Miroslav Krstic and H. Deng. *Stabilization of nonlinear uncertain systems*. 1st. Secaucus, NJ, USA: Springer-Verlag New York, Inc., 1998.

[68] M. Kunisch, M. Haenlin, and J. A. Campos-Ortega. "Lateral inhibition mediated by the Drosophila neurogenic gene delta is enhanced by proneural proteins". In: *Proceedings of the National Academy of Sciences USA* 91.21 (1994), pp. 10139–10143.

[69] T.G. Kurtz. "Strong approximation theorems for density dependent Markov chains". In: *Stochastic Processes and their Applications* 6.3 (1978), pp. 223–240.

[70] Harold J. Kushner. *Stochastic stability and control*. English. Academic Press, New York, 1967, xiv, 161 p.

[71] Zhongwei Lin and Yan Lin. "Passivity and feedback design of nonlinear stochastic systems". In: *Proceedings of the 48th IEEE Conference on Decision and Control, held jointly with the 2009 28th Chinese Control Conference (CDC/CCC)*. 2009, pp. 1575–1580.

[72] Chenli Liu et al. "Sequential establishment of stripe patterns in an expanding cell population". In: *Science* 334.6053 (2011), pp. 238–241.

[73] Anna Lubiw. "Some NP-complete problems similar to graph isomorphism". In: *SIAM Journal on Computing* 10.1 (1981), pp. 11–21.

[74] Elena M. Lucchetta et al. "Dynamics of Drosophila embryonic patterning network perturbed in space and time using microfluidics". In: *Nature* 434.7037 (2005), pp. 1134–1138.

[75] Jan R. Magnus and Heinz Neudecker. *Matrix differential calculus with applications in statistics and econometrics*. 2nd. John Wiley & Sons, Mar. 15, 1999.

[76] Xuerong Mao. "Stochastic versions of the LaSalle theorem". In: *Journal of Differential Equations* 153 (1999), pp. 175–195.

[77] Jerrold E. Marsden and Tudor S. Ratiu. *Introduction to mechanics and symmetry*. Second. Texts in Applied Mathematics 17. New York, NY: Springer-Verlag, 1999.

[78] H. Meinhardt. *Models of biological pattern formation*. Vol. 6. London: Academic Press, 1982.

[79] Hans Meinhardt and Alfred Gierer. "Pattern formation by local self-activation and lateral inhibition". In: *BioEssays* 22.8 (2000), pp. 753–760.

[80] Chris Meissen et al. "Compositional performance certification of interconnected systems using ADMM". In: *Automatica* 61 (2015), pp. 55–63.

[81] A. N. Michel. "Stability analysis of stochastic large-scale systems". In: *ZAMM - Journal of Applied Mathematics and Mechanics / Zeitschrift fur Angewandte Mathematik und Mechanik* 55.2 (1975), pp. 113–123.

[82] A. Michel and R. Rasmussen. "Stability of stochastic composite systems". In: *IEEE Transactions on Automatic Control* 21.1 (Feb. 1976), pp. 89–94.

[83] Renato D.C. Monteiro and Paulo Zanjacomo. "Implementation of primal-dual methods for semidefinite programming based on Monteiro and Tsuchiya Newton directions and their variants". In: *Optimization Methods and Software* 11.1-4 (1999), pp. 91–140.

[84] J. D. Murray. *Mathematical biology II: Spatial models and biomedical applications*. Vol. 18. Interdisciplinary Applied Mathematics. Springer New York, 2003.

[85] Marc AT Muskavitch. "Delta-Notch signaling and Drosophila cell fate choice". In: *Developmental Biology* 166.2 (1994), pp. 415–430.

[86] Stephen Payne et al. "Temporal control of self-organized pattern formation without morphogen gradients in bacteria". In: *Molecular Systems Biology* 9.1 (Jan. 2013).

[87] E. Plahte. "Pattern formation in discrete cell lattices". In: *Journal of Mathematical Biology* 43 (2001), pp. 411–445.

[88] Amirreza Rahmani et al. "Controllability of multi-agent systems from a graph-theoretic perspective". In: *SIAM Journal on Control and Optimization* 48.1 (Feb. 2009), pp. 162–186.

[89] G.N. Rolinson. "Effect of Beta-Lactam antibiotics on bacterial cell growth rate". In: *Journal of General Microbiology* 120 (1980), pp. 317–323.

[90] Wilson J. Rugh. *Linear systems theory*. 2nd. Englewood Cliffs, N.J.: Prentice Hall, 1993.

[91] P. Seiler. "Stability analysis with dissipation inequalities and integral quadratic constraints". In: *IEEE Transactions on Automatic Control* 60.6 (June 2015), pp. 1704–1709.

[92] H.L. Smith. *Monotone dynamical systems: An introduction to the theory of competitive and cooperative systems*. Mathematical Surveys and Monographs. American Mathematical Society, 1995.

[93] T. Sohka, R. Heins, and M. Ostermeier. "Morphogen-defined patterning of Escherichia coli enabled by an externally tunable band-pass filter". In: *Journal of Biological Engineering* 3.10 (July 2009).

[94] E. D. Sontag. "Contractive systems with inputs". In: *Perspectives in Mathematical System Theory, Control, and Signal Processing*. Ed. by Jan C. Willems et al. Vol. 398. Lecture Notes in Control and Information Sciences. Springer Berlin Heidelberg, 2010, pp. 217–228.

[95] E.D. Sontag. "Smooth stabilization implies coprime factorization". In: *IEEE Transactions on Automatic Control* 34.4 (Apr. 1989), pp. 435–443.

[96] David Sprinzak et al. "Cis-interactions between Notch and Delta generate mutually exclusive signalling states". In: *Nature* 465.7294 (May 6, 2010), pp. 86–90.

[97] David Sprinzak et al. "Mutual inactivation of Notch receptors and ligands facilitates developmental patterning". In: *PLoS Computational Biology* 7.6 (June 9, 2011), e1002069.

[98] Ian Stewart, Martin Golubitsky, and Marcus Pivato. "Symmetry groupoids and patterns of synchrony in coupled cell networks". In: *SIAM Journal on Applied Dynamical Systems* 2 (2003), pp. 609–646.

[99] Philip S. Stewart. "Diffusion in biofilms". In: *Journal of Bacteriology* 185.5 (2003), pp. 1485–1491.

[100] Mukund Thattai and Alexander van Oudenaarden. "Stochastic gene expression in fluctuating environments". In: *Genetics* 167.1 (May 1, 2004), pp. 523–530.

[101] A. M. Turing. "The chemical basis of Morphogenesis". In: *Philosophical Transactions of the Royal Society B: Biological Sciences* 237.641 (Aug. 14, 1952), pp. 37–72.

[102] Reha Tutuncu, Kim-Chuan Toh, and Michael Todd. "Solving semidefinite-quadratic-linear programs using SDPT3". In: *Mathematical Programming Series B* 95 (2003), pp. 189–217.

[103] Lieven Vanderberghe and Stephen Boyd. "Semidefinite programming". In: *SIAM Review* 38.1 (1996), pp. 49–95.

[104] Joost Veenman and Carsten W Scherer. "Stability analysis with integral quadratic constraints: A dissipativity based proof". In: *IEEE 52nd Annual Conference on Decision and Control (CDC)*. IEEE. 2013, pp. 3770–3775.

[105] M. Vidyasagar. *Input-output analysis of large-scale interconnected systems: decomposition, well-posedness, and stability*. Lecture Notes in Control and Information Sciences. Springer-Verlag, 1981.

[106] Yunjiao Wang and Martin Golubitsky. "Two-colour patterns of synchrony in lattice dynamical systems". In: *Nonlinearity* 18.2 (2005), p. 631.

[107] H.J. Wearing and J.A. Sherrat. "Analysis of juxtacrine patterns". In: *SIAM Journal on Applied Mathematics* 62 (2001), pp. 283–309.

[108] Julia S Webb et al. "Delivery of CdiA nuclease toxins into target cells during contact-dependent growth inhibition". In: *PloS ONE* 8.2 (2013), e57609.

[109] Ron Weiss et al. "Genetic circuit building blocks for cellular computation, communications, and signal processing". In: *Natural Computing* 2 (1 2003), pp. 47–84.

[110] Jan Willems. "Dissipative dynamical systems Parts I-II". In: *Archive for Rational Mechanics and Analysis* 45.5 (1972), pp. 321–393.

[111] L. Wolpert and C. Tickle. *Principles of development*. fourth. Oxford University Press, 2011.

[112] Luping Xu et al. "Microcontact printing of living bacteria arrays with cellular resolution". In: *Nano Letters* 7.7 (2007), pp. 2068–2072.

[113] Yohei Yokobayashi, Ron Weiss, and Frances H. Arnold. "Directed evolution of a genetic circuit". In: *Proceedings of the National Academy of Sciences USA* 99.26 (2002), pp. 16587–16591.

[114] G. Zames. "On the input-output stability of time-varying nonlinear feedback systems - Parts I and II". In: *IEEE Transactions on Automatic Control* 11.2 (Apr. 1966), pp. 228–238.

[115] K. Zhou and J.C. Doyle. *Essentials of robust control*. Prentice Hall, 1998.